Master Thesis in Geosciences

Structural Analysis of The Hoop Fault Complex, SW Barents Sea

Agus Fitriyanto

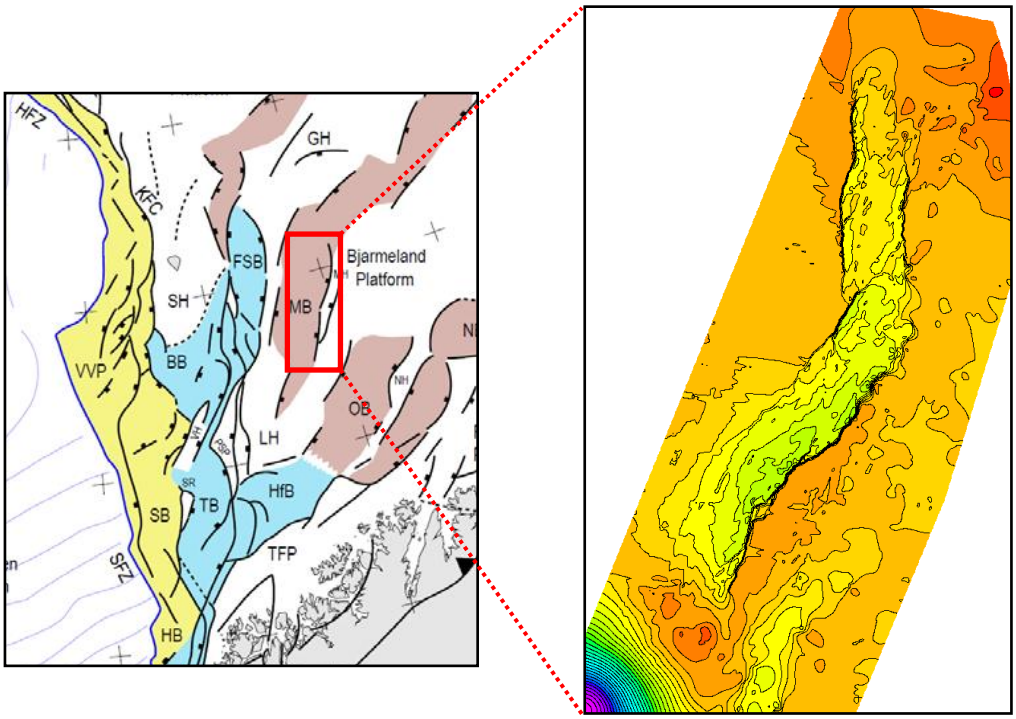

UNIVERSITY OF OSLO
FACULTY OF MATHEMATICS AND NATURAL SCIENCES

Structural Analysis of The Hoop Fault Complex, SW Barents Sea

Agus Fitriyanto

Master Thesis in Geosciences

Discipline: Petroleum Geology and Petroleum Geophysics

Department of Geosciences

Faculty of Mathematics and Natural Sciences

UNIVERSITY OF OSLO

June 2011

Abstract

The Hoop Fault Complex is an old zone of weakness in SW Barents Sea which intersects Bjarmeland Platform and separates Maud Basin from Mercurius High. Reactivations during its long-lived activity have brought to the complex of geometry, style and geological history of this fault complex. A set of 2D and 3D seismic lines has been interpreted to map and characterize the structural geometry, genesis and evolution of the Hoop fault Complex.

The Hoop Fault Complex is an obviously extensional fault complex with graben system. It can be divided laterally and vertically into distinct major segments of different fault geometry, orientation and style. Laterally, this fault complex comprises NE-SW trending half graben in the south, NE-SW trending full graben in the central part and N-S trending full graben in the north. Vertically, this fault complex consists of several depth-dependent segments which are characterized by different fault geometry and separated by detachments. The main detachment coincides with upper Carboniferous-lower Permian carbonate-evaporite succession separating late Carboniferous interval from the post-early Permian interval. Late Carboniferous interval is characterized by a set of extensional planar normal faults defining a wide graben with tilted fault blocks and faulted platform which are formed by late Carboniferous major rifting. Post-early Permian interval is characterized by complex geometry of moderate-steeply dipping, slightly curved, extensional master normal faults which are segmented into three depth-dependent intervals. Each depth-dependent interval has different normal fault characteristics which are influenced by different reactivation process, from growth faulting in early-middle Triassic, mild inversion in middle-earliest late Triassic and major extension in late Jurassic-early Cretaceous. Organic rich-shales within upper Permian Ørret Formation and middle Triassic Snadd-Kobbe Formations have acted as minor detachments separating mentioned depth-dependent intervals.

Evolution of the Hoop Fault Complex in study area was started from late Carboniferous ESE-WNW regional rifting which was followed by thermal subsidence in early-late Permian. No indication of faulting related to late Permian-early Triassic regional rifting can be observed in study area. Growth faulting active during early-middle Triassic which was followed by mild inversion related to the NW-SE head-on contraction in middle-earliest late Triassic. Subsidence occurred during early-middle Jurassic, which was broke by the late Jurassic-early Cretaceous NW-SE rifting. Late Cretaceous was marked by the regional uplift and erosion, which was followed by Paleogene subsidence and Neogene glaciation uplift and erosion.

Preface

This master thesis completes the two year master program in Petroleum Geology and Geophysics undertaken at the Department of Geosciences, University of Oslo. This master thesis has been supervised by Prof. Jan Inge Faleide and Prof. Roy Helge Gabrielsen.

Acknowledgements

I would like to express my special thanks to my supervisors for their guidance, encouragements and interesting discussions during period of writing this thesis. I would also like to thank to Dr. Michael Heeremans who has helped in preparing all of the data set needed to accomplish this thesis.

TGS-NOPEC is acknowledged for making seismic data available.

Last but not least, thanks to my family and friends for encouragement and care.

Agus Fitriyanto

Contents

1. Introduction

Geographically, the Barents Sea is a continental shelf (*fig. 1.1*), covering the area of approximately 1.2 million km^2 (Worsley, 2008), which is bounded by the Svalbard archipelago and Franz Josef Land to the north, Norwegian-Greenland Sea to the west, northern Norwegian coast and Kola Peninsula to the south, and Novaya Zemlya to the east (Faleide et al., 1984).

Barents Sea region has demonstrated potentials of hydrocarbon reserves with major discoveries found in Snøhvit gas field and Goliat oil field. Both fields are located within Hammerfest Basin of southwestern Barents Sea. The most recent promising oil and gas discovery was made in Skrugard prospect, which is located north of Snøhvit gas field or west of the Loppa High (www.npd.no). Complex structural and stratigraphic developments interpreted from regional seismic studies and well data, have brought to the about 20 years of exploration history in this area (Gabrielsen, 1984; Larssen et al., 2002).

Structural elements of Barents Sea show a complicated network of fault complexes, basins, platforms, and highs with various geometrical and genetic characteristics which are influenced and developed by several regional tectonic phases, including three major post-Caledonian events (Gabrielsen et al., 1990; Gabrielsen, 1984; Faleide et al., 1984; see chapter 2 for more details). Reactivation of long lived fault zones during mentioned tectonic phases and inhomogeneous tectonic patterns (Gabrielsen, 1984) may have contributed to the complexity of arrangement of the structural elements in this area. Based on mentioned background, this thesis work which focuses on structural analysis of Hoop Fault Complex as one of the old weakness zones in southwestern Barents Sea (*fig. 1.1*) is conducted.

The main objective of this thesis work is to study the structural geometry, style and evolution of Hoop Fault Complex in the southwestern Barents Sea. Result of this study can lead to increase of knowledge and understanding about geometry, style and relationship between regional tectonic events and evolution of the Hoop Fault Complex in southwestern Barents Sea.

Grids of regional 2D seismic lines and 3D seismic data, which are main data set used in this thesis work, will be tied and stratigraphicaly calibrated first to the well data before detail seismic interpretation is performed using Schlumberger's Petrel seismic interpretation. Detail

fault analysis on selected key profiles, construction of time-structure maps, fault maps and time-thickness map are also performed in order to achieve the objectives of the work.

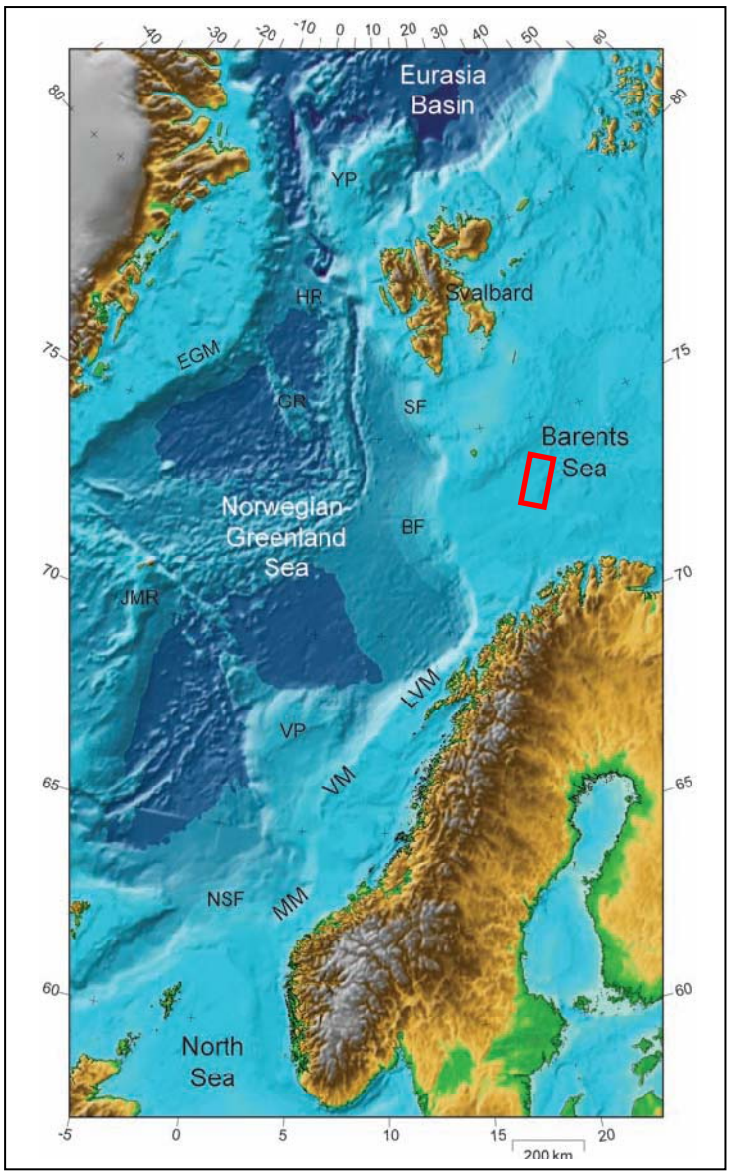

Figure 1.1: Regional setting and location of the study area (modified from Faleide et al., 2008).

2. Geological Framework

2.1 Regional Setting

Geologically, Barents Sea is a wide epicontinental sea covering northwestern corner of Eurasian continental shelf. Originally, this continental shelf was formed by two major continental collisions, followed by younger continental separations (Doré, 1995). Those collisions are Caledonian Orogeny in mid Paleozoic time, which represented by closure of Iapetus Ocean located in present North Atlantic, and late Paleozoic collision between Laurasian Continent and western Siberia in the eastern margin of present Barents Sea. Younger extensional tectonics recorded during late Paleozoic-Mesozoic time, reflect the breakup of continents formed by previous collisions. Cenozoic opening of Norwegian-Greenland Sea and Eurasia Basin completed the construction of Barents Sea and created young passive continental margin to west and north of Barents Sea (Doré, 1995; Faleide et al., 2008).

Stratigraphy of Barents Sea consists of thick, relatively complete succession of sedimentary strata ranging from late Paleozoic to Quaternary (Gudlaugsson et al., 1998) showing both lateral and vertical variations in thickness and facies. This succession is characterized by late Paleozoic mixed carbonates, evaporites and clastics, overlain by Mesozoic-Cenozoic clastic sedimentary rocks (Faleide et al., 2010).

2.1.1 Geological Province

Based on its structural elements, western Barents Sea can be divided into three regional geological provinces (*fig. 2.1*): (1) basinal province between Svalbard Platform and the Norwegian coast; (2) Svalbard Platform; and (3) the western continental margin (Faleide et al., 2010).

The basinal province between Svalbard platform and the Norwegian coast is defined mainly by the distribution of the sediment and characterized by number of sub-basins and highs. This province is bounded to the south by the line of basement outcrop along the coast. To the east, this basinal province continues with a bifurcation of the trend into the Pechora Basin and the Novaya Zemlya Basin. Further to the west, it is limited to the continental margin (Faleide et al., 1984).

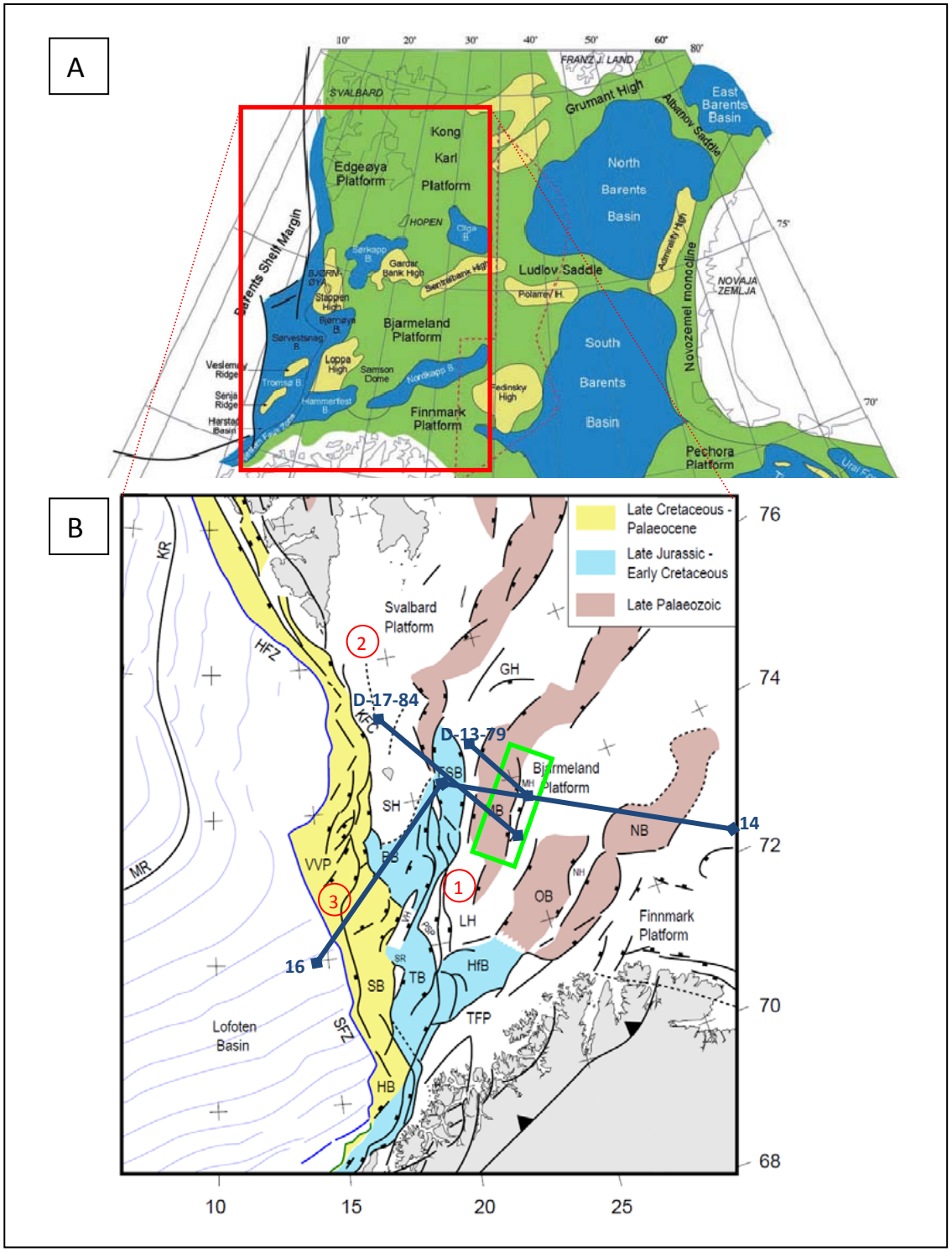

Figure 2.1: A. Major structural elements of Barents Sea. Red square is western Barents Sea; B. Structural elements of the western Barents Sea. Red numbers 1-3 shows the locations of three geological provinces in western Barents Sea. Blue lines illustrate profile lines in *fig. 2.2, 2.4 and 2.5*. Green square is the location of the study area of this thesis. SFZ: Senja Fracture Zone. TFFC: Troms-Finnmark Fault Complex. RLFC: Ringvassøy-Loppa Fault Complex.BFC: Bjørnøyrenna Fault Complex. LFC: Leirdjupet Fault Complex (modified from Worsley, 2008 and Faleide et al. 2008).

Western continental margin is developed close to and along De Geer Zone mega shear system which linked the rifting and spreading in the Norwegian-Greenland Sea to the Eurasian Basin

(Faleide et al., 2008). This margin can be divided into central rifted segments and 2 large shear segments in the southern and northern parts. Southern sheared margin segment is marked by the Senja Fracture Zone, whereas complex of sheared and rifted margin north of Bjørnøya mark the northern sheared margin. These two sheared margins are separated by Vestbakken Volcanic Province in the central rifted segment (Faleide et al., 2008).

The Svalbard Platform covers the area north of the regional basin province. The Stappen High and its northern continuation form the western boundary of the Svalbard Platform. The extension of this platform toward north and east is relatively difficult to be determined due to lack of available data (Faleide et al., 1984).

More specific to the southwestern portion of Barents Sea, which covers southern part of western continental margin and basinal regional geological provinces, can be divided into three more detailed geological provinces based on its tectonic style, crustal structure and sedimentary fills (Faleide et al., 1993a,b); (A) Cenozoic oceanic Lofoten Basin and Vestbakken Volcanic Province in the west, (B) Cretaceous-early Tertiary southwestern Barents Sea deep basins (Harstad, Tromsø, Bjørnøya and Sørvestsnaget basins) that are separated by intrabasinal highs (Veslemøy and Stappen highs, Senja Ridge), (C) eastern, between 20-25^0 E, Mesozoic basins and highs which have not experienced pronounced Cretaceous-Tertiary subsidence (Hammerfest Basin, Fingerdjupet Subbasin, Loppa High). Each province is separated by major fault zones. The Hoop Fault Complex is one of the fault complexes separating late Paleozoic basins to the relatively more stable Bjarmeland Platform to the east (see chapter 2.2 for more detail).

2.1.2 Structural Elements

Structurally, Barents Sea is dived into 2 major regions *(fig. 2.1)*, eastern and western regions, separated by north-south trending monoclinal structure (Worsley, 2008). Eastern Barents Sea shows development closely linked to that of Uralides, Timan-Pechora and Novaya Zemlya. The western Barents Sea, which will be explained more in this regional setting section, shows a much more complex tectonic development (Gabrielsen et al., 1990; Faleide et al., 1984).

The structural elements in western Barents Sea *(fig. 2.1 and 2.2)*, shows a mosaic of basins, platforms, structural highs and fault complexes that reflect interplay through time between major tectonic processes along the western and northwestern margins of the Eurasian plate (Worsley, 2008).

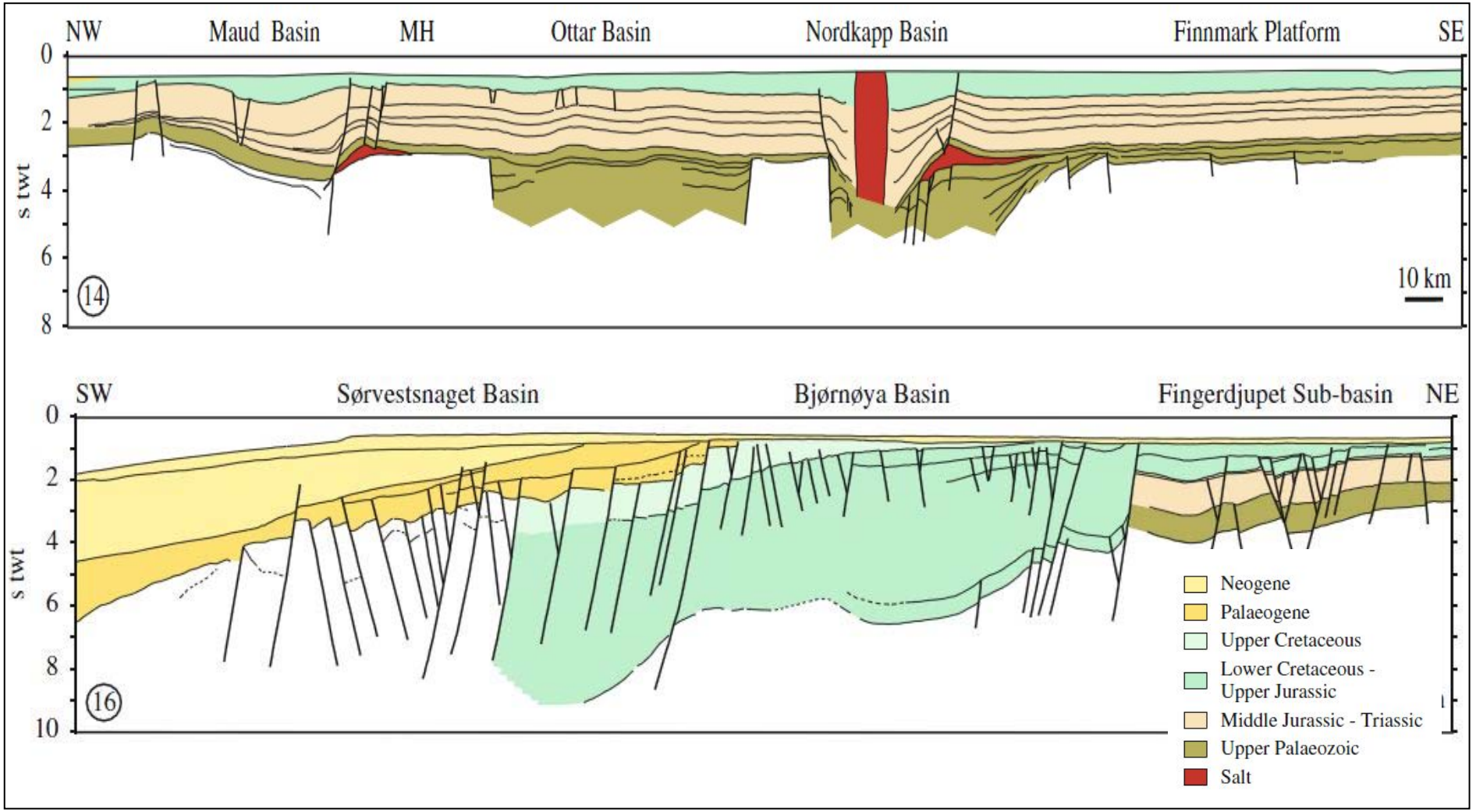

Figure 2.2: Regional profiles across western Barents Sea (modified from Faleide et al., 2010). See *fig. 2.1* for the location of the sections.

Main structural elements of western Barents Sea are dominated by ENE-WSW trends. In the south, ENE-WSW trends are defined by the major fault complexes bordering Hammerfest and Nordkapp basins. These trends are sub-parallel to another major zone in the north which is defined by the Veslemøy High and fault complexes separating Loppa High from Bjørnøya Basin. Some influences of N-S trends prevail in the west and northwest area, like Tromsø Basin, Knølegga Fault Complex and Hornsund Fault Complex (Gabrielsen et al., 1990). The arrangement of structural elements (*fig. 2.1*) shows that the age of basins were older toward the east. It definitely correlates to the tectonic evolution of this area (see chapter 2.1.3).

The main structural elements observed in the western Barents Sea region have been influenced by several post-Caledonian tectonic phases; late Devonian-early Carboniferous, middle Jurassic-early Cretaceous, and Cenozoic phases (Faleide et al., 1984). Glørstad-Clark et al. (2010) subdivided the evolution of the western Barents Sea into tectonic megasequences including the same three main tectonic phases as described above, with addition of late Permian rifting event as seen in *fig. 2.3*. Nonetheless, some major structures may still relate, through reactivation processes, to structures formed during Caledonian Orogeny (Faleide et al, 1984, Gabrielsen et al., 1990). It is mainly due to within certain limits, an old fault system will reactivate instead of initiating of new ones, even when the new stress field is different from the old one (Gabrielsen, 1984). The Hoop Fault Complex, as one of ENE-WSW old weakness zones, has also experienced this reactivation (Gabrielsen et al., 1990).

2.1.3 Stratigraphy and Structural Evolution

Evolution of southwestern Barents Sea has been controlled by several tectonic events that influenced the sedimentation. These events include two phases of Caledonian compressional deformation, and post-Caledonian tectonic phases (Gabrielsen et al., 1990). The stratigraphy and structural evolution of western Barents Sea can be summarized as seen in *fig. 2.3*.

Western Barents Sea is underlain by metamorphic basement formed by consolidation of plates during Caledonian Orogeny, which culminated in the closure of Iapetus Ocean and continental collision of Laurentia and Baltica in the Silurian-Devonian times (Gudlaugsson et al., 1998; Ritzmann and Faleide, 2007; Dengo and Røssland, 1992). The influence of this Caledonian still can be observed on the pattern of younger tectonic events as seen in the N-S structural grain of western Barents margin and Svalbard, and the NE-SW grain of the southwestern Barents Sea (Doré, 1995; Gabrielsen, 1984; Ritzmann and Faleide, 2007).

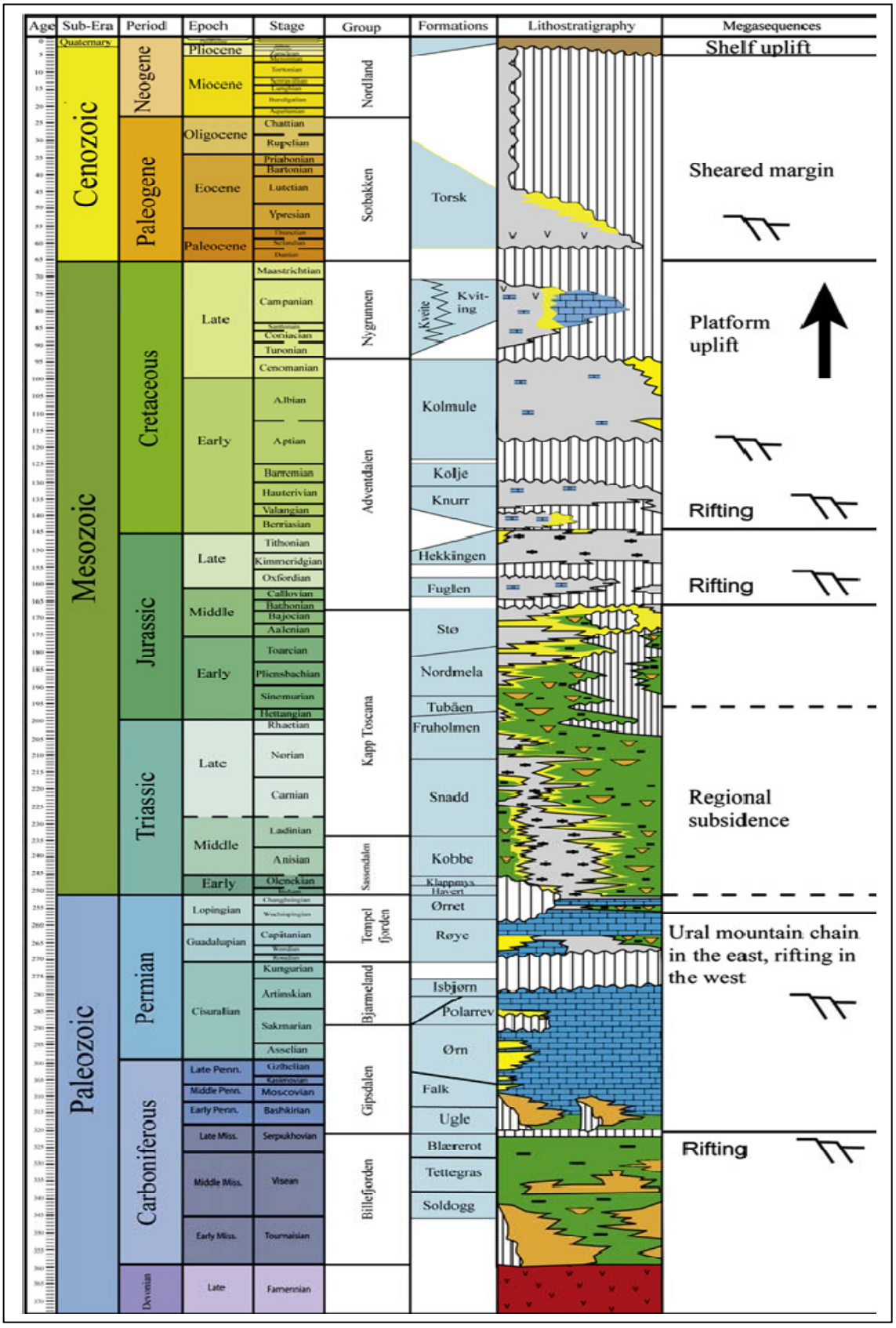

Figure 2.3: Stratigraphy of western Barents Sea (modified from Glørstad-Clark et al., 2010).

Paleozoic evolution of western Barents Sea is marked by several tectonic events; late Devonian extensional and compressional events (also known as Svalbardian), late Carboniferous and late Permian rifting events followed by development toward regional subsidence and formation of sag basin in Triassic (Gudlaugsson et al., 1998).

In late Devonian, Caledonian compressional regime changed to a left-lateral shear regime with large-scale northeasterly strike-slip movements creating transpression and transtension of Svalbardian events that controlled post-orogenic sedimentation in northwestern Barents Sea, so far only known on Svalbard. Late Devonian - Early Carboniferous continental clastic sediments with coals were deposited syn-tectonically in extensional basin formed by mentioned transtension events (Gabrielsen et al., 1990; Faleide et al., 2010; Faleide et al., 1984).

In late Carboniferous, major rifting event occurred related to the direct continuation of North-East Atlantic rift and subordinate tectonic link to Arctic rift. This rifting created northeasterly to northerly oriented fan-shaped array of interconnected, segmented rift basins and intrabasinal highs (Gudlaugsson et al., 1998). Maud Basin, which is correlated to the Hoop Fault Complex, has been interpreted as a basin which formed at this time (Faleide et al., 2010). At eastern area, fault activity has ceased down toward end of Carboniferous and allowing structural relief to be infilled and covered by thick, widespread shelf succession of carbonates with a variety of facies, evaporites and some clastics during latest Carboniferous-Permian times (Gudlaugsson et al., 1998; Faleide et al., 1984; Faleide et al., 2010). During late Permian-early Triassic, renewed rifting, faulting, and uplifting affected the N-S trending structures in western part of Carboniferous rift system. (Gudlaugsson et al., 1998; Faleide et al., 2010).

Mesozoic evolution in western Barents Sea is marked by regional subsidence and formation of huge interior sag basin in Triassic-middle Jurassic following late Permian rifting event, and late Jurassic-early Cretaceous rifting (Glørstad-Clark et al., 2010).

Regional subsidence during Triassic-middle Jurassic, coupled with high sedimentation rate, led to the development of thick shelf sequences of marine shales, siltstones and sandstones with an increased content of coarse clastic material toward younger intervals, especially in early Jurassic-lower middle Jurassic time when throughout Barents Sea was dominated by

sandstones. Intervals of non-deposition and local erosion related to the fluctuation of sea level also occurred intermittently (Faleide et al., 1984; Faleide et al., 2010). Differential loading, which related to this thick sequence, might have triggered salt diapirism in eastern Barents Sea and later also in southwestern Barents Sea (Faleide et al., 2010).

Block faultings started again in western Barents Sea during late Jurassic-early Cretaceous. It related to the major rifting phases and basin formation which closely linked to the tectonic phases in North Atlantic-Arctic region. These rifting phases were characterized by regional crustal extension accompanied by strike-slip adjustments along old late Paleozoic lineaments (Faleide et al., 1993a; Gabrielsen et al., 1990). Rifting events led to the deposition of shale, claystone with interbeds of silt, limestone and dolomite in the distal marine environment of faulted blocks with periodic restricted bottom circulation (Faleide et al., 2010). In southwestern Barents Sea, unconformity marked the onset of these rifting phases in upper middle Jurassic which later gave rise to very deep basins. Some unconformities also formed during late Jurassic time reflected interplay between continued faulting and sea level changes (Faleide et al., 2010; Breivik et al., 1998).

In eastern platform region, which is the main study area, mentioned late Jurassic-early Cretaceous rifting occurred without large scale post-rift subsidence (Faleide, et al., 1993b). In fact, in some basins such as Hammerfest, base Cretaceous tectonism was not a major event.

Following the late Jurassic-early Cretaceous rifting, western Barents Sea in early-middle Cretaceous time was subsided progressively. Magmatism occurred in the northern Barents Sea without any sign of faulting in early Cretaceous. It caused regional uplift and erosion in Barents Sea except in southwestern Barents Sea which continued to subside in response to the extensional faulting in the Sørvestsnaget basin and thermal subsidence in Tromsø. This regional uplifted resulted large amount of sediments transported and deposited in southwestern Barents Sea until late Cretaceous time (Feleide et al., 2010; Faleide et al., 1984).

During Cenozoic time, tectonic evolution was mainly related to opening of Norwegian-Greenland Sea and formation of predominantly sheared western Barents Sea continental margin. These tectonic events were preceded by a phase of rapid late Paleocene rifting, and completed in Eocene time. It culminated with a 3-6 m.y. period of massive magmatic activity (Faleide et al., 2008; Talwani and Eldholm, 1977). Furthermore, mentioned magmatic

activity evoked the regional uplift in late Paleogene-early Neogene, prior to the glaciations in Miocene-Pliocene-Pleistocene (Dimakis et al., 1998; Faleide et al., 1996; Nyland et al., 1992). Post-Miocene repeated glaciations in late Pliocene-Pleistocene created major uplift related to erosions and glacial isostasy during that time. High sedimentation rates toward shelf margin were observed creating thick deposits of glacial sediments as submarine fans and wedges (Faleide et al., 1996; Nyland et al., 1992; Kjemperud and Fjeldskaar, 1992). In general this Tertiary succession is missing in the eastern platform region, which is the main study area, due to mentioned uplifting and erosion.

2.2 Bjarmeland Platfrom

Bjarmeland Platform represents relatively stable area since late Paleozoic time which includes the Norsel and Mercurius Highs, the Svalis, Samson and Norvarg Domes, the Swaen graben, the Maud Basin and parts of the Hoop Fault Complex (Gabrielsen et al., 1990). This platform lies between Hammerfest and Nordkapp Basins to the south and southeast, Sentralbanken and Gardarbanken Highs to the north, Loppa High and Fingerdjupet sub-basin to the west (Gabrielsen et al., 1990).

Bjarmeland Platform was started to develop as stable platform in late Carboniferous time. A pronounced structural high parallel to relatively north-south trending fault zone in the west of this platform existed throughout late Permian and early Triassic. Later during late Triassic, this high was transformed into deep basin. Late Mesozoic and Tertiary tectonics gave rise Loppa High and Fingerdjupet sub-basin which bound the platform to the west (Gabrielsen et al., 1990).

2.3 Loppa High

Loppa High is positive structural element which associated with positive gravity and magnetic anomalies caused by a relatively shallow, steeply easterly dipping flank, metamorphic basement block of Caledonian age underlying its western part (Gudlaugsson et al., 1998; Gabrielsen et al., 1990). This high consists of an eastern platform, crestal western and northwestern margins. It is bounded on the north by Svalis Dome and Maud Basin.

The development of Loppa High was started with Carboniferous rift topography followed by renewed tectonic uplift and tilting of the flank during late Permian and early Triassic. After being depocenter during late Triassic-Jurassic, Loppa High was uplifted again during early

Cretaceous time (Faleide et al., 1993a,b; Dengo and Røssland, 1992; Glørstad-Clark et al., 2010).

2.4 Hoop Fault Complex

Hoop Fault Complex (*fig. 2.4 and 2.5*) is an old zone of weakness which cuts across the Loppa High and Bjarmeland Platform between 72^0 50' N, $21^0$50' E and 74^0 N, 26^0 E (Gabrielsen et al., 1990). (*fig. 2.1 and 2.2*). It also separates Maud Basin and Mercurius High. This fault complex is one of several NE-SW trending structures in the southwestern Barents Sea.

The Hoop Fault Complex is characterized by normal block faulting and can be divided into three portions (Gabrielsen et al., 1990). Northern part includes swarm of normal faults cutting the Bjarmeland Platform. The central part of Hoop Fault Complex relate to the development of Maud Basin, Svalis Dome and Mercurius High, and may control pattern of late Carboniferous to Permian sedimentation in this area. The southern part of Hoop Fault Complex comprises a narrow graben which is part of minor grabens arranged in en échelon pattern in northern Loppa High (Gabrielsen et al., 1990).

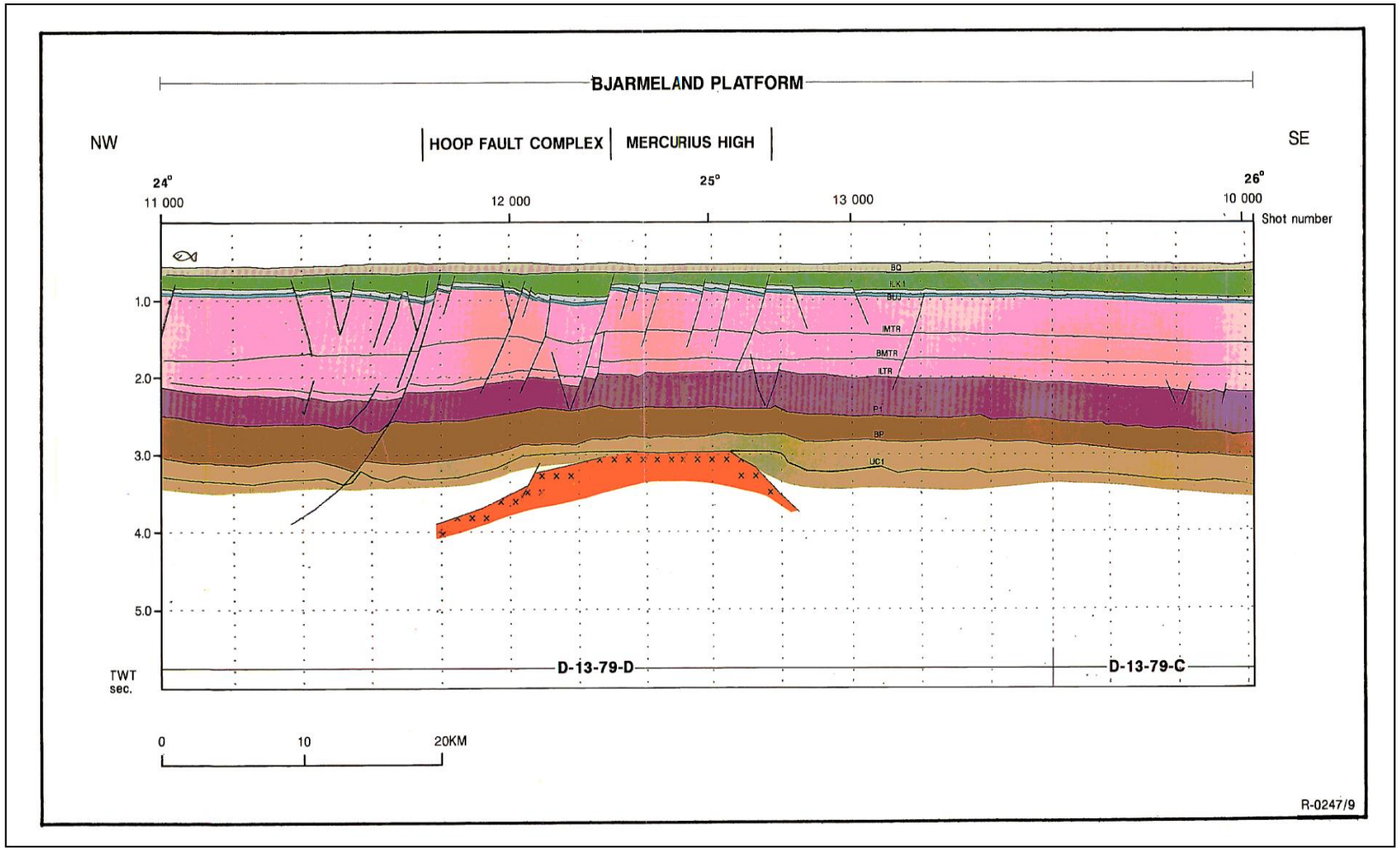

Figure 2.4: Profile line across the Hoop Fault Complex, D-13-79 (modified from Gabrielsen et al., 1990). See the location of line in *fig. 2.1.* Color codes: Quaternary (grey), Cretaceous (Green), Jurassic (light-blue, dark-blue), Triassic (pink), Upper Permian (brown), Lower Permian (olive), Basement (red).

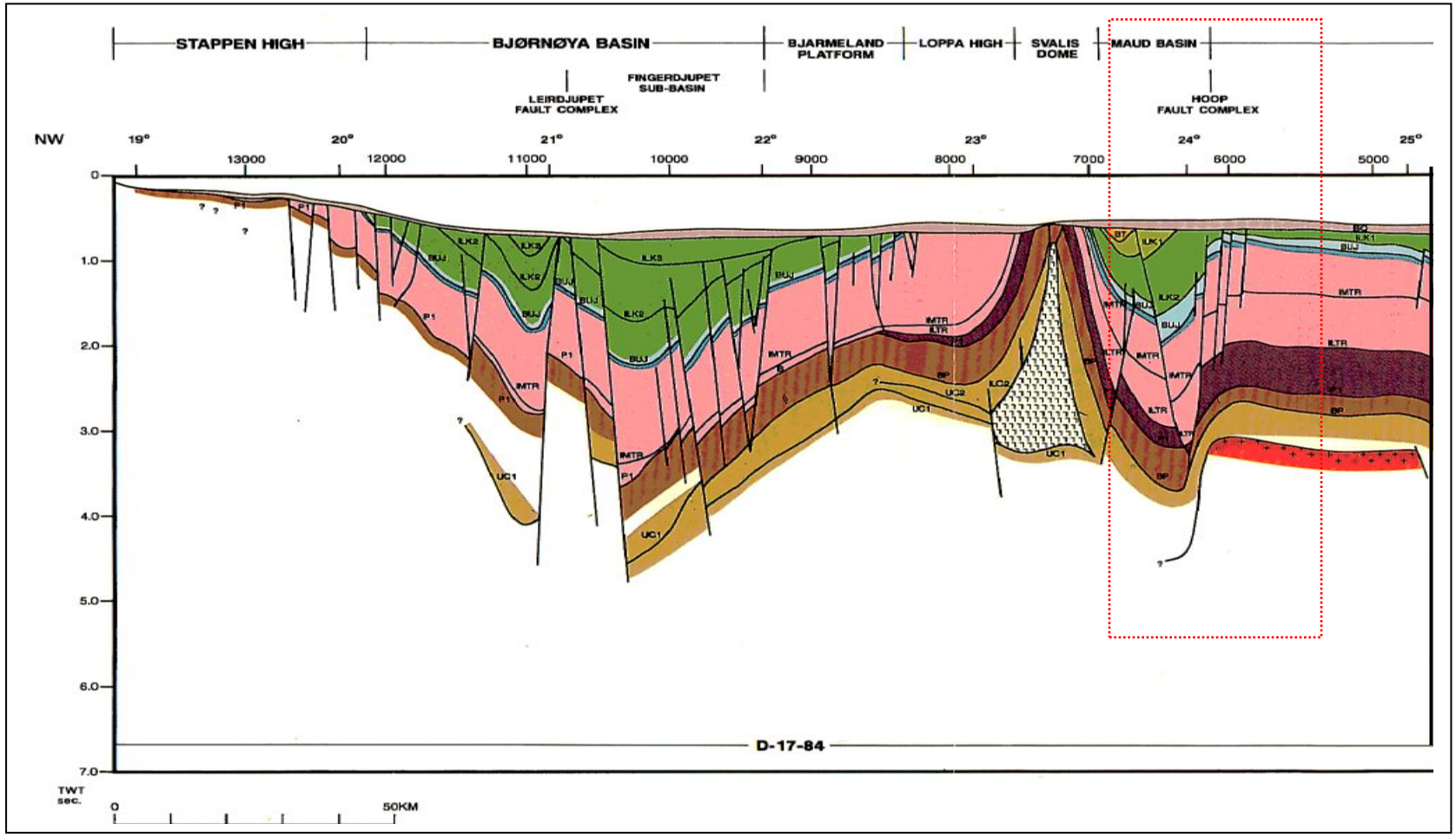

Figure 2.5: Profile line across the Hoop Fault Complex, D-17-84 (modified from Gabrielsen et al., 1990). See the location of line in *fig. 2.1*. Color codes: Quaternary (grey), Cretaceous (Green), Jurassic (light-blue, dark-blue), Triassic (pink), Upper Permian (brown, dark brown), Lower Permian (olive), Basement (red). Red square is the study area.

3. Seismic Interpretation

Generalized interpretation workflow of this study, including data and methods, can be summarized as seen in *fig. 3.1*.

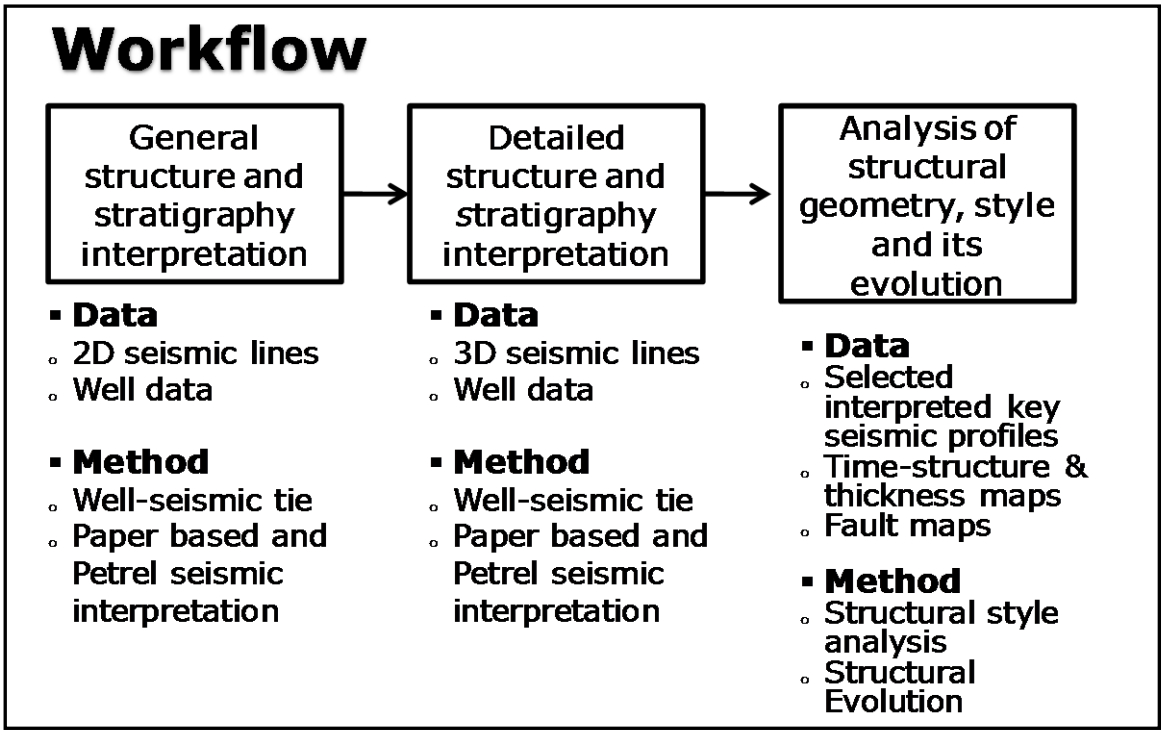

Figure 3.1: Generalized workflow of the study.

3.1 Data

3D seismic data and a grid of 2D seismic lines from five different surveys are used in this study as data set (*fig. 3.2*), the lithostratigraphy of which is calibrated against one exploratory well data (7324/10-1).

A grid of 2D seismic lines with line spacing of about 8 x 9 km, located in central part of study area, was utilized in the interpretation of detail structural pattern of the Hoop Fault Complex. Additional 2D lines are located in the periphery of the study area which is not covered by 3D data was also utilized to link the observed structures to the more regional structural features.

3D seismic data of HFC09 Survey, which was acquired in 2009 and covered about 4300 square kilometer area (www.TGSNOPEC.com), are provided by TGS-NOPEC. The high

resolution 3D seismic data, which covers all main features of the Hoop Fault Complex in the study area, has been the key data set for the study. The extent of effective 3D data cube is 4300-11300 for crossline and 1900-3200 for inline (*fig. 3.2*).

Exploration well 7324/10-1 is the only well in the study area. This well data is used to calibrate the interpretation of seismic data. The general information of well 7324/10-1 can be seen in *table 3.1*.

Wellbore name	7324/10-1
Geodetic datum	ED50
NS degrees	73° 9' 49.45 " N
EW degrees	24° 18' 47.62 " E
Drilled in production license	162
Drilling operator	Den norske stats oljeselskap a.s
Completion date	19-08-1989
Type	Exploration
Purpose	Wildcat
Status	Plug & abandoned
Content	Shows
Total depth (MD) [m RKB]	2919.0
Formation at TD	Havert Formation (early Triassic)
Maximum inclination [°]	2.8

Table 3.1: General information of well 7324/10-1 (modified from www.npd.no).

Well 7324/10-1 is located with an offset of 2 km toward west to the closest seismic line (*fig. 3.2*). All the formation tops in this well can be identified with acceptable confidence to the reflections of those in the seismic line (*fig. 3.3* and *3.4*). Known well formation tops, namely base Cretaceous (top of Fuglen Formation.), middle Triassic (near top of Kobbe Formation.) and early Triassic (top of Havert Formation.) are of particular importance for seismic interpretation (*fig. 3.4*). Two more reflections are picked below the drilled depth, which assumed as late Permian and late Carboniferous reflections.

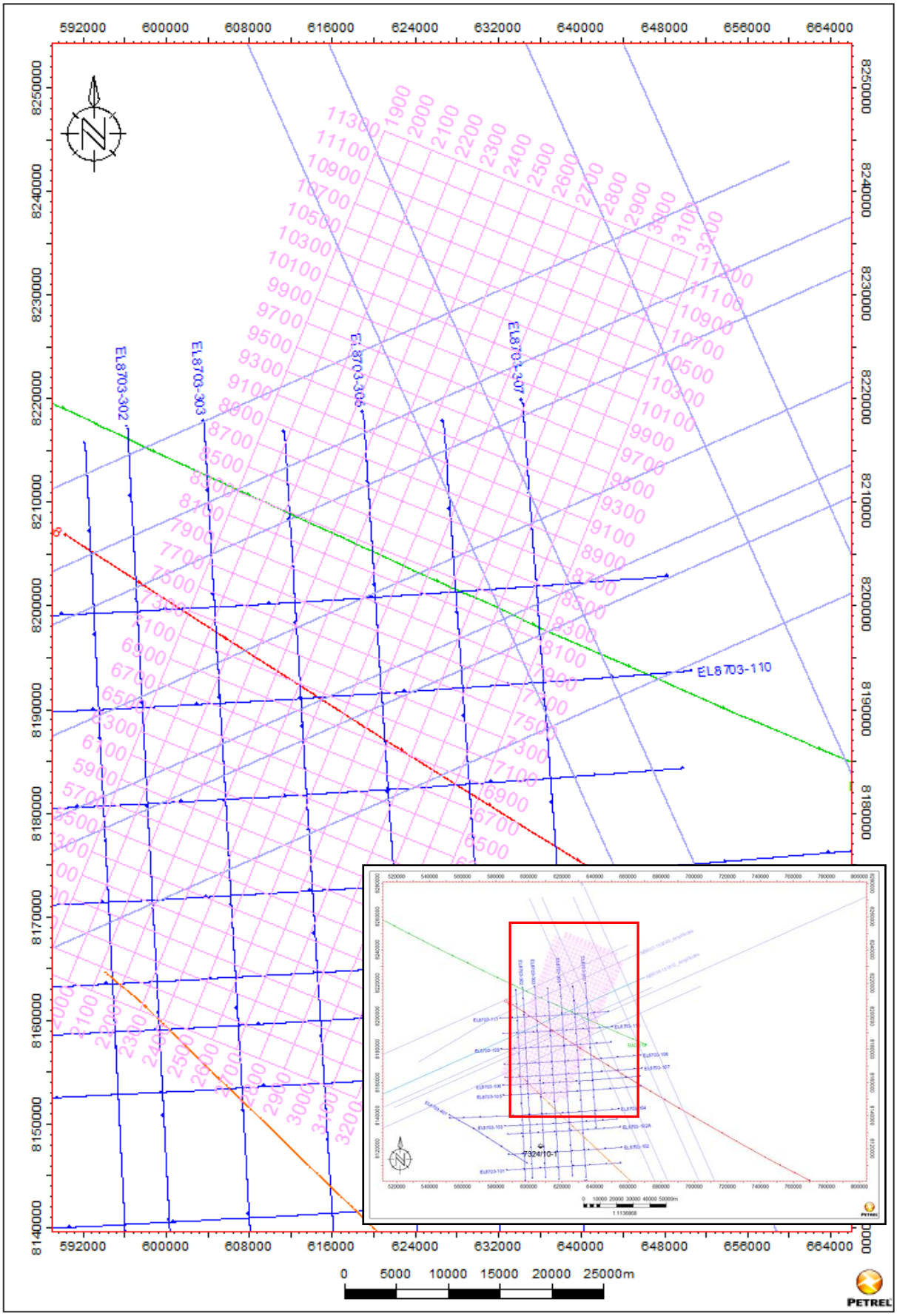

Figure 3.2: Base map of study area, showing location of the data used in the study.

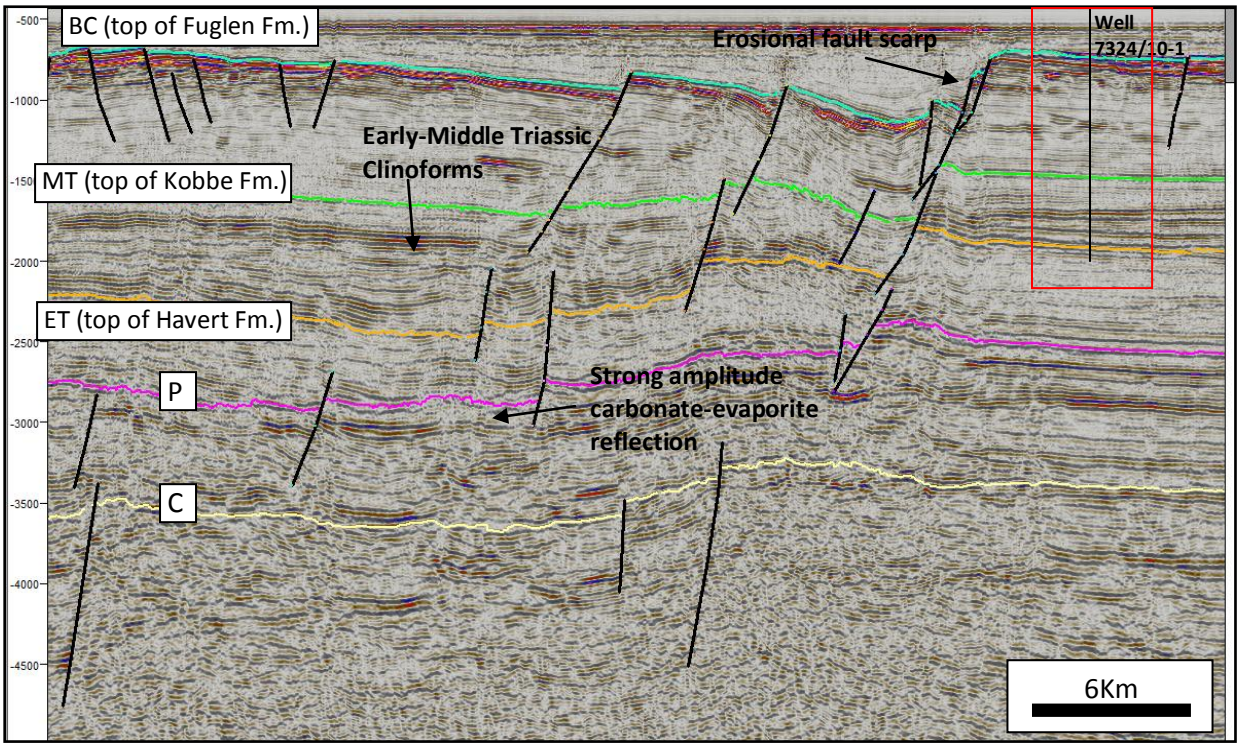

Figure 3.3: Well 7324/10-1 shown on 2D seismic line with interpreted reflections. BC: base Cretaceous, MT: middle Triassic, ET: early Triassic, P: late Permian, C: late Carboniferous. Red rectangle is zoomed area in *fig. 3.4.*

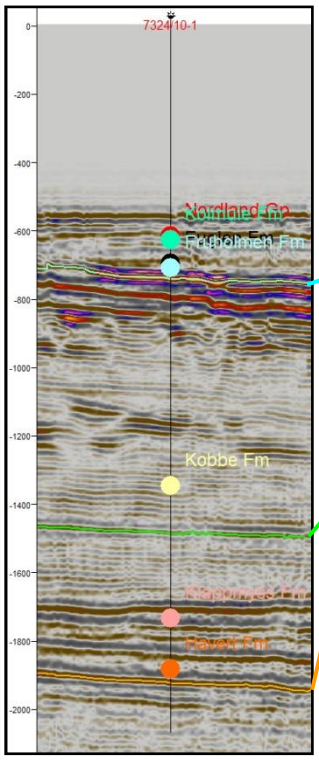

Depth [mMDKB]	Formation Top	Age	
		Sub-Era	Periode
431	NORDLAND GP	Cenozoic	Neogene
480	ADVENTDALEN GP	Mesozoic	Cretaceous
480	KOLMULE FM		
553	KNURR FM		
561	FUGLEN FM		Jurassic
569	KAPP TOSCANA GP		
569	STØ FM		
577	FRUHOLMEN FM		Triassic
606	SNADD FM		
1607	SASSENDALEN GP		
1607	KOBBE FM		
2272	KLAPPMYSS FM		
2512	HAVERT FM		

Figure 3.4: Formation tops of well 7324/10-1 and their ages (modified from www.npd.no and Glørstad-Clark et al., 2010).

Base Cretaceous reflection is represented by uppermost distinctive strong amplitude, high frequency, positive reflection, close to the top of Fuglen Formation or at about 600-1700 ms (TWT). This reflection represents regional unconformity which can be followed easily across the study. It is characterized by erosional fault scarp, especially along the master faults (*fig. 3.3*). Most of the faults are terminated at or below this strong amplitude reflection. Above base Cretaceous unconformity, younger reflections onlap onto it particularly in the area close to the master fault. Farther towards the platform area, where less topographic contrast is expected, this reflection is seen to be conformable with other reflections.

The middle Triassic reflection is represented by strong-moderate amplitude, high-medium frequency, positive reflection near the top of Kobbe Formation at about 1200-2400 ms (TWT). It is characterized as the uppermost reflection of clinoform-progradational seismic facies of early-middle Triassic age (*fig. 3.3*) where younger reflection onlap onto. This reflection can be followed well within main study area, even though the complex sigmoid seismic facies of Triassic succession may bring difficulties in interpreting the continuation of this reflection, especially across the master fault.

The early Triassic reflection is represented by strong amplitude, medium frequency, positive reflection at about 1700-2800 ms (TWT). It serves as the base of complex sigmoid seismic facies where early-middle Triassic clinoform-progradational reflections onlap onto (*fig. 3.3*), as clearly seen in the western part of the study area or distal part of clinoform.

The assumed late Permian reflection (*fig. 3.3.*) is a reflection below the penetrated depth in well 7324/10-1 at 2400-4000 ms (TWT). This reflector is characterized by a strong-moderate amplitude reflection interpreted as boundary between upper Permian-Triassic shale and underneath upper Carboniferous-lower Permian carbonate-evaporite succession. The carbonate-evaporite succession itself is characterized by distinctive strong amplitude of fair to poor lateral continuation with local patchily distributed, positive reflections (Gérard and Buhrig, 1990; Glørstad-Clark et al., 2011). Most of master faults are terminated within this carbonate-evaporite succession.

The assumed late Carboniferous reflection is represented by moderate amplitude, moderate-low frequency, positive reflector which observed at the base of interpreted strong amplitude carbonate-evaporite layers. This reflection is also observed below drill depth in well 7324/10-1 at about 2600-4200 ms (TWT). The poor quality in greater depth and presence of possible pegleg multiples in 2D seismic data (*fig. 3.3* and *3.5*) have increased the uncertainties of this

reflection interpretation, especially at great depth and edge of study area. In 3D lines, this reflection is observed as the lowermost moderate amplitude, positive reflection which still can be observed (*fig. 3.5*).

3.2 Seismic Interpretation Procedures

In order to obtain general pictures of structural elements and regional geology in study area, this thesis work was started by interpreting and analyzing hard copy version of regional 2D seismic data.

The next step was structural and stratigraphical interpretation of seismic lines using PETREL software. Due to limitation of this software, manual interpretations of selected seismic lines were performed to represent the fault geometry and its detail. The 2D seismic interpretation is presented first, to display the regional picture before interpretation moves to the much denser and focus 3D seismic data. All main interpreted seismic reflections were tied in and calibrated to the well data. The objectives of this step are to map out main seismic reflections and geometry of fault complex.

In general, 2D seismic interpretations need to be correlated to the interpretation of arbitrary 3D seismic data. It is performed to compensate for occasional poor resolution in the 2D seismic data, especially at great depth. A comparison of the data quality and interpretation of 2D and its 3D seismic data is displayed in *fig. 3.5*.

In 3D seismic interpretation, crosslines which are oriented perpendicular to trend of the master faults were interpreted within much denser spacing, such as every 50-100 crosslines, compared to that of inline which only interpreted for every 200 lines. The interpretation of denser spacing lines, are also performed in the area with more complicated structures, such as area along the master faults.

Loop interpretation method, which is performed by combining inline and crossline or with arbitrary line in one screen display, is used for 3D data interpretation. This method is very useful to minimize shifting between tracked horizons on different seismic sections.

Structural maps, which consisted of time-structure and fault maps, and time-thickness maps were constructed mainly to identify lateral geometry of structural element and possible depositional patterns respectively. Time-structure and time-thickness maps were built using PETREL software, whereas fault maps were built manually to represent detail lateral pattern

of the faults, including minor faults with small throw which were not clearly observed in time-structure and time-thickness maps.

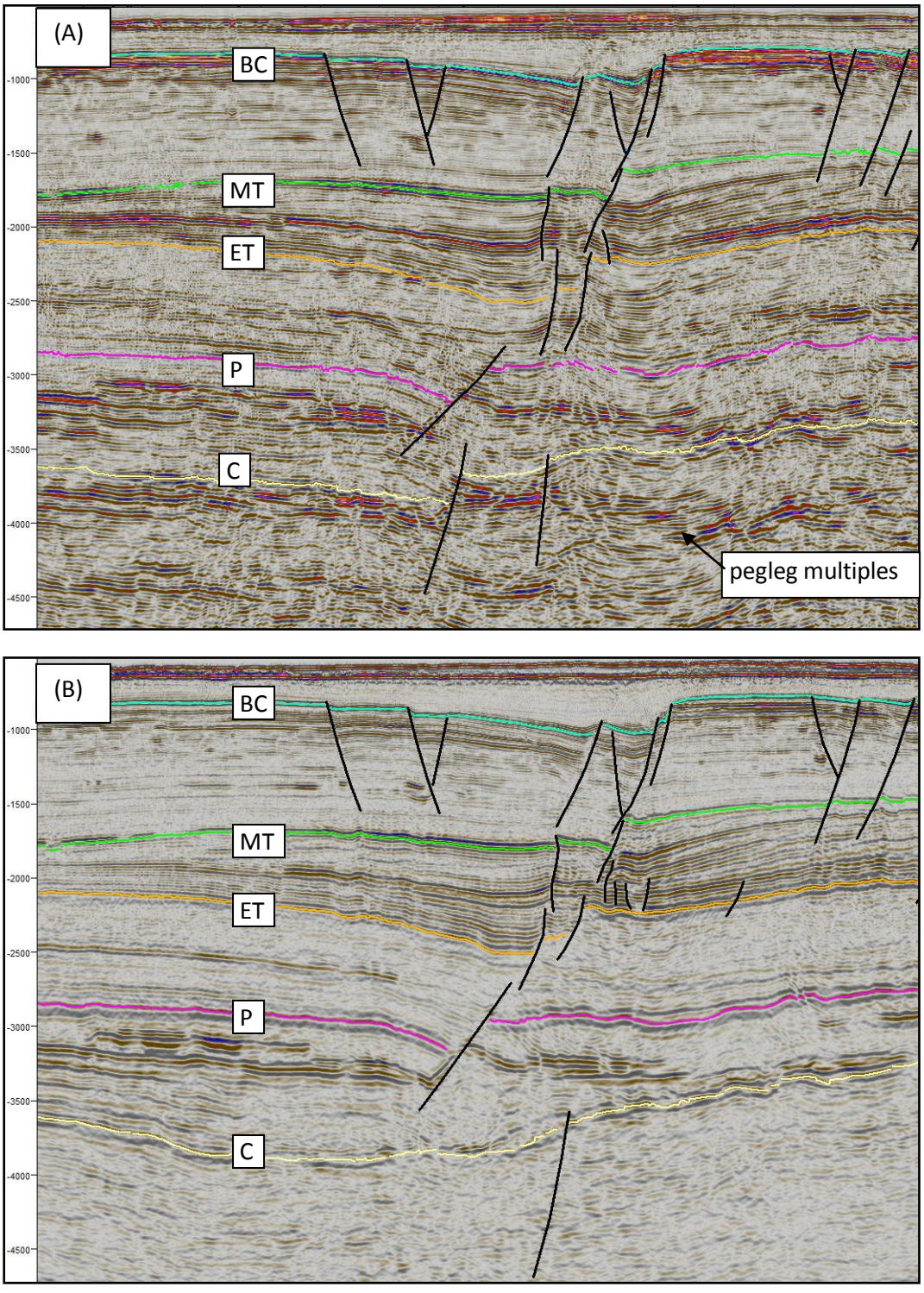

Figure 3.5: Comparison of interpreted 2D seismic line (A) and its arbitrary 3D seismic line (B). BC: base Cretaceous, MT: middle Triassic, ET: early Triassic, P: late Permian, C: late Carboniferous.

The final step was selections of key lines which represent variations and details of different segments of the master faults. These key lines are used to analyze the geometry, pattern and style of structural elements, timing of faulting and interplay between faulting with the erosion and sedimentation.

3.3 Geometry and Structuring of the Hoop Fault Complex

Referring to Gabrielsen et al. (1990), the Hoop Fault Complex is the NE-SW trending normal faults which transects the Loppa High and Bjarmeland Platform. The northern portion of fault complex comprises a swarm of normal faults cutting the Bjarmeland Platform. The central portion is related to the development of the Svalis Dome and Maud Basin, whereas southern part is a narrow graben on the Loppa High.

The local structural elements of the study area (*fig. 3.6)* only cover the northern and central portions of overall Hoop Fault Complex mentioned above. It is characterized by set of NE-SW trending normal faults at the southern part which turn to N-S trend at the north. The southern termination of fault complex is placed at the area close to northeastern flank of the deep Maud Basin which is part of rim syncline around the Svalis Dome in the southwest. The deep Maud Basin itself, which is more related to the development of the Loppa High and Svalis Dome, is excluded from this detail study.

The NE-SW and N-S trending normal faults of the Hoop Fault Complex, as seen in base Cretaceous time-structure map (*fig. 3.6* and *3.7*), comprises four master faults and a swarm of minor normal faults in both hanging and footwalls which form elongated half graben in the south and full graben topography along the strike of master faults toward north. The transition between the two structural trends is sharp and characterized by narrow area with overstepping of master faults (*fig 3.6*, *3.7, 3.10*). A few minor normal faults also occur at the platform area at southeastern side of study area (*fig. 3.7*). The dip-slip component of master faults, as measured in seismic sections, varies along the strike between 100-300 ms (TWT) and tends to increase toward central part of the study area before it diminishes toward north where the master faults terminate.

Based on the pattern of structural elements, the Hoop Fault Complex can be divided into three major lateral segments. Segment 1 in the south, comprises NE-SW trending normal fault (master fault F1). It throws to NW and defines SE tilted half graben topography at

downthrown side. The dip-slip of master fault F1 increases toward north. A swarm of minor normal faults can also be observed, especially at downthrown side.

Segment 2 in the central part, consists of a set of NE-SW trending normal faults (master fault F1 and F2) which together form full graben topography. Master fault F1 is throwing toward northwest, whereas master fault F2 is throwing toward southeast. The magnitude of dip-slip of master fault F1 is generally higher than master fault F2 which creating slightly tilted full graben toward southeast (*fig 3.6* and *3.15*). The size of this full graben is slightly smaller compared to the half-graben in segment 1.

Segment 3 in the north, consist of set of major N-S trending normal faults (master fault F3 and F4) which are together forming a symmetric full graben topography. Master fault F3 is throwing toward west, whereas master fault F4 is throwing toward east. In general, magnitude of dip-slip in both master faults F3 and F4 are relatively similar. Compared to segment 2, magnitude of dip-slip of master faults in segment 3 is smaller. It creates a shallower N-S trending full graben but more symmetric compared to the NE-SW trending full graben in segment 2. Toward the north end of the study area, master fault F3 is terminated. It dismisses the symmetric graben in segment 3 and changes to be westward tilted half graben topography. A swarm of minor normal faults are observed in the downthrown side of master fault F4. Generally, the arrangement of structural element in this north end part of segment 3 represents the geometry of the Hoop Fault Complex before it terminates toward the Bjarmeland Platform.

Similar structural trends and configurations are also recognized at deeper interval (see section 3.4.3). Even though the trends are similar, slightly different arrangement of structural element is observed in late Carboniferous interval (*fig. 3.19*). Selected key lines, both in 2D and 3D, are presented in next section to represent fault geometry and its style in every segment.

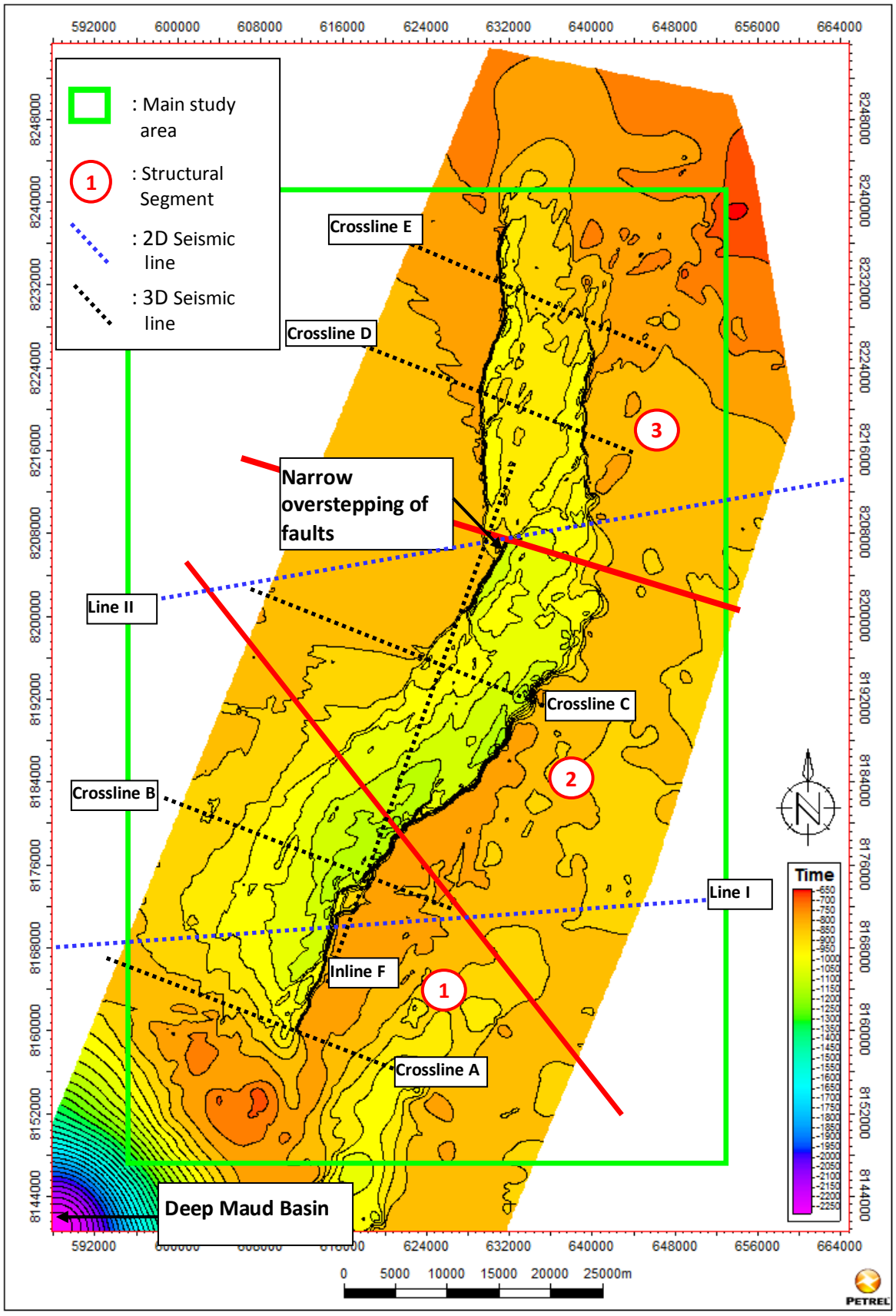

Figure 3.6: Time-structure map and structural segments of main study area. Contouring (TWT) at base Cretaceous. Position of seismic lines used is indicated

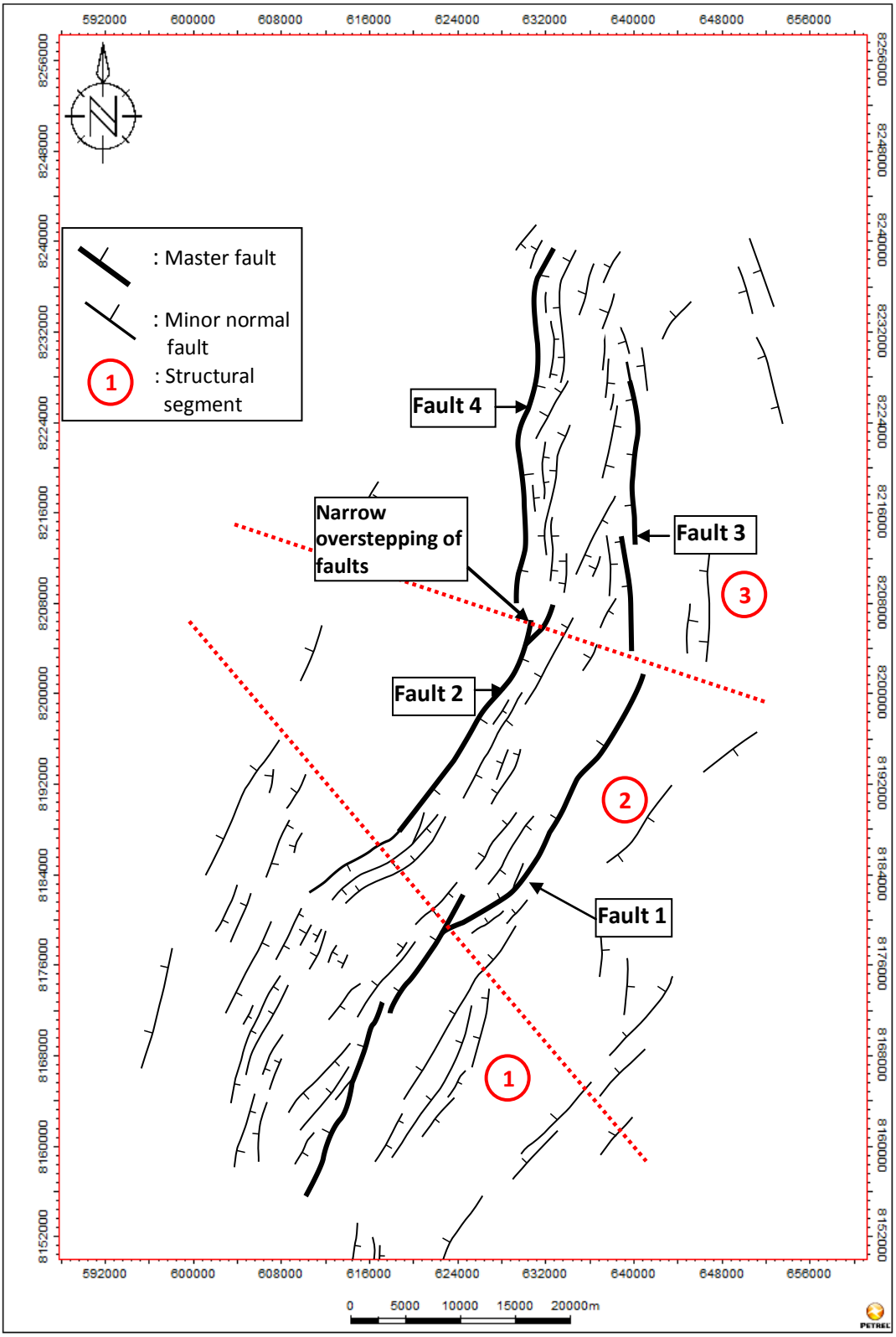

Figure 3.7: Fault map of base Cretaceous.

3.3. 1 2D Seismic Interpretation

Two 2D lines were selected for illustrating the main structural and stratigraphical unit in the study area, namely Line I and II (*fig. 3.6*). Line I (*fig. 3.8* and *3.9*) particularly illustrates the configuration of structural segment 1 where NE-SW trending faults are the main controlling structural feature, whereas Line II (*fig. 3.10* and *3.11*) illustrates structural segment 3 where N-S trending faults is the main controlling structures.

Line I

This line (*fig. 3.8*) is located at the southern part of study area within structural segment 1 (*fig. 3.6*). Generally it displays one steeply dipping (55-65^0) master normal fault (F1), located at the central part of section, controlling the main structural feature in this line. It strikes to the NE-SW (*fig. 3.6*) and separates a flat platform in the footwall from the eastward tilted half graben in the hanging wall. A set of normal faults (F6-a,b,c,e) is observed in platform area forming minor rotated fault blocks at base Cretaceous reflection. A set of normal faults (F5-a,c,g) and its antithetic faults are also observed within half graben defining minor horst-graben topography inside the half graben. These normal faults only cut upper Triassic-upper Jurassic succession.

Master fault F1 initiates at late Permian-early Triassic interval, or not basement involved, as a planar normal fault and branches upward into series of synthetic normal faults in early-middle Triassic and a normal fault with its antithetic accommodation structures in middle Triassic-base Cretaceous interval. These different fault geometries suggest that post-early Permian interval may include three separated fault segments; namely middle Triassic-base Cretaceous (fault F1-a), early-middle Triassic (fault F1-b) and late Permian-early Triassic (fault F1-c) intervals. Beneath of master fault F1 within late Carboniferous succession, there is one steeply dipping (70^0) deep planar normal fault FD1-1 which together with FD1-2 forms half graben at the downthrown side. The quality of seismic data does not allow interpreting whether faults FD1-1,2 are basement involved or not. The disconnection of fault FD1-1 to F1 suggests that there is a detachment within upper Carboniferous-lower Permian succession defining separate tectonic intervals below and above it. The presence of carbonate and evaporite layer within upper Carboniferous-lower Permian strata (Faleide et al., 2010) can be one candidate for mentioned detachment.

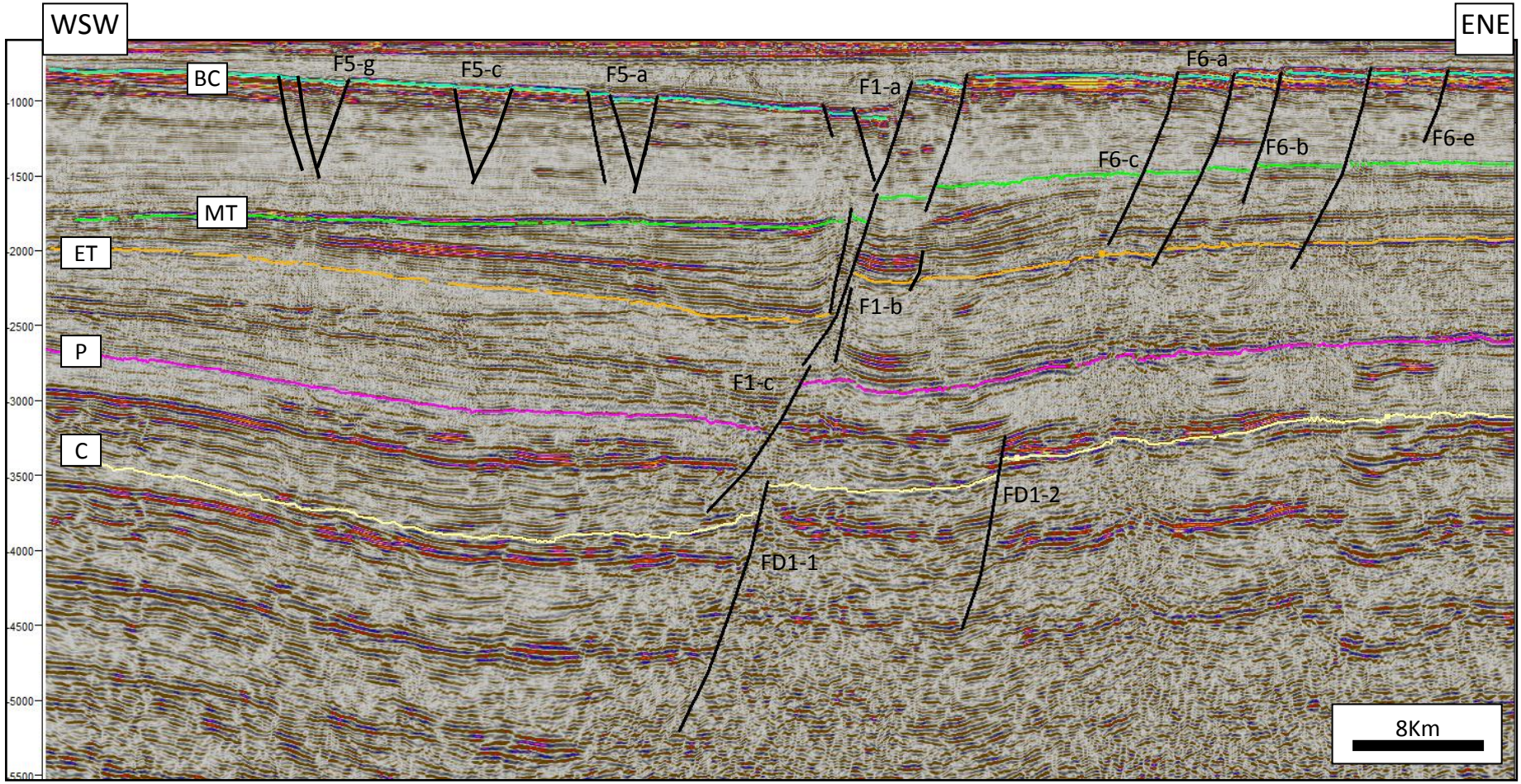

Figure 3.8: 2D seismic line I across segment 1. See *fig. 3.6* for location of the line. BC: base Cretaceous, MT: middle Triassic, ET: early Triassic, P: late Permian, C: late Carboniferous.

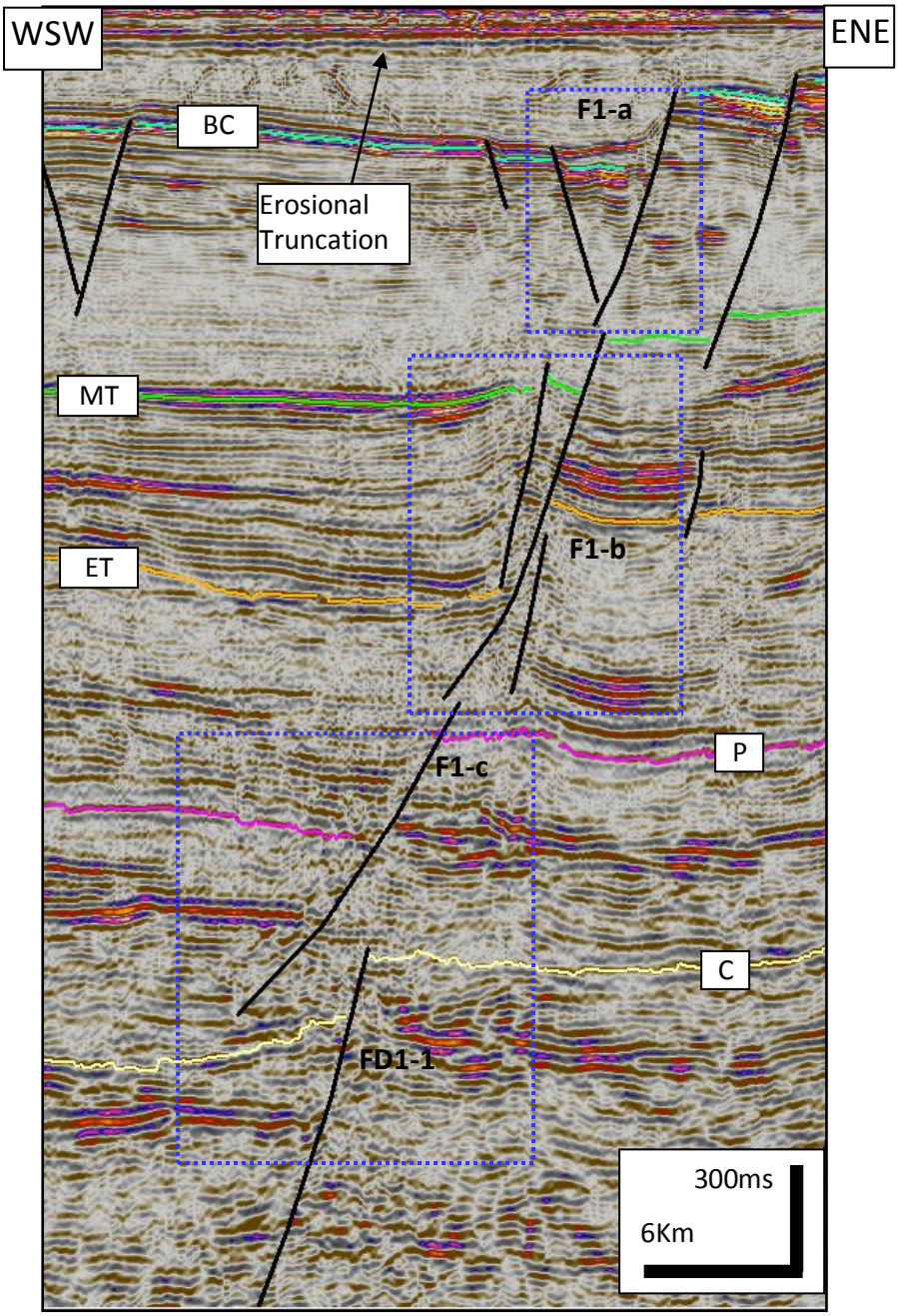

Figure 3.9: 2D seismic line I (close-up from *fig. 3.8*). BC: base Cretaceous, MT: middle Triassic, ET: early Triassic, P: late Permian, C: late Carboniferous. Lower blue square: late Permian-early Triassic interval, middle blue square: early-middle Triassic interval, upper blue square: middle Triassic-base Cretaceous Interval.

The disconnection between deep fault FD1-1 to the fault F1-c is more clearly observed in *fig 3.9* (lower blue square). FD1-1 is characterized by planar normal fault with no drags observed in hanging wall. Reflections in footwall are relatively flat with small dip-slip (<40 msTWT). This small dip-slip magnitude in FD1-1 is very different to the fault F1-c which has bigger dip-slip magnitude.

The separation of tectonic intervals within master fault F1 is also more observed in *fig. 3.9*. F1-c is characterized by planar normal fault which terminated below late Permian reflection. No drags are observed in hanging wall of F1-c, whereas flat to minor undulated reflections are observed in the footwall with dip-slip about 100 ms (TWT). F1-b has different characteristics compared to F1-c. F1-b is characterized by fault zone consists of 2 synthetics normal splay faults with normal drags observed at the lower part and folded reflections at the upper part of hanging wall. F1-a is characterized by planar normal fault and its antithetic faults with large magnitude of dip-slip and steep apparent angle (65^0) defining the fault scarp topography, as also seen in the base Cretaceous time-structure map (*fig. 3.6*). Minor fault blocks are also observed in the foot wall of F1-a.

For the stratigraphy interpretation, the thickening of sediment package can be observed above the base Cretaceous reflection across the master fault F1-a. It is interpreted as the result of basin infilling after faulting activity ceased down. Slight sediment thickening across master fault (F1-b) can also be observed within lower-middle Triassic succession. The progradational succession itself is generally getting thinner toward west or distal part of the clinoform. There is no clear and significant thickening of sediment package across fault F1-c. Erosional truncation, which represents unconformity, is observed at upper part of the section within upper Cretaceous-lower Tertiary succession.

Line II

This 2D line (*fig. 3.10*) is located in the northern part of study area within structural segment 3 (*see fig. 3.6*). Since it is located in different structural segment, some variations of structural geometry are observed in this line compared to the ones observed in previous 2D line.

This line displays two contrasting structural patterns which are not clearly observed in previous line, namely late Carboniferous and post-early Permian intervals, separated by strong amplitude reflections of upper Carboniferous-lower Permian succession. Late Carboniferous interval is characterized by a set of steeply dipping, deep planar normal faults (FD4-1,2,3,4,5) defining wide horst-graben topography and tilted fault blocks, as also seen in late Carboniferous time-structure map (*fig. 3.19*).

Dissimilar to the previous 2D line, post-early Permian interval is characterized by 2 master faults, namely F3 and F4, defining full graben in the hanging walls and flat platform

reflection in footwalls. Both faults are N-S trending normal faults (*fig. 3.6*) with F3 throwing toward west and F4 throwing toward east.

Faults F3 and F4 in this line, have also included three separating fault segments as seen in the master fault of previous 2D line. They are middle Triassic-base Cretaceous (F3-a, F4-a), early-middle Triassic (F3-b, F4b) and late Permian-early Triassic (F3-c, F4-c) intervals as seen in *fig. 3.10*.

F3-c is characterized by a planar normal fault which together with F4-c defines a narrow graben the hanging wall (*fig. 3.11*). Minor undulated reflections are observed in footwall of both faults. Similar to F1-c in previous 2D line, both F3-c and F4-c are detached from late Carboniferous deep fault (FD4-1). FD4-1 is characterized by planar normal fault with strongly tilted reflections in hanging wall and minor undulated reflections in footwall.

Dissimilar to fault F1-b in previous 2D line which shows a synthetic splay fault zone, two simpler planar normal faults F3-b and F4-b (*fig. 3.11*), defining full graben in their hanging walls, are observed. F4-b is characterized by planar normal fault with no drag to normal drag observed in the hanging wall. F3-b shows more complicated normal faults compared to F4-b. F3-b is characterized by a slightly curved normal fault with normal drag in lower part of hanging wall and folded reflections in the upper part of hanging wall.

In middle Triassic-base Cretaceous interval, similar fault characteristics are observed in this section to the one in previous line. F3-a and F4-a are characterized by planar normal faults and its antithetic fault with no drag to normal drag observed in the hanging wall. Both faults are defining SW tilted full graben topography in hanging wall and flat reflection in footwall. The difference in reflection characteristics inside the graben has marked the separation of this interval to the early-middle Triassic interval at below.

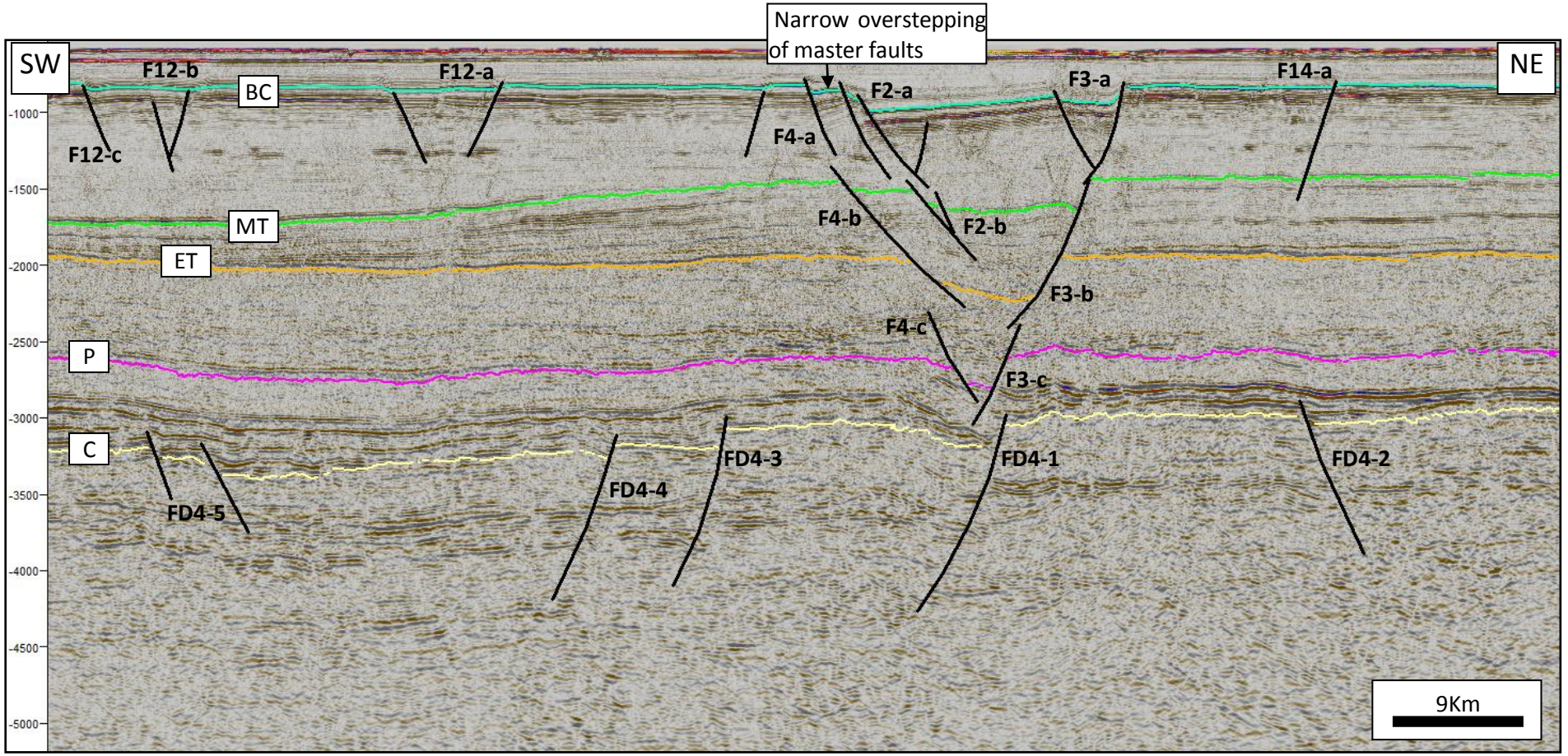

Figure 3.10: 2D line II across segment 3. See *fig. 3.6* for location of the line. BC: base Cretaceous, MT: middle Triassic, ET: early Triassic, P: late Permian, C: late Carboniferous.

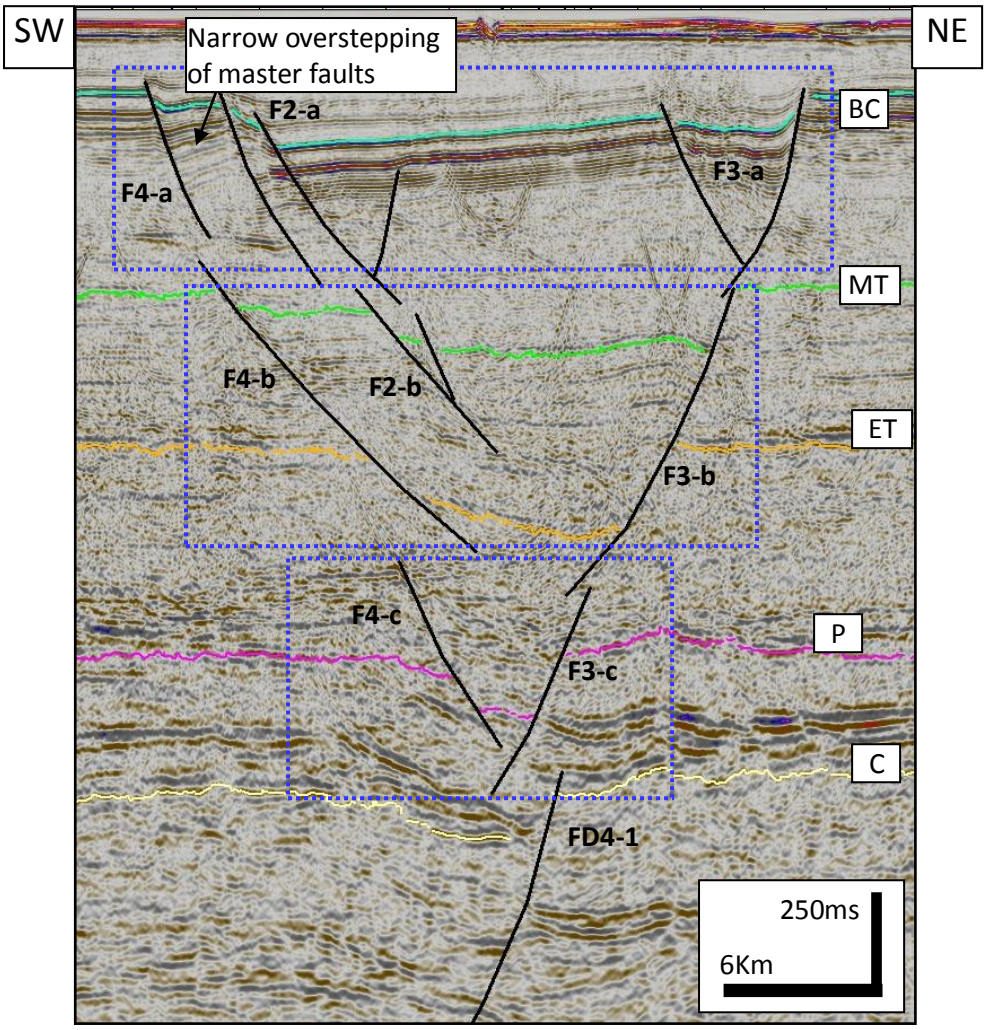

Figure 3.11: 2D line II seismic interpretation (close-up from *fig. 3.10*). BC: base Cretaceous, MT: middle Triassic, ET: early Triassic, P: late Permian, C: late Carboniferous. Blue squares are the focus discussion area. Lower blue square: late Permian-early Triassic interval, middle blue square: early-middle Triassic interval, upper blue square: middle Triassic-base Cretaceous Interval.

Parts of NE-SW trending master fault F2, which has the same apparent dip as N-S trending master fault F4, are also observed in this line (*fig. 310, 3.11*). The area between fault F2 and F4 represents a narrow transition zone which connects NW-SE trending normal fault F2 to the N-S trending normal fault F4. Fault F2 only cuts the succession from lower Triassic – lower Cretaceous. Fault F2 also shows separated fault segments, namely middle Triassic-base Cretaceous interval (F2-a) and early-middle Triassic interval (F-2b). F2-b is characterized by planar normal fault with no drag and synthetic normal fault. The reflections, both in footwall and hanging wall, are relatively flat to slightly undulating. F2-a is characterized by two slightly curved normal faults with antithetic normal fault defining minor tilted fault block feature at foot wall.

For the stratigraphy interpretation, similar to the previous 2D line, the thickening of sediment package across the master fault is observed above the base Cretaceous reflection and also within lower-middle Triassic succession.

3.3. 2 3D Seismic Interpretation

Five 3D crosslines and one inline are selected to represent the variation of fault geometry and style within three different lateral structural segments (*fig. 3.6*).

Crossline A

This line (*fig. 3.12*) is located in southern part of study area (*fig 3.6*) within similar structural segment as 2D line I. In general, it also displays similar structural geometry as observed in 2D line I (*fig. 3.8*). It displays one master fault (F1) striking to the NE-SW, as seen in base Cretaceous structure map (*fig. 3.6*) and separating a flat platform in the footwall from the half graben in the hanging wall. This master fault is detached from deeper fault FD1-1 by strong amplitude, limited lateral continuity, low frequency seismic reflections of upper Carboniferous-lower Permian succession. FD1-1 is characterized by steeply dipping planar normal fault defining half graben topography.

Similar to that observed in 2D line I (*fig. 3.8*), post-early Permian interval in this line also includes three separating fault segments (F1-a,b,c) which are represented by the changes of geometry in dip dimension of master fault F1. More complex geometry of fault F1-b marks the difference of geometry of master fault F1 in this line compared to the one in 2D line I.

Fault F1-c is characterized by a planar normal fault with normal drag in the lower part to no drag in the upper part of hanging wall. Slightly undulated reflections are observed in the footwall. Together with its antithetic normal fault, it is defining minor graben as seen in lower blue square in *fig. 3.13*. Fault F1-b (*fig. 3.13*) has very different characteristics compared to F1-c. It is characterized by complex fault zone with kind of lensoid geometry consisted of one master fault and minor reverse fault in lower part, and two synthetic normal splays in upper part. Fault F1-a is characterized by two planar normal faults and its antithetic faults defining half graben in the hanging wall and minor fault block at the edge of the half graben..

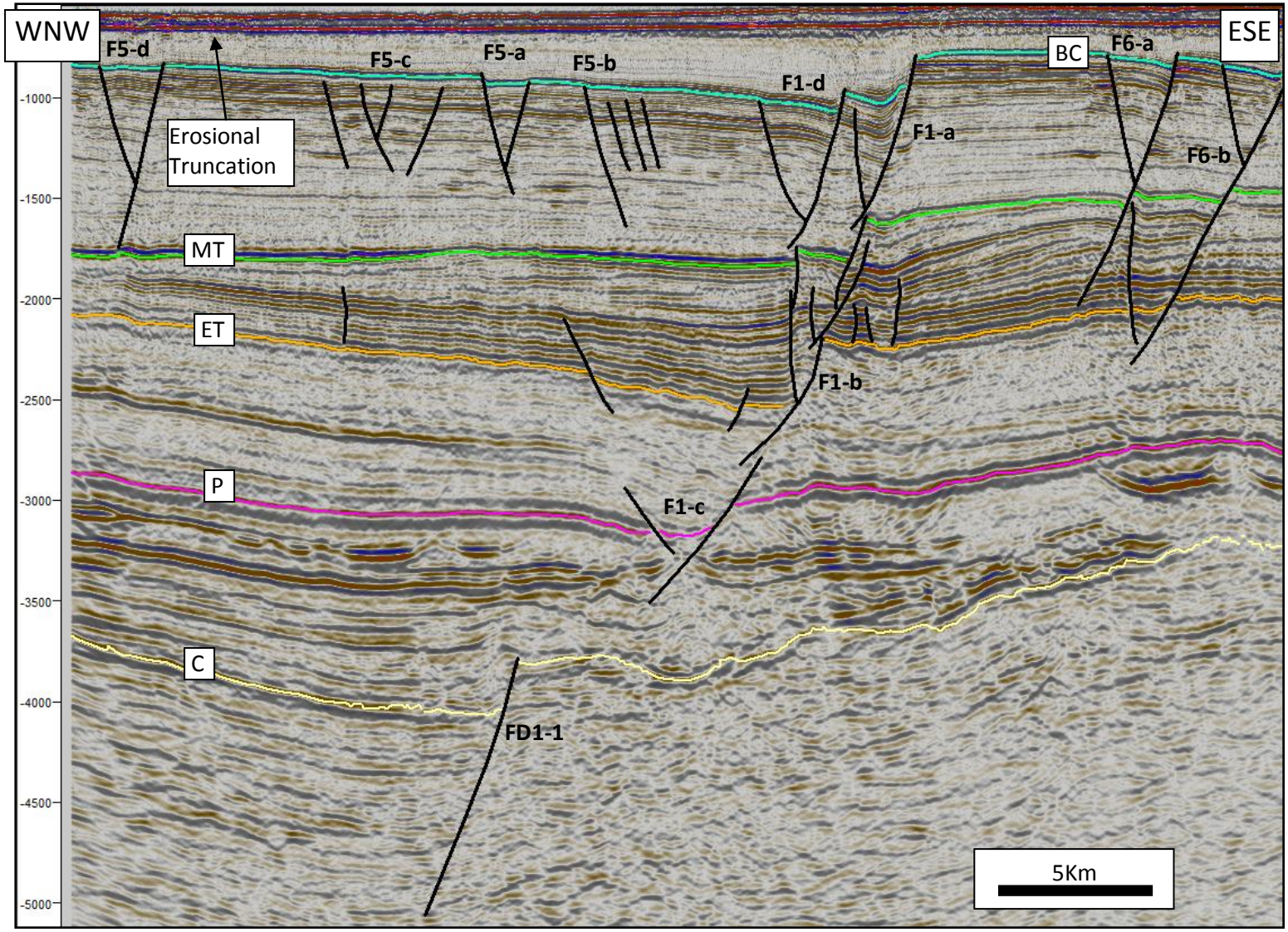

Figure 3.12: 3D crossline A. See *fig. 3.6* for location of the line. BC: base Cretaceous, MT: middle Triassic, ET: early Triassic, P: late Permian, C: late Carboniferous.

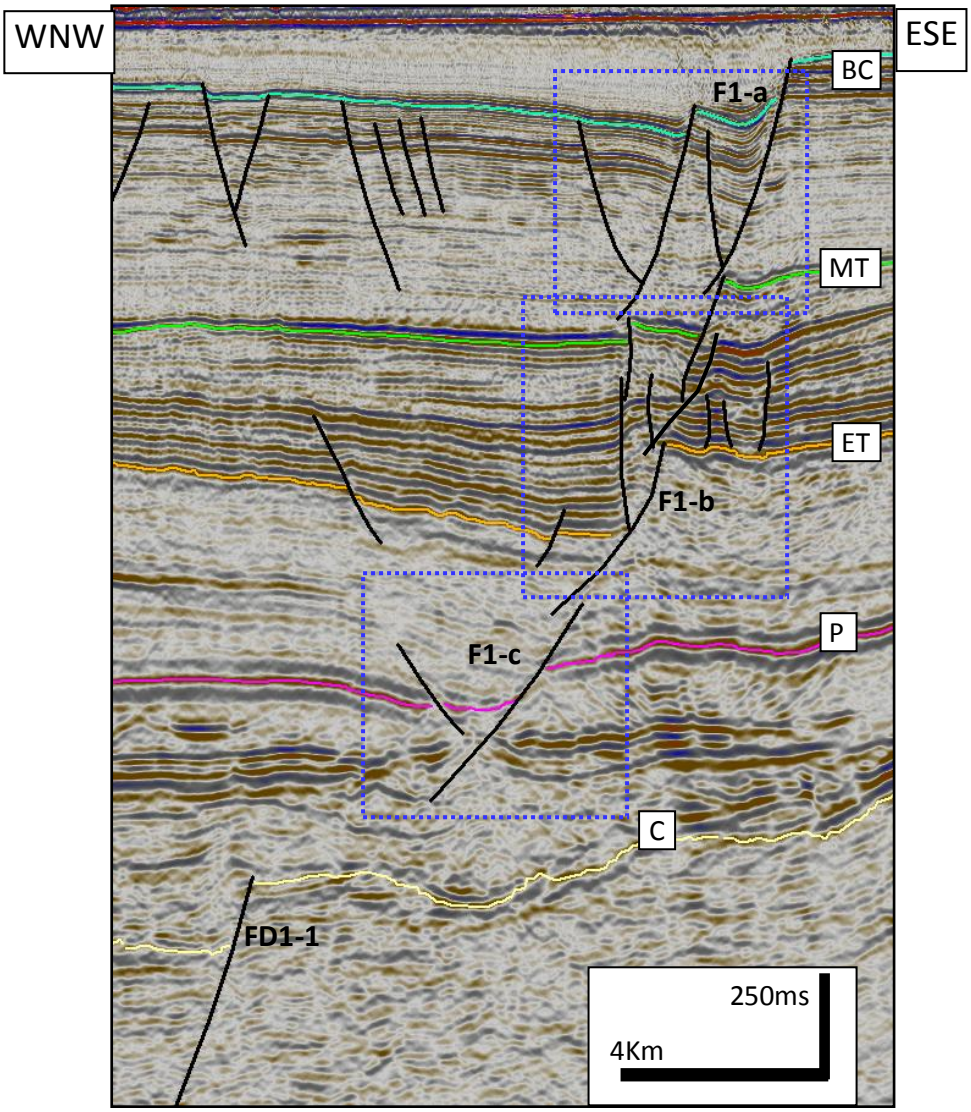

Figure 3.13: 3D crossline A seismic interpretation (close-up from *fig. 3.12*). BC: base Cretaceous, MT: middle Triassic, ET: early Triassic, P: late Permian, C: late Carboniferous. Blue squares are the focus discussion area. Lower blue square: late Permian-early Triassic interval, middle blue square: early-middle Triassic interval, upper blue square: middle Triassic-base Cretaceous Interval.

A set of normal faults, namely F5-a,b,c,d and F6-a,b, with their antithetic faults are also observed within half graben and platform area respectively. These normal faults only cut upper Triassic-Upper Jurassic succession.

For the stratigraphy interpretation, the thickening of sediment across master fault is observed within upper Carboniferous-lower Permian succession, lower-middle Triassic and lower Cretaceous successions, which are related to the activity of the faults. Erosional truncation is observed at the upper part of seismic section (*fig. 3.12*) which represents late Cretaceous-early Tertiary unconfomity.

Crossline B

This line (*fig. 3.14*) is located at the north of crossline A but still within lateral structural segment 1 (*fig. 3.6*). Similar to crossline A, it displays clear separation of structural patterns above and below strong amplitude reflections with locally mounded and patchy reflection patterns of upper Carboniferous-lower Permian succession. Late Carboniferous interval is characterized by set of planar normal faults (FD1-1,2,3,4) defining wide graben topography with fault block at the edge of the graben, as also seen in the southern part of late Carboniferous structure map (*fig. 3.19*), whereas post-early Permian interval is characterized by one master normal fault (F1) separating flat platform reflections in the footwall to the slightly tilted narrower half graben in the hanging wall. Master fault (F1) in this line shows much simpler normal fault geometry compared to that in crossline A. A set of normal faults (F5-a,e,f,d and F6-a,d), which only cut upper Triassic-upper Jurassic succession, and their antithetic faults are also observed within half graben and platform area.

Generally, segmentation within post-early Permian interval into three fault segments in this line is similar to the one observed in crossline A. F1-c (*fig. 3.14*) is characterized by one simple planar normal fault with no drag in hanging wall and moderate dip-slip (about 200 ms TWT), whereas F1-b is characterized by planar to slightly curved normal fault, large dip-slip (about 400 ms TWT) with normal drag in the lower part and folded reflection in the upper part of hanging wall (*fig. 3.14*). Thickening and sagging of sediment sequence in the hanging wall across F1-b are also observed in this lower-middle Triassic succession. F1-a is characterized by slightly curved normal fault with antithetic normal fault defining fault scarp and half graben topography in the hanging wall (*fig. 3.14*), as also seen in base Cretaceous structure map (*fig. 3.6*). The difference in dip-slip magnitude and reflection characteristics in the hanging and footwalls have characterized separation of F1-a, F1-b and F1-c.

Similar to crossline A, thickening of sediment is observed within upper Carboniferous-late Permian succession across the deep faults FD1-1,2,3,4 and above the base Cretaceous reflection across master fault F1-a. Thickening, sagging of sediment across fault F1-b and increasing of dip-slip toward down dip are also observed within lower-middle Triassic succession. Late Cretaceous-early Tertiary erosional truncation is also observed at the upper part of seismic section.

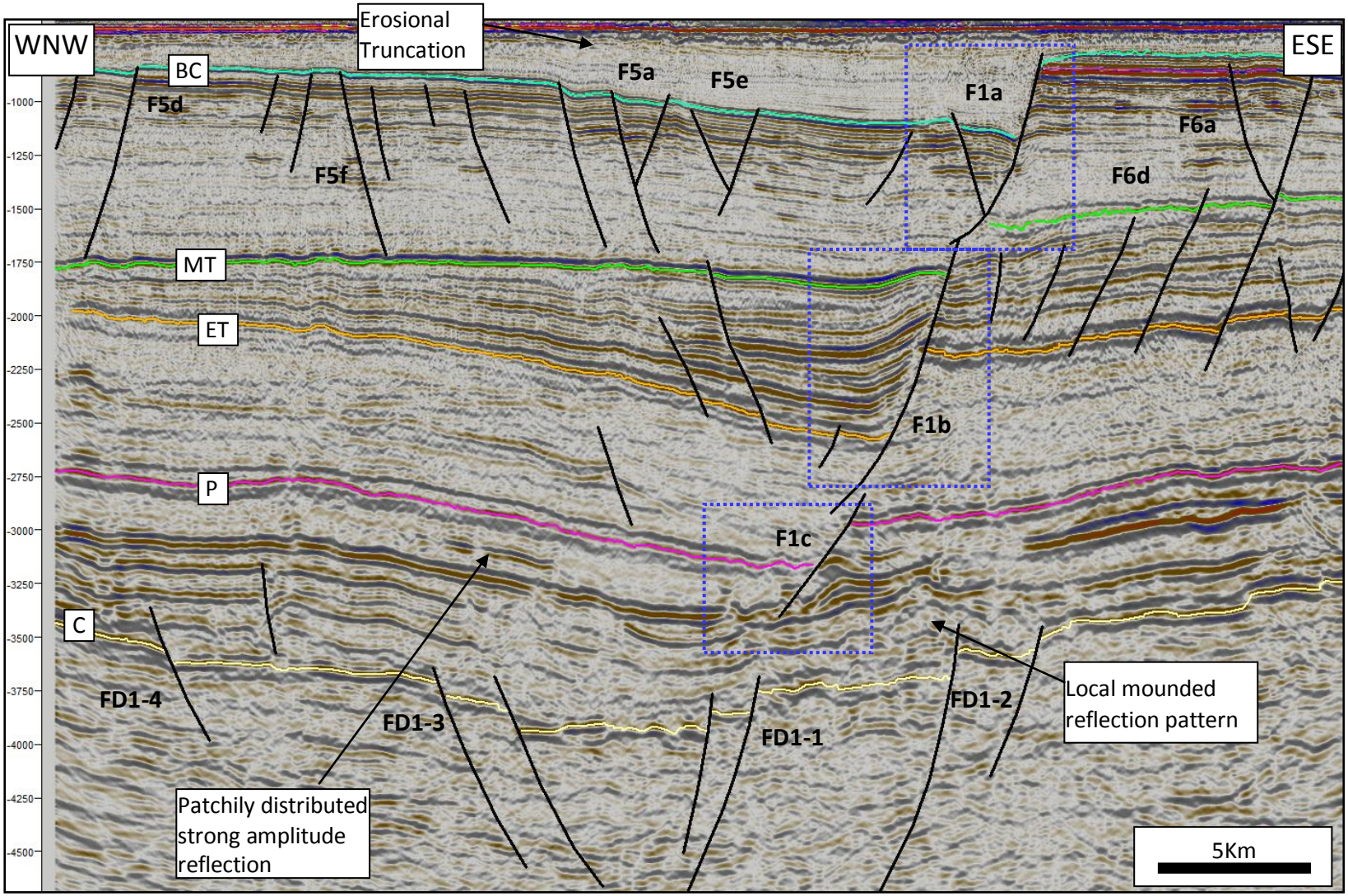

Figure 3.14: 3D crossline B. See *fig. 3.6* for location of the line. BC: base Cretaceous, MT: middle Triassic, ET: early Triassic, P: late Permian, C: late Carboniferous. Blue squares are the focus discussion area for characteristics of master fault. Lower blue square: late Permian-early Triassic interval, middle blue square: early-middle Triassic interval, upper blue square: middle Triassic-base Cretaceous Interval.

Crossline C

This line (*fig. 3.15*) is located at north of crossline B or within lateral structural segment 2 (*fig. 3.6*). Similar to crossline B, the separation of structural patterns below and above upper Carboniferous-lower Permian succession is also observed in this line. The late carboniferous tectonic interval is characterized by a set of planar normal faults defining wider graben topography with fault blocks. The significant difference of structural pattern between this line to the one in crossline B is the presence of two master normal faults (F1 and F2) defining full graben topography in the hanging wall and flat platform reflections in the footwall within post-early Permian interval. Both faults are NE-SW trending normal faults (*fig.3.6*) with fault F1 is throwing toward NW, whereas F2 is throwing toward SE. Minor normal fault (F7-a) and antithetic normal faults are observed within full graben. The size of this full graben is relatively the same as the half graben observed in crosslines A and B within segment 1, as seen in base Cretaceous structure map (*fig. 3.6*).

Fault segmentation in the post-early Permian interval into three separate fault segments is also observed in this line (blue squares in *fig. 3.15*). The characteristics of master fault F1 in this line are very similar to that observed in crossline B, except smaller size of fold is observed in the hanging wall of F1 compared to the one observed in previous line.

Segmentation of fault F2 in this line is not clearly observed, especially between F2-a and F2-b. Both fault segments are characterized by planar normal faults, with one antithetic normal fault associated with F2-b. Slightly different reflection patterns in the hanging wall of both intervals may suggest separation between them (upper blue square in *fig. 3.15*). The separation of both fault segments can also be observed within inline F (*fig 3.18,*), which intersects fault F2 obliquely in the same structural segment with this crossline C, which may be used as secondary data to settle the separation between faults F2a and F2b.

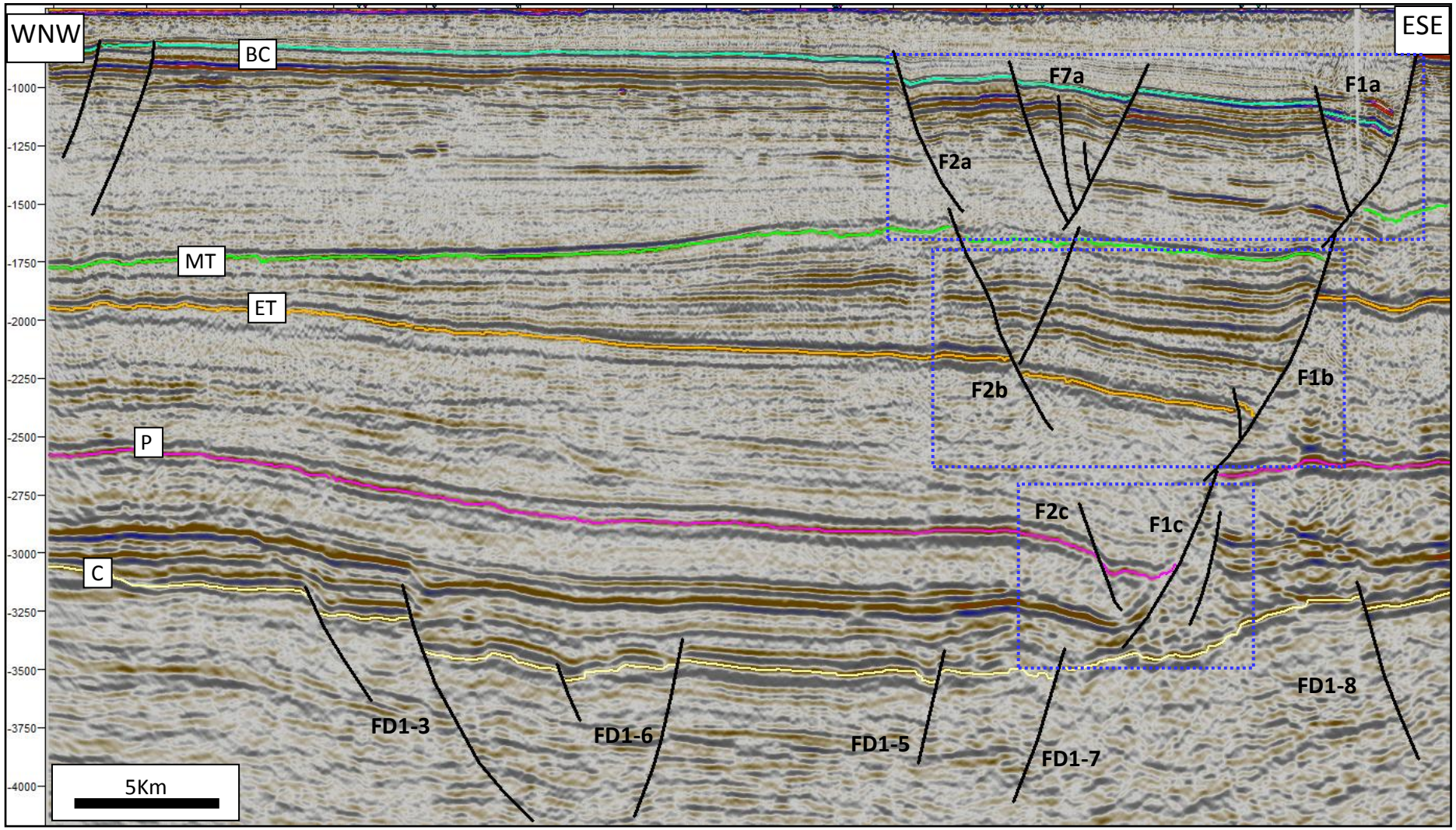

Figure 3.15: 3D crossline C. See *fig. 3.6* for location of the line. BC: base Cretaceous, MT: middle Triassic, ET: early Triassic, P: late Permian, C: late Carboniferous. Blue squares are the focus discussion area. Lower blue square: late Permian-early Triassic interval, middle blue square: early-middle Triassic interval, upper blue square: middle Triassic-base Cretaceous Interval.

The thickening of sediment package is observed within lower-middle Triassic succession across fault F1-b, but it absent across fault F2-b. Other sediment thickening is also observed above base Cretaceous reflection across master faults F1-a and F2-a.

Crossline D

Crossline D (*fig. 3.16*) is located at the southern part of structural segment 3 (*fig. 3.6*). Similar to other previous lines, the separation of structural patterns below and above strong amplitude reflections of upper Carboniferous-lower Permian succession is clearly defined in this line. A set of planar deep normal faults (FD4-2,3,6) defining large horst and tilted fault block in the WNW of the section.

Sets of N-S trending master normal faults (F3 and F4) defining symmetric full graben in the hanging wall and relatively flat platform in footwall are observed within post-early Permian interval, as also seen in base Cretaceous structure map (*fig. 3.6*). F3 is throwing toward west, whereas F4 is throwing toward east. The segmentation of master faults (blue squares in *fig. 3.16*) within post-early Permian intervals, which may represents separate tectonic intervals, is also observed in this line. In general, characteristic and fault geometry of these master faults (F3 and F4) are relatively similar to the characteristic of NE-SW trending master faults (F1 and F2) observed in crossline C, except more undulated reflections are observed in the hanging wall of F3 and F4 within the graben, especially in lower-middle Triassic succession (*fig. 3.16*).

Crossline E

Crossline E (*fig. 3.17*) is located in the northern part of segment 3 (*fig. 3.6*). In general, this line represents the geometry of the Hoop Fault Complex before terminates toward Bjarmeland Platform in the north.

This line generally displays one master normal fault (F4) at central part of the section defining slightly tilted half graben in the hanging wall. Set of minor normal faults (F11-a,b,c,d) observed within half graben forming minor tilted fault blocks. These minor normal faults are interpreted as the continuation of master fault F3 observed in the previous line.

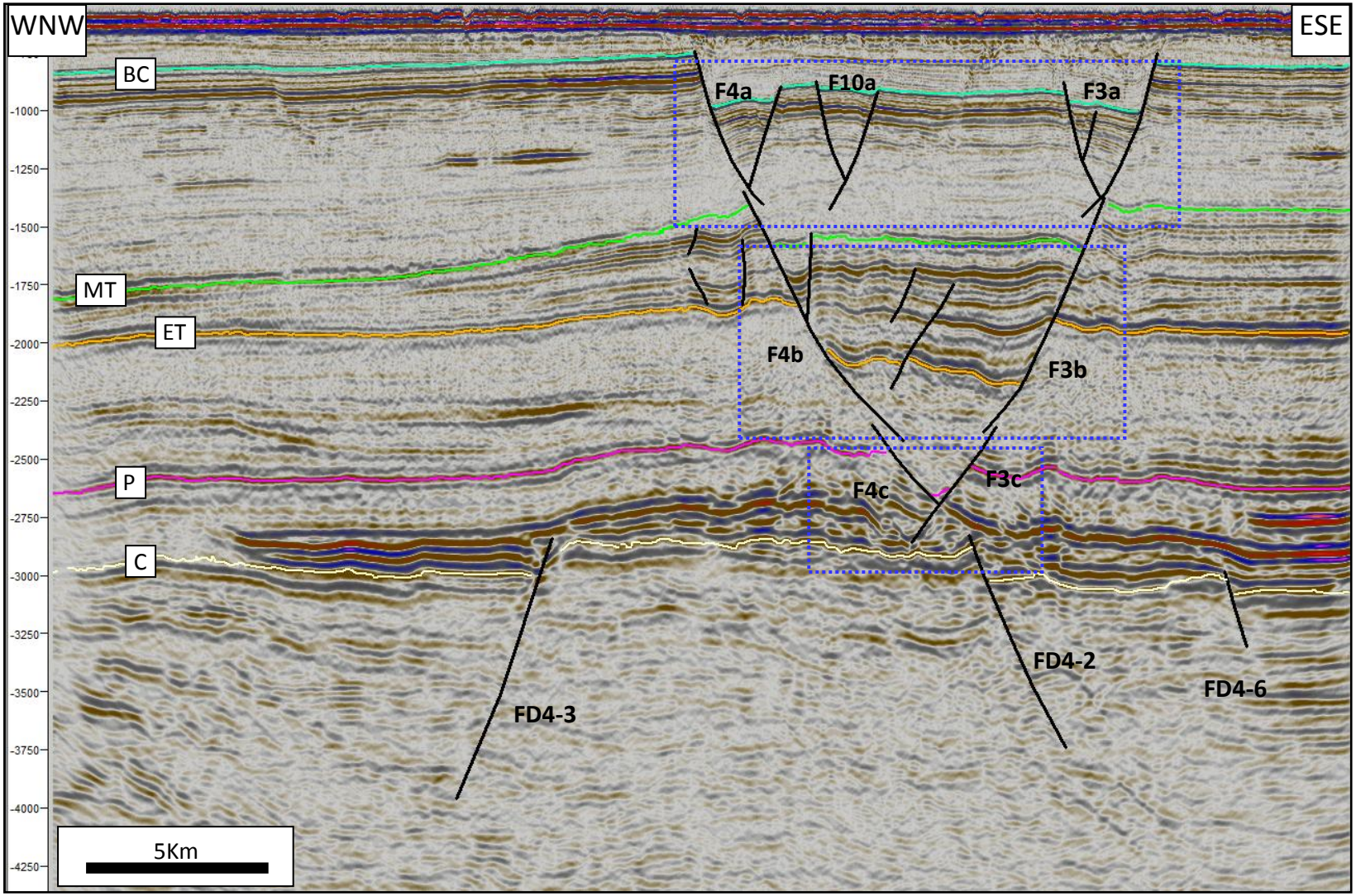

Figure 3.16: 3D crossline D. See *fig. 3.6* for location of the line. BC: base Cretaceous, MT: middle Triassic, ET: early Triassic, P: late Permian, C: late Carboniferous. Blue squares are the focus discussion area. Lower blue square: late Permian-early Triassic interval, middle blue square: early-middle Triassic interval, upper blue square: middle Triassic-base Cretaceous Interval.

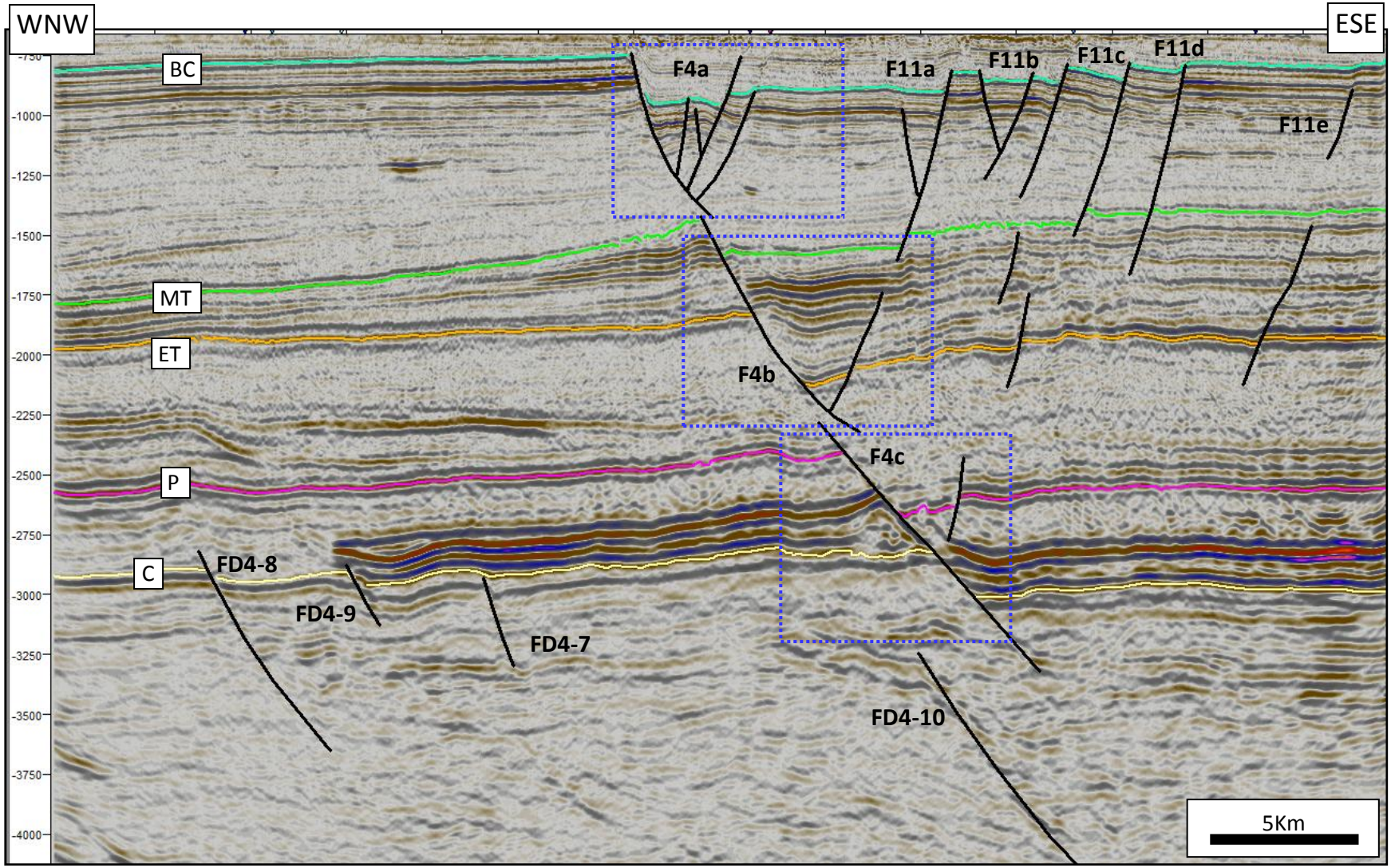

Figure 3.17: 3D crossline E. See *fig. 3.6* for location of the line. BC: base Cretaceous, MT: middle Triassic, ET: early Triassic, P: late Permian, C: late Carboniferous. Blue squares are the focus discussion area. Lower blue square: late Permian-early Triassic interval, middle blue square: early-middle Triassic interval, upper blue square: middle Triassic-base Cretaceous Interval.

Similar to the previous lines, the separation of structural patterns below and above strong amplitude reflections of upper Carboniferous-lower Permian succession is also clearly defined in this line. A set of planar normal faults (FD4-7,8,9,10) defining fault block system is observed in late Carboniferous interval.

Similar to the master fault F4 observed in previous line, the segmentation of master fault (F4) into F1-a, F1-b and F1-c still can be observed (blue squares in *fig. 3.17*). Fault F4-c is characterized by planar normal fault with no drag and one antithetic normal fault (*fig 3.17*). It braches upward in early-middle Triassic interval (F4-b) which characterized by planar-slightly curved normal fault with normal drag at lower part and no drag at the upper part of hanging wall. One antithetic normal fault is associated with this fault F4-b. The thickening of lower-middle Triassic succession across the F4-b and increase of dip-slip toward down dip are also observed. F4-a is characterized by one slightly curved normal fault and three antithetic normal faults.

Inline F

This line is (*fig. 3.18*) oriented relatively NNE-SSW. It crosses the three separated lateral structural segments (*fig. 3.6*) and intersects obliquely three master faults (F1, F2 and F4).

In general, this line also displays separated two major structural patterns below and above strong reflection of upper Carboniferous-lower Permian succession, as seen in all crosslines described before. Late Carboniferous interval in this line is characterized by a set of steeply dipping planar normal faults defining large tilted fault block system. Above this interval, post-early Permian interval is characterized by three master normal faults defining half graben to full graben in different lateral structural segments.

Emphasized on the segmentation of master fault within post-early Permian interval into three separated fault segments as observed in previous crosslines, the separations between faults F1-a, F1-b and F1-c are clearly observed (blue square in *fig. 3.18*) in this inline. Fault F1-c is characterized by a planar normal fault with normal drag. Together with fault F2-c, which has similar characteristics with F1-c, they are defining minor graben. Fault F1-b is characterized by a planar normal fault with normal drag in the lower part and minor folded reflections in upper part. F1-a is characterized by three synthetic normal faults defining minor tilted fault blocks in footwall and half graben in hanging wall.

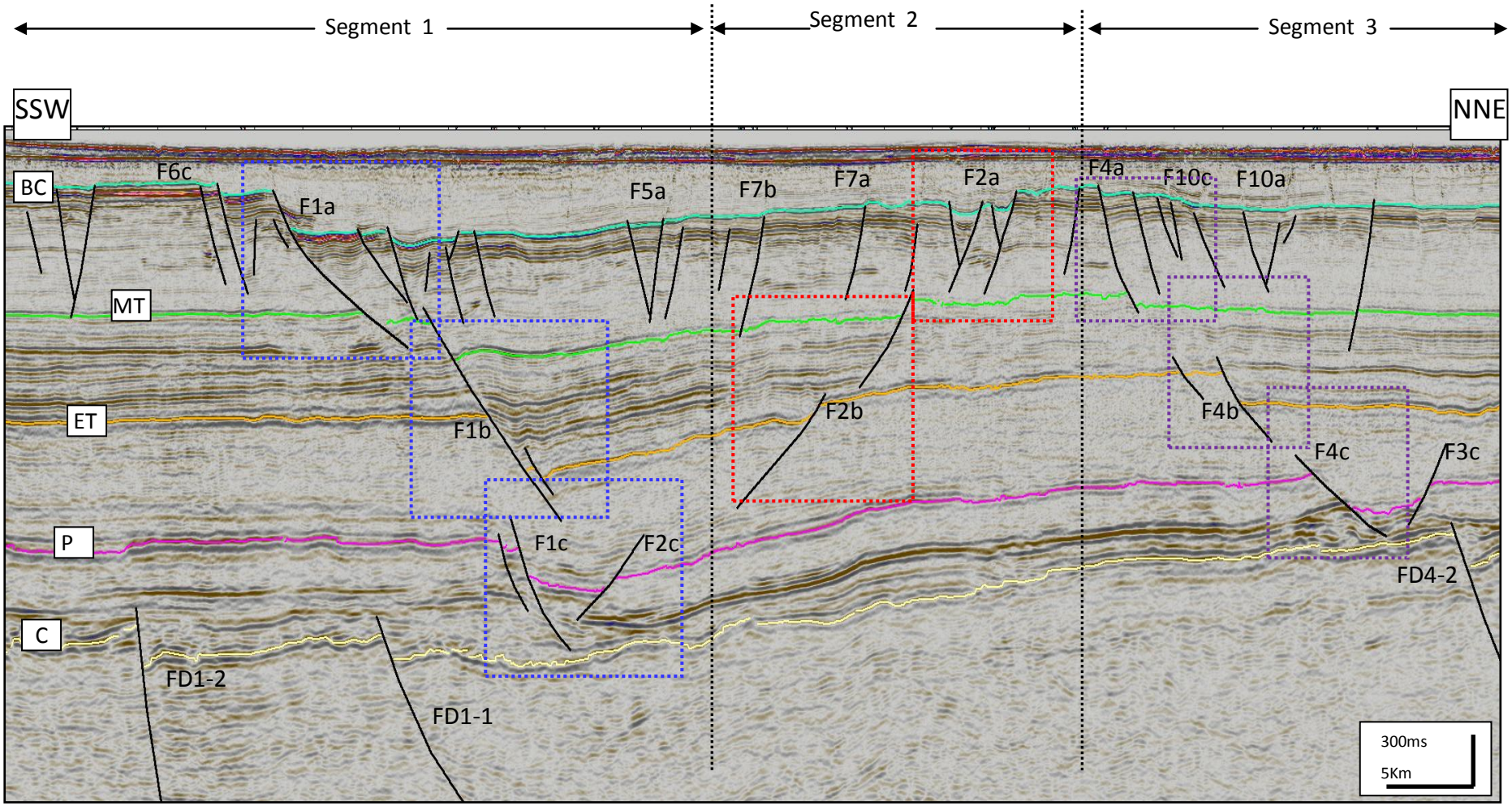

Figure 3.18: 3D inline F shows separating intervals of master faults within segment 1, 2 and 3. See *fig. 3.6* for location of the line. BC: base Cretaceous, MT: middle Triassic, ET: early Triassic, P: late Permian, C: late Carboniferous. Squares are the focus discussion area.

For master Fault F2, even though all of fault segments F2-a, F2-b and F2-c have relatively similar characteristics, but the separations of these fault segments are clearly observed (red squares in *fig. 3.18*). The similar separation is also observed for master fault F4 which is segmented into F4-a, F4-b and F4-c (purple squares in *fig. 3.18*).

The thickening of sediment across master faults within lower-middle Triassic succession and also above base Cretaceous reflection can be observed in all segments crossed by this inline, whereas slightly thickening of sediment above late Carboniferous reflection is only observed in SSW of the section.

3.3. 3 Time-Structure and Fault Maps

Beside the base Cretaceous time-structure and fault maps (*fig. 3.6-3.7*), which have been used to identify general lateral orientation of structural element and subdision of lateral structural segment, the other time-structure and fault maps of other interpreted reflections, such as late Carboniferous, late Permian, early and middle Triassic, were also constructed to identify lateral orientation of structural element in the study area at corresponding reflection and their changes throughout the time.

Late Carboniferous

Late Carboniferous structural elements (*fig. 3.19* and *3.20*) in the study area mainly consist of a set of NE-SW trending normal faults defining graben in the south (segment 1), and a set of NNE-SSW trending normal faults defining local horst with minor half grabens within platform area in the north (segment 3). Segment 2 in the central part is characterized by presence of both NE-SW and NNE-SSW trending faults. In general, the fault configuration within segment 2 and 3 in this late Carboniferous is slightly different to the fault configuration in base Cretaceous (*fig. 3.6* and *3.7*) which is mainly consisted by full graben topography. The fault activity in base Cretaceous is also seen to be more concentrated in fewer master faults compared to faulting activity in late Carboniferous which is affected much wider area.

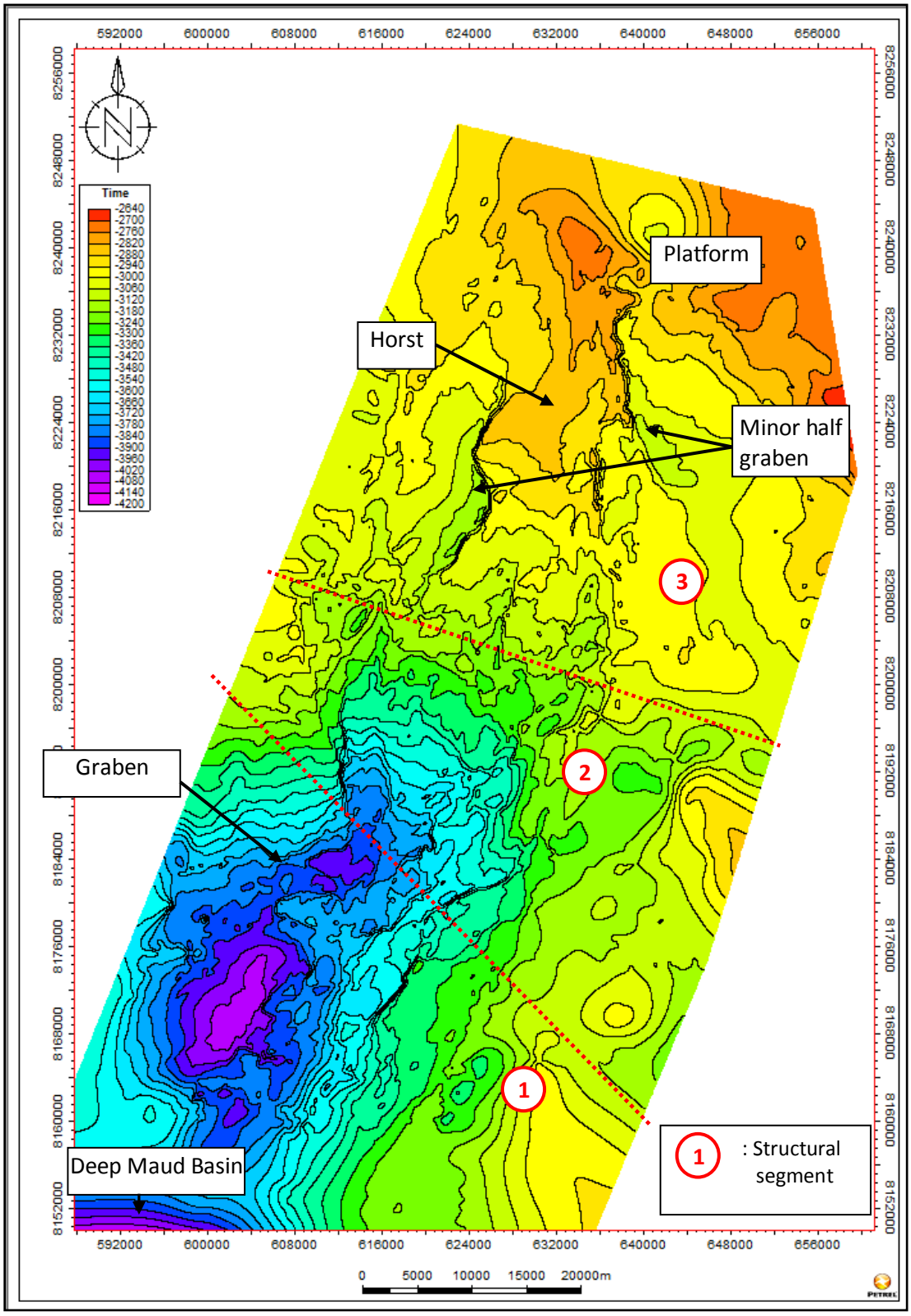

Figure 3.19: Late Carboniferous time-structure map.

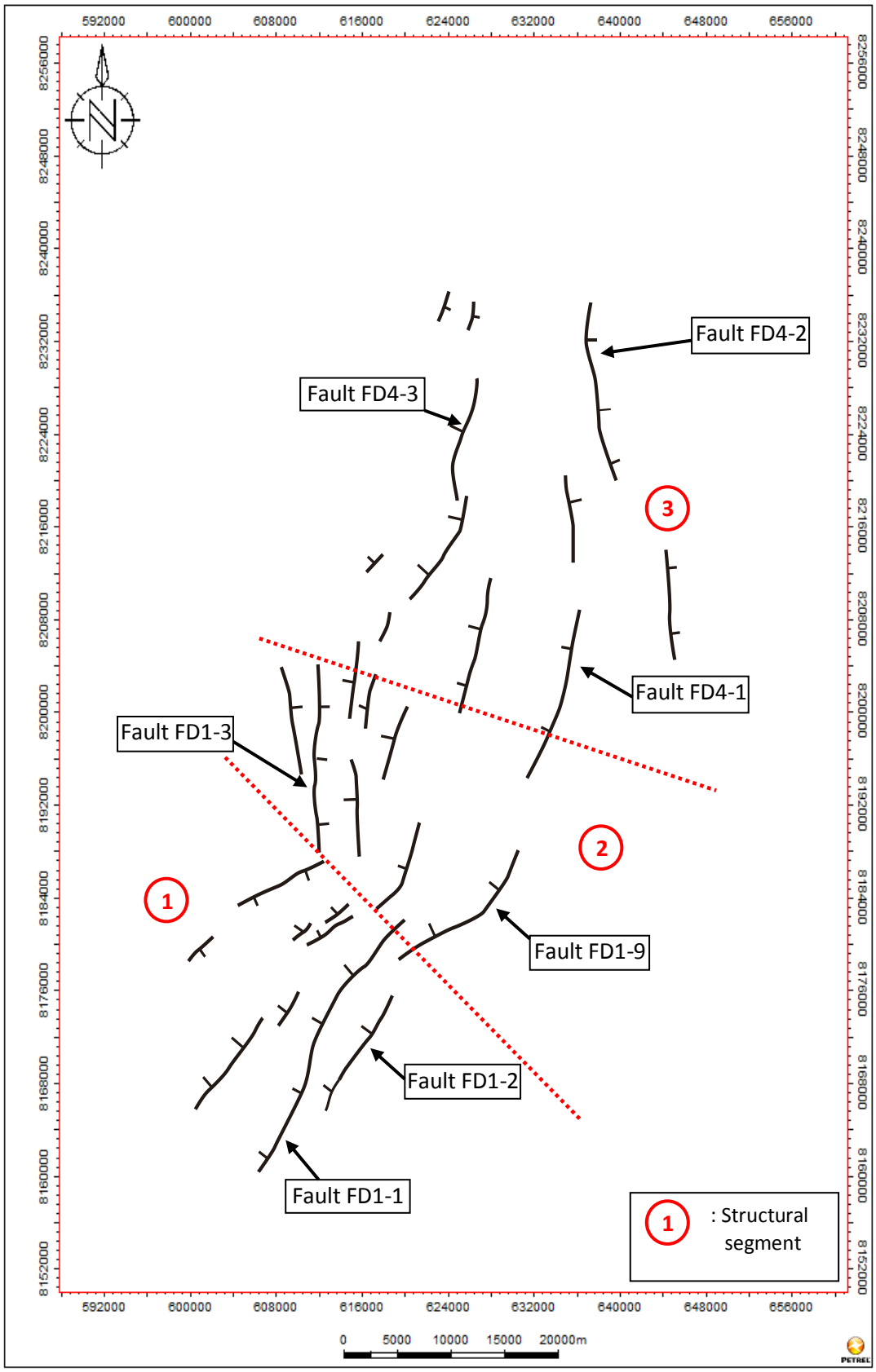

Figure 3.20: Late Carboniferous fault map.

A set of NE-SW trending normal faults (FD1-1, FD1-2, FD1-9), which throwing toward NW and defining a wide graben in the downthrown side, is observed in the southern and central parts of study area or segment 1-2 (*fig. 3.19* and *3.20*). A set of minor normal faults is also observed within this graben which form fault blocks geometry toward the deepest part of the graben (*fig. 3.14*). It is observed that the graben connects to the deep Maud Basin in the southwest to some extent.

In the central part or within segment 2, the structures turn to be more NNE-SSW trending and mark the edge area of graben area. The presence of both NE-SW and NNE-SSW trending faults in this segment indicate that segment 2 is kind of the transition area between those two structural trends and also transition from wide graben in the south to platform area in the north.

In the north area or within segment 3, platform area is dominated by NNE-SSW trending normal faults. Normal fault FD4-2, FD4-1 which throwing toward east and FD4-3 which throwing toward west are defining a wide horst topography with the minor half grabens observed at the hanging wall of these faults (*fig. 3.19, 3.10,* and *3.16*).

Late Permian

Generally, the structural elements in late Permian (*fig. 3.21* and *3.22*) is similar to the ones observed in base Cretaceous (*fig. 3.6* and *3.7*) which consist of NE-SW and N-S trending master normal fault defining three different segments. However, the faulting activity in late Permian is more concentrated in several master faults only which form narrower half and full grabens.

Compared to the late Carboniferous structural element (fig. 3.19 and 3.20), late Permian structural arrangement also shows much narrower graben. The presence of N-S trending normal faults is also marked the differences to that in late Carboniferous.

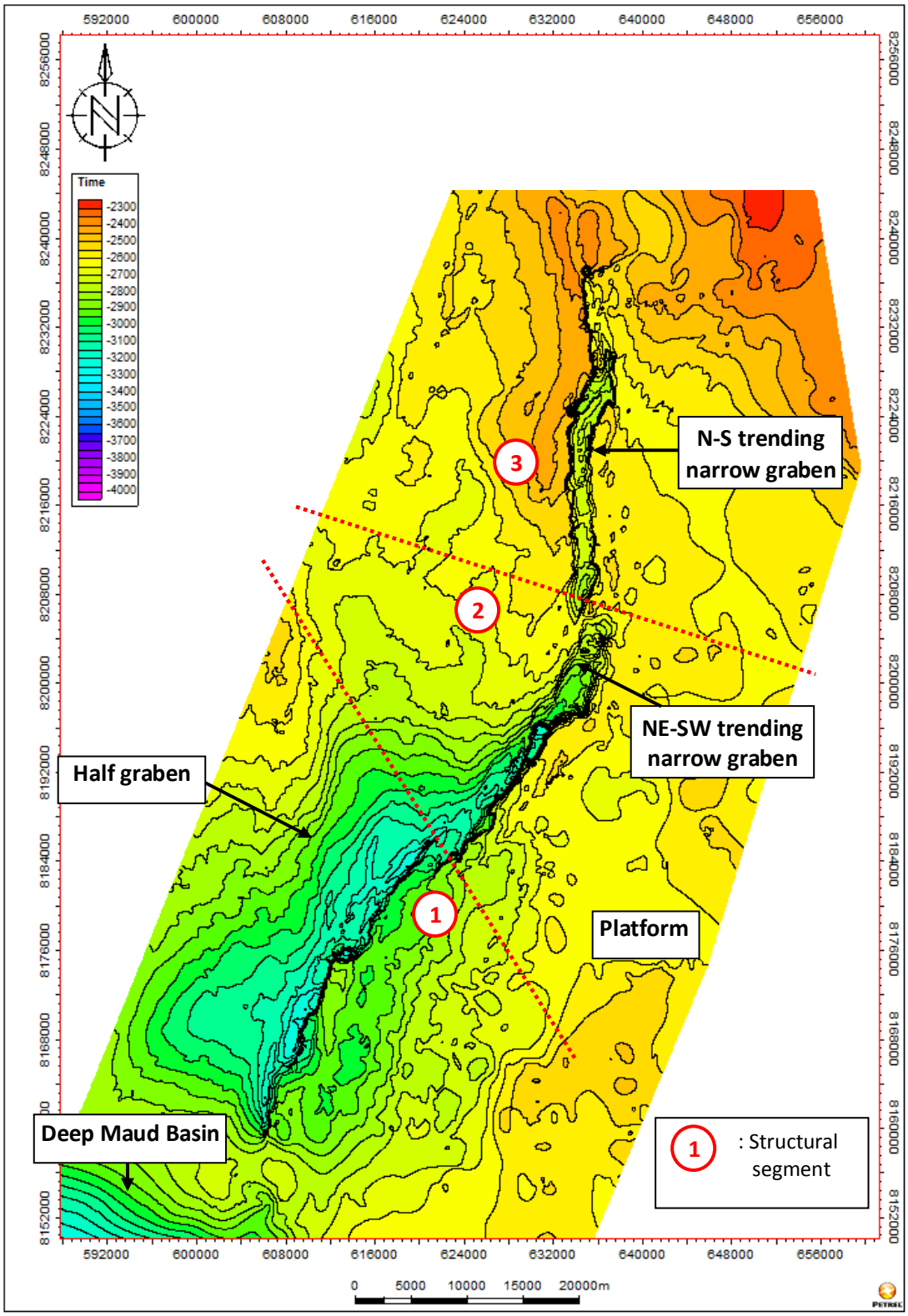

Figure 3.21: Late Permian time-structure map

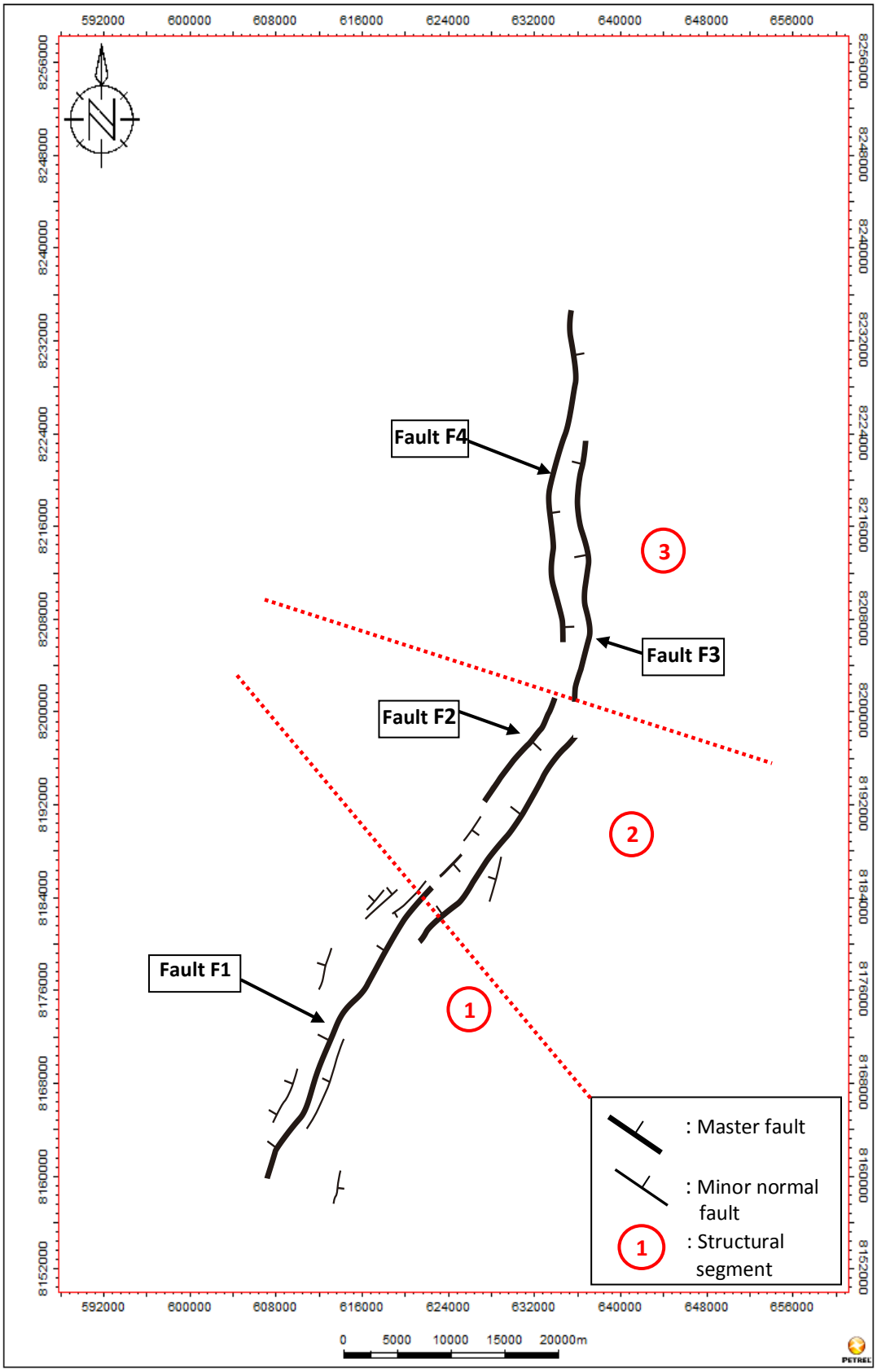

Figure 3.22: Late Permian fault map.

Early Triassic

In general, structural elements in early Triassic are principally similar to the ones observed in late Permian which is mainly consisted of one NE-SW trending master normal fault (F1) defining half graben in the south, two NE-SW trending master normal faults (F1 and F2) defining narrow full graben in central part of study area and two N-S trending master normal faults (F3 and F4) defining N-S narrow full graben in the north (*fig. 3.23* and *3.24*).

The main difference between this interval and the late Permian interval is the size of both, half and full grabens in this interval, is wider compared to the one in late Permian. It marks the starting of development of basin with sag sediment package of lower-middle Triassic succession, especially in half graben area as seen in seismic section (*fig. 3.12 - 3.14*).

Middle Triassic

The arrangement of structural element of the study area in middle Triassic can be seen in time structure and fault map as below (*fig. 3.25* and *3.26*). Principally, middle Triassic structural elements have the same arrangement as the one observed in early Triassic.

Even though the structural elements in middle Triassic seems to be similar to the one in early Triassic, but actually there are minor folds located in the hanging wall of the master faults within the graben which mark the difference between structureal element in middle and early Triassic, as seen in all seismic sections especially at segment 2 and 3. However, these minor folds do not visible in structural maps due to the minor size of the fold and low resolution of the map.

Base Cretaceous

The detail arrangements of structural elements in the study area in base Cretaceous (*fig. 3.6* and *3.7*) have been already described at the beginning of subchapter 3.4.

Higher density of faulting, both NE-SW and N-S trending faults has marked the differences of structural elements in base Cretaceous from the ones observed in other time intervals. Most of the minor normal faults, both within hanging and footwall of master faults, are shallow faults which only cut through the upper Triassic-upper Jurassic succession, as seen in seismic section (*fig. 3.8 – 3.18*).

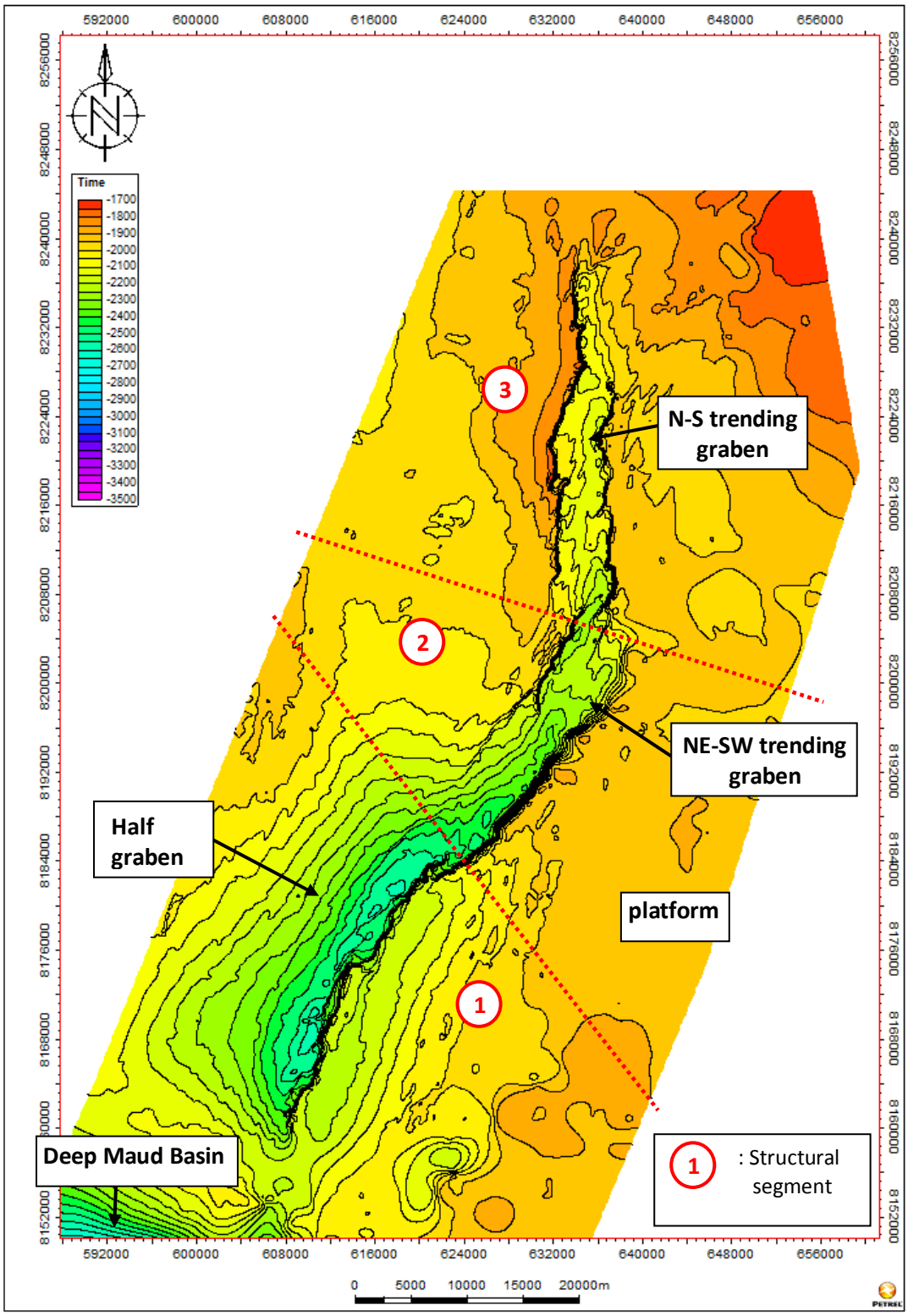

Figure 3.23: Early Triassic time-structure map.

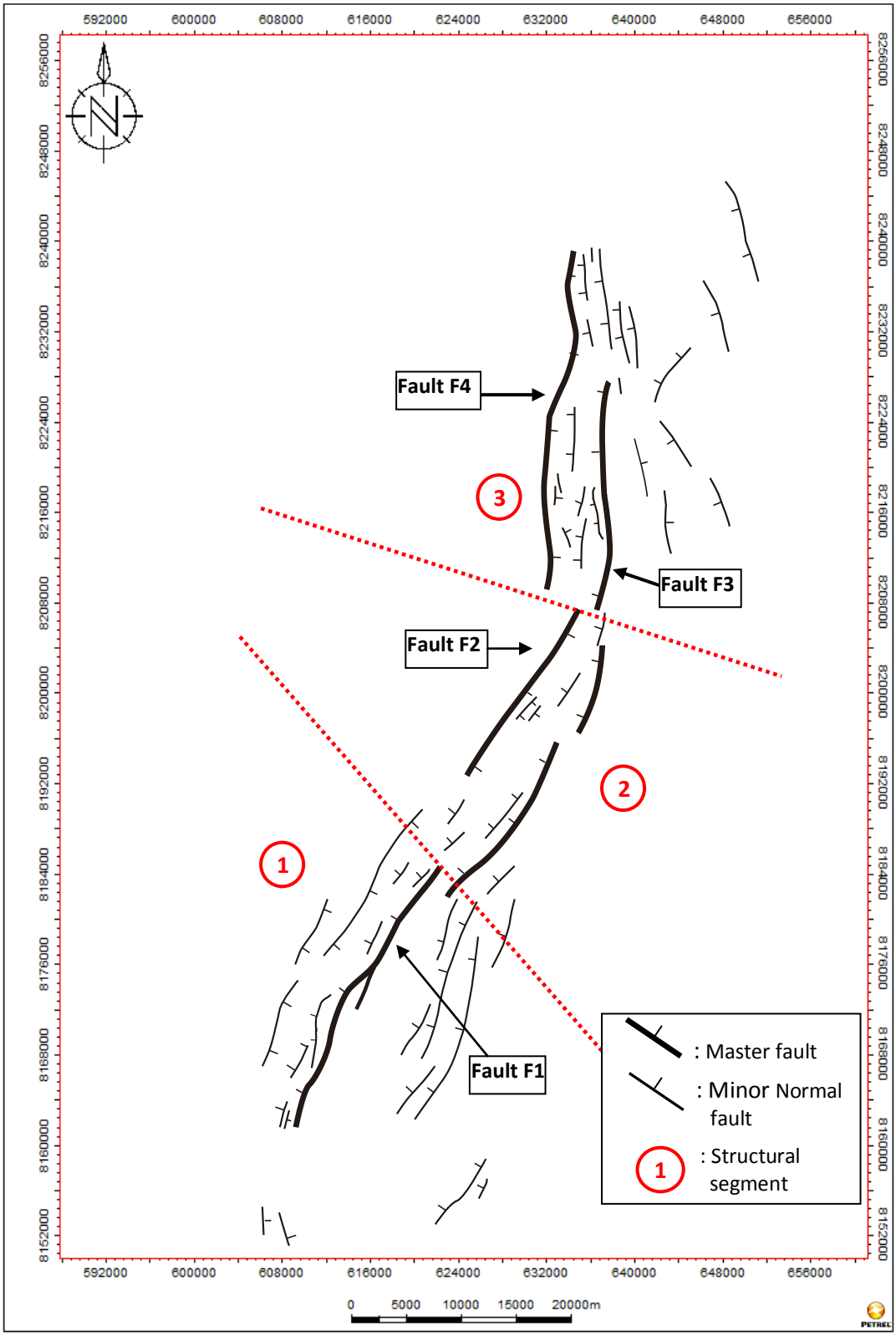

Figure 3.24: Early Triasic fault map.

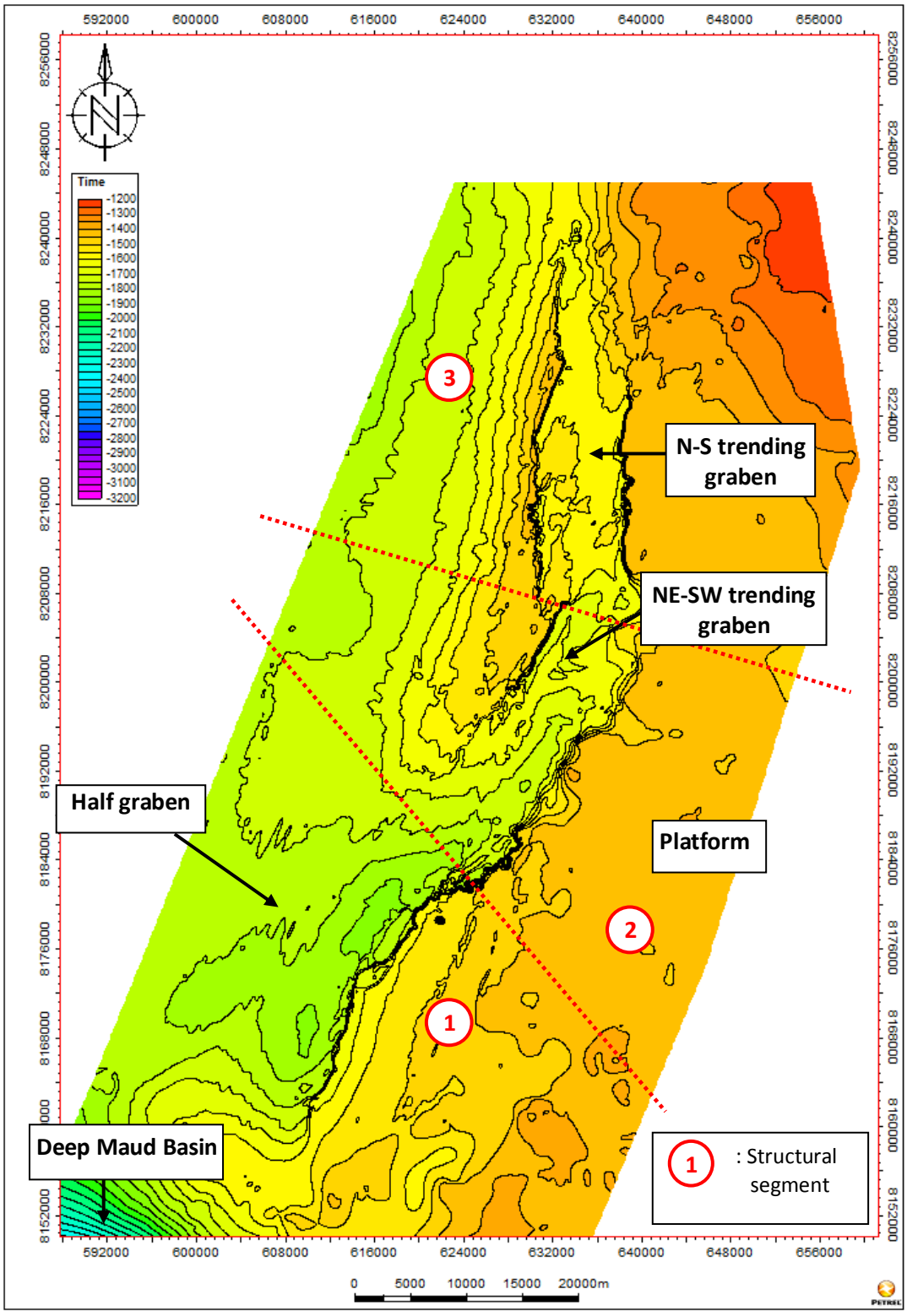

Figure 3.25: Middle Triassic time-structure map.

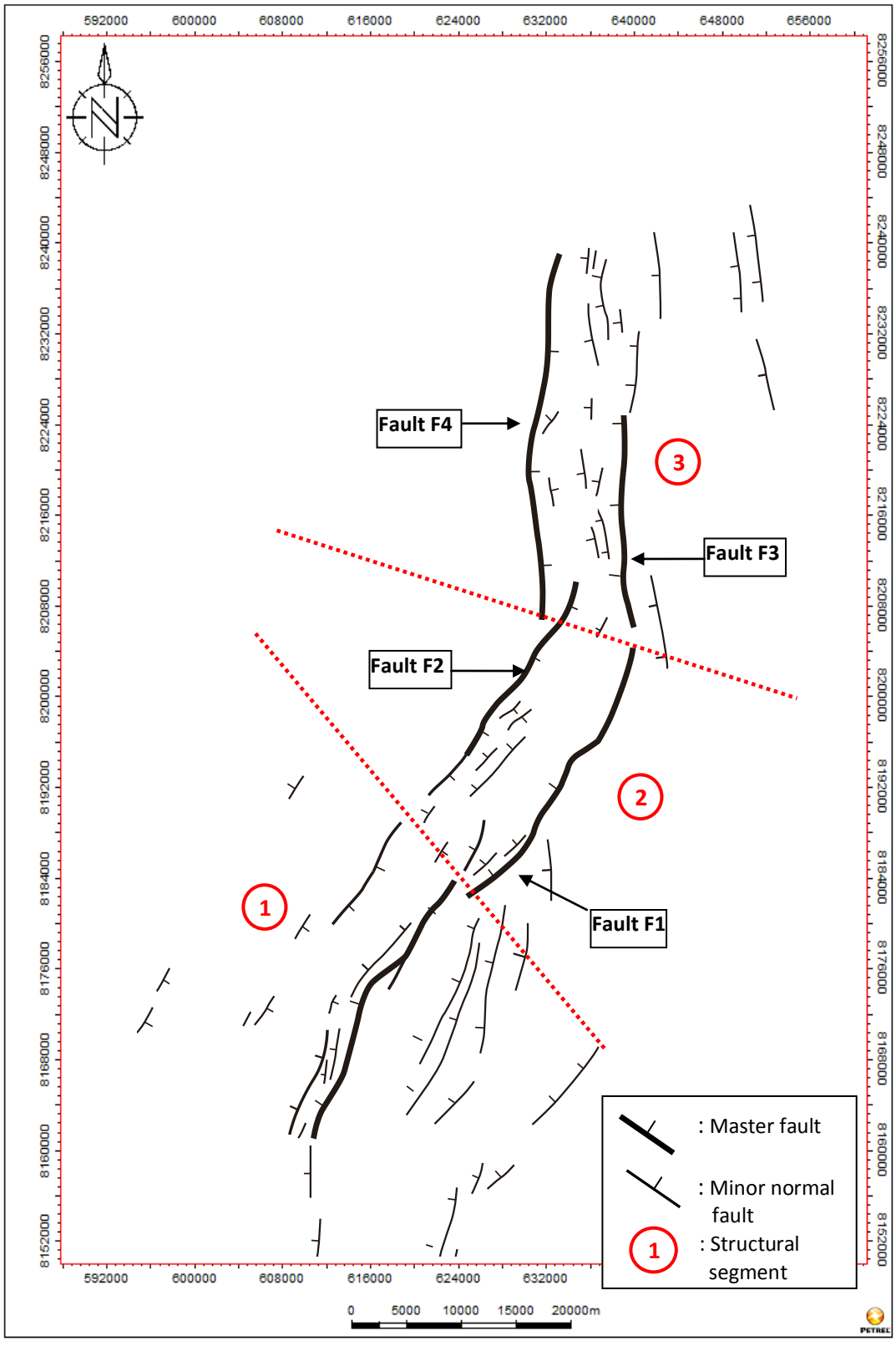

Figure 3.26: Middle Triassic fault map.

3.3.4 Time-Thickness Maps

Time-thickness maps between interpreted reflections were constructed to identify the lateral thickness variation of sediments which is related to the faulting activity and depositional patterns within certain time interval.

Late Carboniferous-Late Permian

Lateral variation of sediment thickness at late Carboniferous-late Permian interval can be seen in *fig. 3.27*. It is observed that there is a relatively NE-SW trending thick sediment package at the southern part of study area representing the graben, whereas in the platform area in the north, the thickness of the sediments are relatively uniform except in some small areas close to the fault where minor half graben is formed. This thickening of sediment may indicate faulting activity during this time interval.

Late Permian-Early Triassic

Lateral variation of sediment thickness at late Permian-early Triassic interval can be seen in *fig. 3.28*. It is observed that there are a no significant changes of sediment thickness across the master faults in the study area. It can be interpreted that normal faulting which occur during previous late Carboniferous-late Permian interval has stopped in this time interval. However, in general sediment thickness within this time interval seems to decrease toward NE as the morphology changes from half graben in the south to the platform in the north.

Early-Middle Triassic

Lateral variation of sediment thickness at early-middle Triassic interval can be seen in *fig. 3.29*. It can be observed that there is thickening of the sediment across the master faults both in half graben and full graben, as also seen in the seismic sections (*fig. 3.8-3.18*). The magnitude of sediment thickening in the half graben is higher compared to the one in full graben. It is also observed that in general, sediment is getting thinner toward NW which may correlates to the direction toward distal part of lower-middle Triassic prograding succession within this time interval, as observed in the seismic sections.

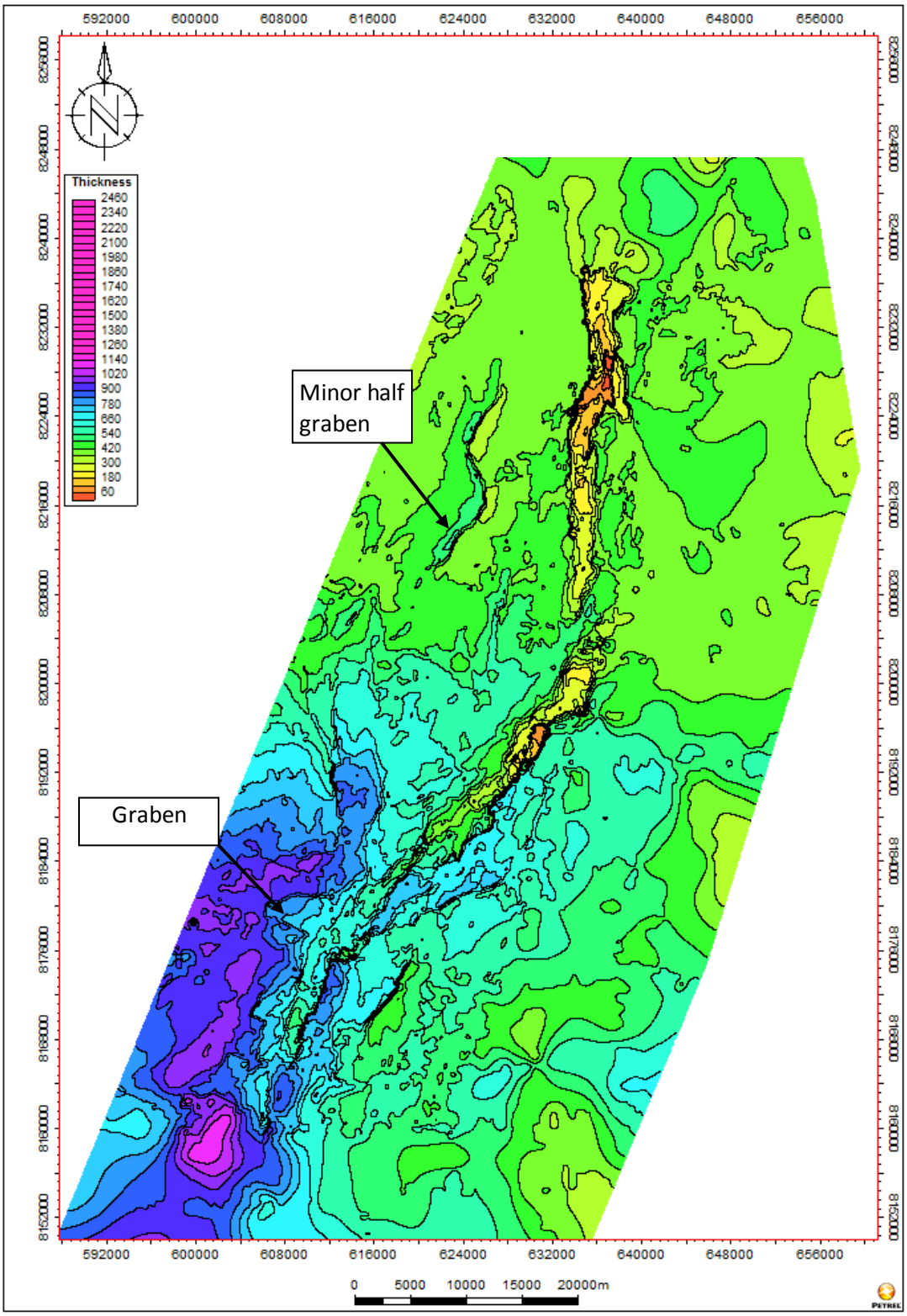

Figure 3.27: Late Carboniferous-late Permian time-thickness map.

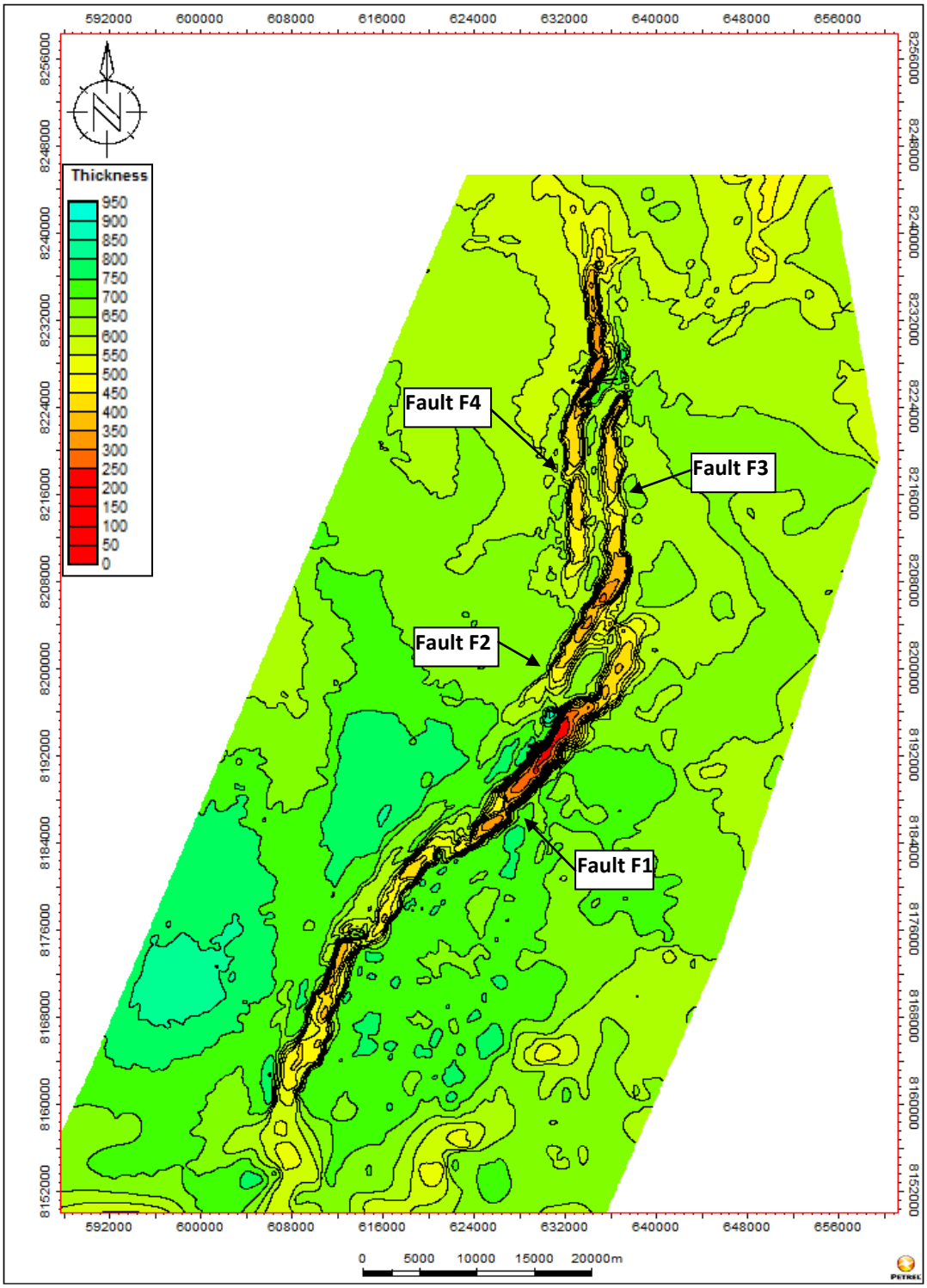

Figure 3.28: Late Permian-early Triassic time-thickness map.

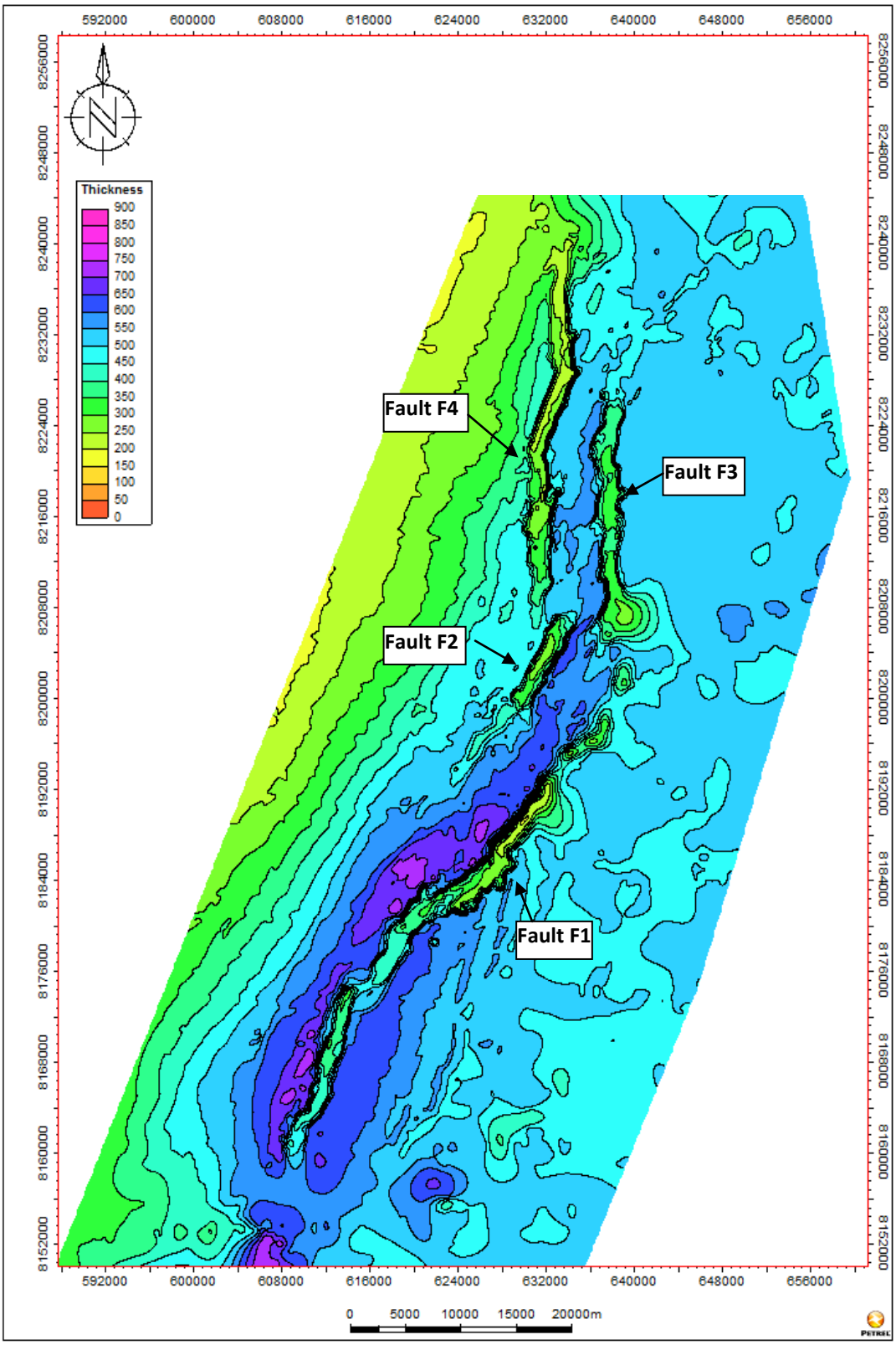

Figure 3.29: Early-middle Triassic time-thickness map

Middle Triassic-Base Cretaceous

Lateral variation of sediment thickness at middle Triassic-base Cretaceous interval can be seen in *fig. 3.30*. It can be observed that there is no changes of sediment thickness across the master faults which may be indicated no active faulting during this time interval. However, the general sediment thickness is increased toward NE as the sediment infilling continues toward that direction.

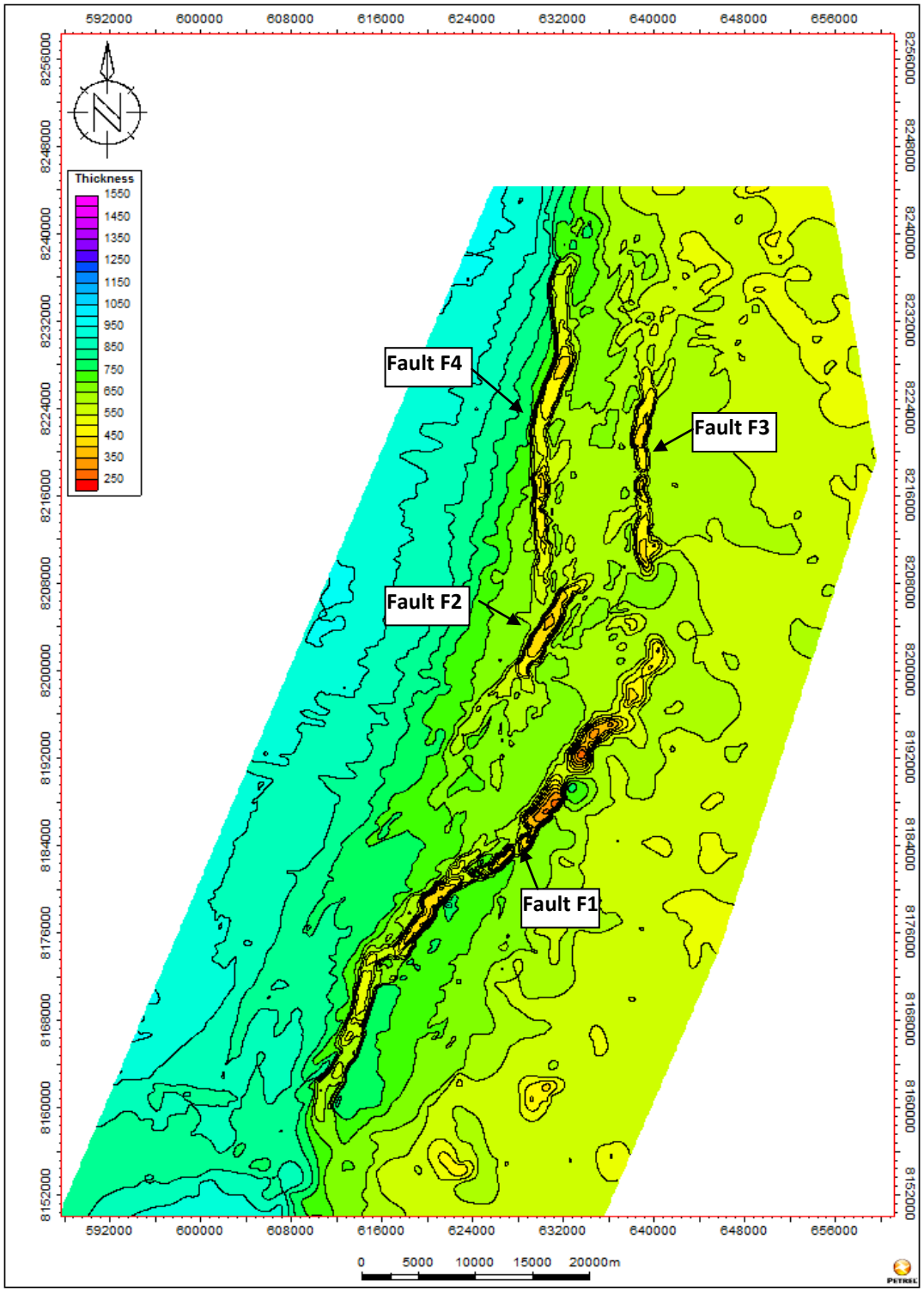

Figure 3.30: Middle Triassic-base Cretaceous time-thickness map.

4. Discussion

This chapter is focused on discussion of the structural characteristics and development of the Hoop Fault Complex in study area based on data described in the previous chapter and literatures. The detail topics of discussion are (1) fault geometry and its genesis, including the time of activation, (2) indication of detachment, (3) indication of inversion or potentially strike-slip influences, and (4) geological history of the Hoop Fault Complex.

The Hoop Fault Complex is an obviously extensional fault complex with graben system. It can be divided laterally and vertically into distinct major segments of different fault geometry, orientation and style which are separated by detachments. This fault complex was resulted from roughly NW-SE to E-W extension which has been repeatedly active since late Carboniferous time and being reactivated during early-middle Triassic, middle-earliest late Triassic and late Jurassic-early Cretaceous. An indication of inversion and potentially strike-slip movement, which observed within middle-upper Triassic succession, has increased complexity of fault geometry and geological history.

4.1 Fault Geometry and Its Genesis of The Hoop Fault Complex

4.1.1 Lateral Configuration

The Hoop Fault Complex is an extensional fault system which is consisted of NE-SW and N-S trending normal faults (*fig. 3.6, 3.7* and *4.1A*) forming half graben and full graben morphologies. This fault complex can be divided into three lateral distinct major segments of different structural orientation, namely segment 1, 2 and 3. Segment 1 in the south is characterized by one NE-SW trending master normal faults defining a SE tilted half graben along the strike of master fault. A set of minor normal faults are also observed inside the half graben. Segment 2 in the central part is characterized by a set of NE-SW trending master normal faults and minor normal faults which are developed mainly in the hanging wall of master fault, defining full graben morphology. Segment 3 in the north is characterized by a set of N-S trending normal faults defining a full graben in between the master faults. Similar lateral segmentation is also found in other extensional system, such as in Lake Tanganyika of the East African Rift System (*fig. 4.1B*).

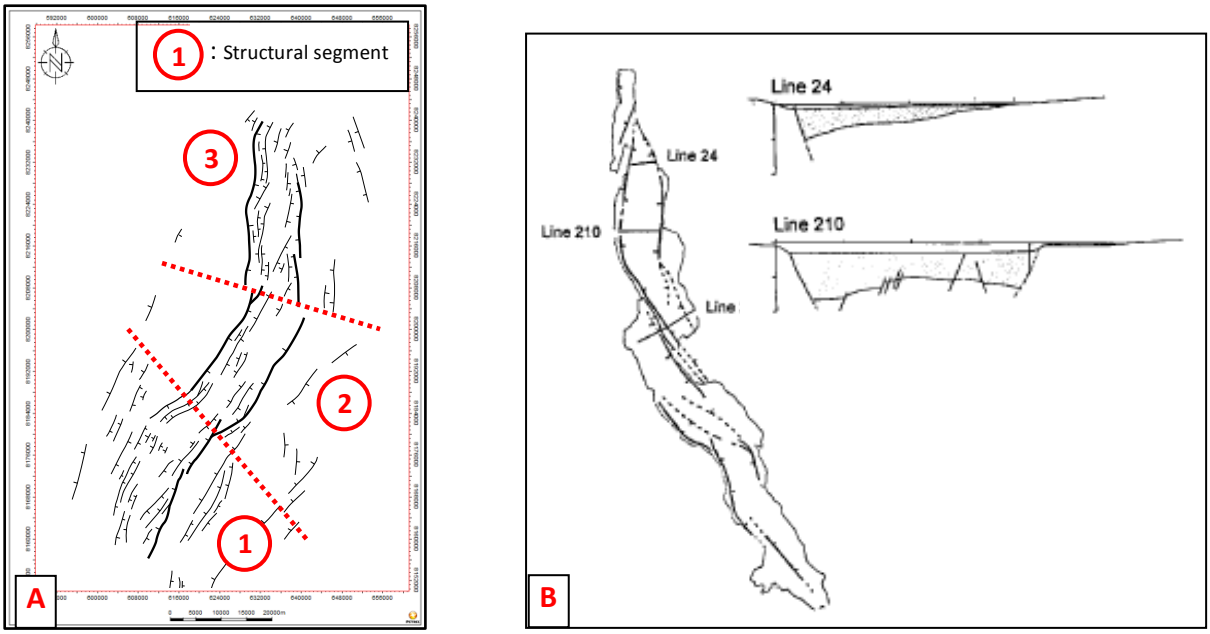

Figure 4.1: (A) Base Cretaceous fault map. (B) Cross sections across Lake Tanganyika, East African Rift System, showing half and full grabens within one rift system (Kusznir et al., 1995).

4.1.2 Fault Geometry in Dip Dimension and Its Genesis

The detailed fault geometry of the Hoop Fault Complex along its dip can be seen in *fig. 4.2*. It can be observed that there is a contrast of geometry between faults within late Carboniferous interval to the faults in post-early Permian interval which are separated by upper Carboniferous-lower Permian carbonate-evaporite layer.

The deep fault system in the late Carboniferous interval is characterized by a set of planar extensional normal faults defining wide graben with tilted fault blocks at the flank of the graben. The post-early Permian interval shows more complex fault geometry compared to the late Carboniferous. It can be divided into several depth-dependent segments, namely late Permian-early Triassic, early-middle Triassic and middle Triassic-base Cretaceous intervals. Each of segment is characterized by different fault geometry which is resulted from different style and timing of fault activity. Late Permian-early Triassic interval is characterized by simple planar to slightly curved normal fault, whereas early-middle Triassic is characterized by slightly curved, growth normal fault defining a kind of narrow sag sediment package in the hanging wall. Minor fold is observed at the upper part of early-middle Triassic interval which possibly related to the inversion. The middle Triassic-base Cretaceous interval is characterized by a set of planar to slightly curved extensional normal faults and its antithetic fault defining a wide SE tilted half graben in the hanging wall. The detailed genesis of the fault geometry for every depth dependent segment is discussed in 4.1.2.1 – 4.1.2.3.

Besides the presences of different fault activity with different tectonic style, as mentioned before, the variation of vertical mechanical strength in the rock column of upper Permian to upper Jurassic strata may also contributes, to some extent, to the formation of complex fault geometry as seen in *fig. 3.13*. Childs et al. (1996) mentioned the influence of rock competency to the dip of the fault trace within fault zone, where dip of the fault trace in less competent rock is shallower than in the more competent rock.

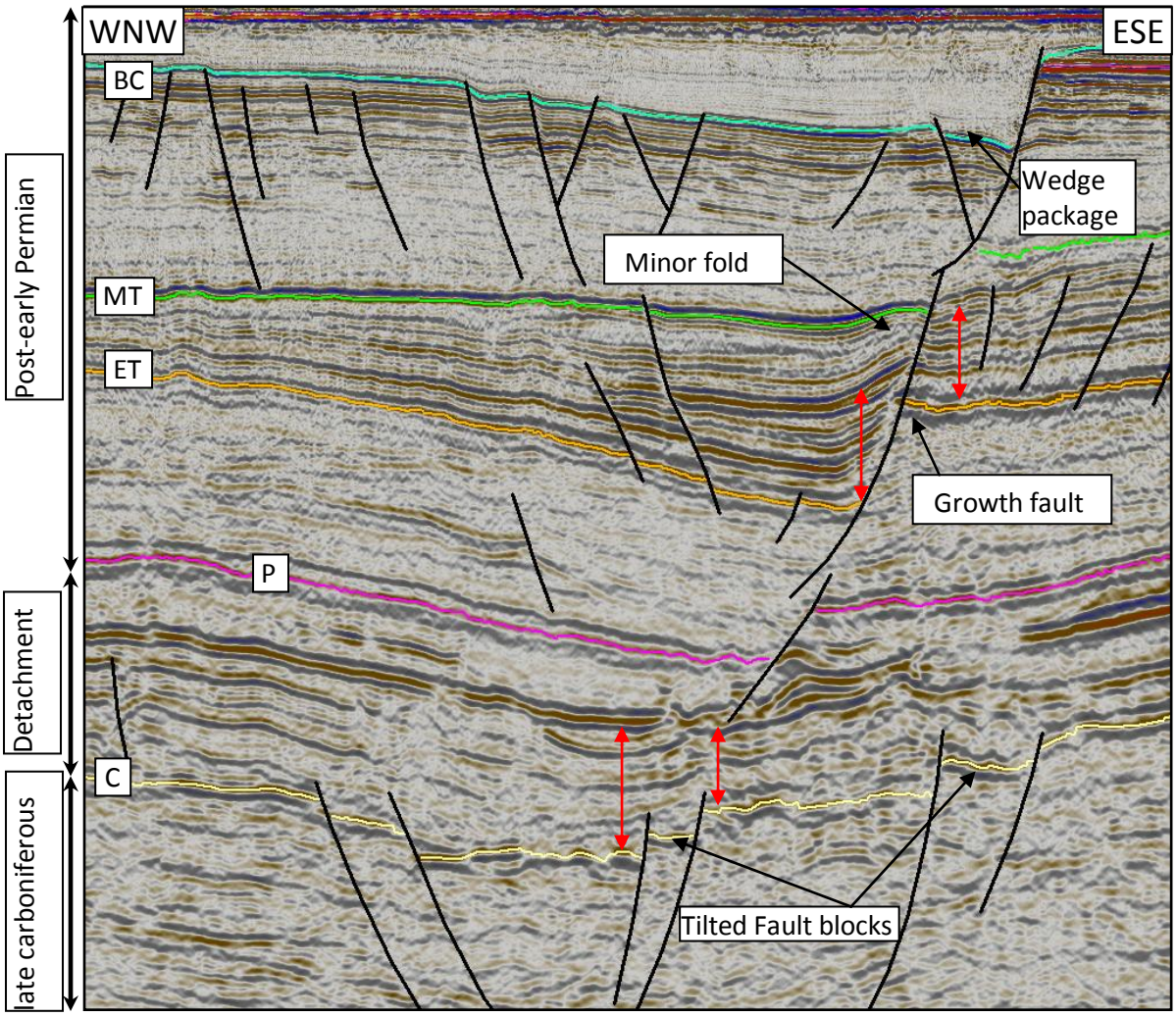

Figure 4.2: 3D crossline B shows general fault geometry along the dip. Red arrows are indicating the thickening of sediment across the fault. BC: base Cretaceous, MT: middle Triassic, ET: early Triassic, P: late Permian, C: late Carboniferous.

4.1.2.1 Late Carboniferous Interval

A set of steeply dipping, small dip-slip magnitude, deep planar normal faults in late Carboniferous interval, as described before, reflects the extension which occurs during that time interval. It is shown by presence of tilted fault blocks and sediment thickening toward the fault, as seen in the lower part of *fig.4.2*. Tilted fault blocks and sediment thickening toward the fault are very common in the extensional basin. It is related to the development

stages of extensional basin itself, especially during the active stretching and thermal subsidence stages (*fig. 4.4-4.6*). Clearer view of indications of extension, including wedge shaped sediment package, sediment thickening toward the fault and tilted fault block can be seen in *fig. 4.3*.

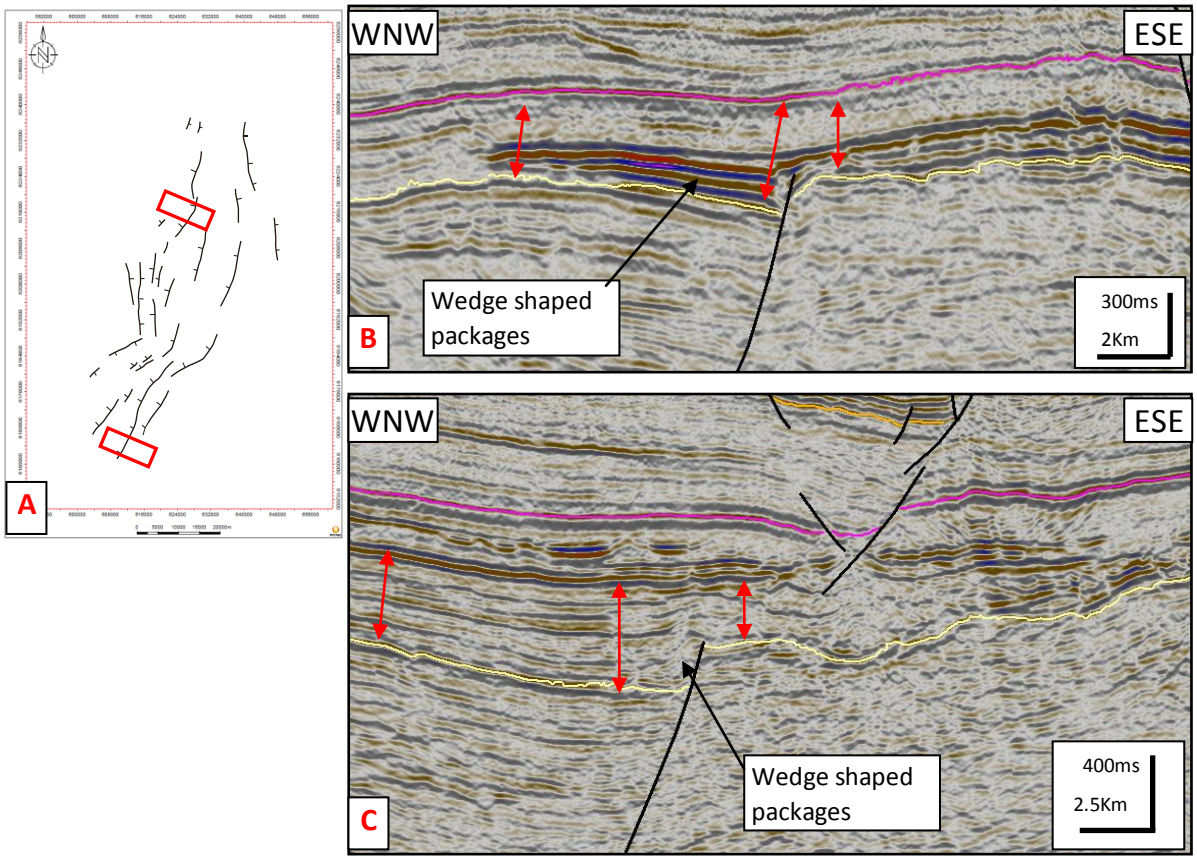

Figure 4.3: (A) Late Carboniferous fault map and location of seismic sections (red rectangles), (B) and (C) 3D crosslines show the fault geometry of late Carboniferous interval. Red arrows indicate sediment thickening.

The presences of fault block which tilted away from basin axis and wedge sediment package, which is located just above the late Carboniferous reflection (*fig 4.2* and *fig 4.3)*, indicate and separate syn-rift deposit from pre- and post-rift deposits at below and above it, as seen in the *fig. 4.5* and *4.6*. There is no clear unconformity observed in the section, which perhaps related to the gradual transition between the development stages of the rift.

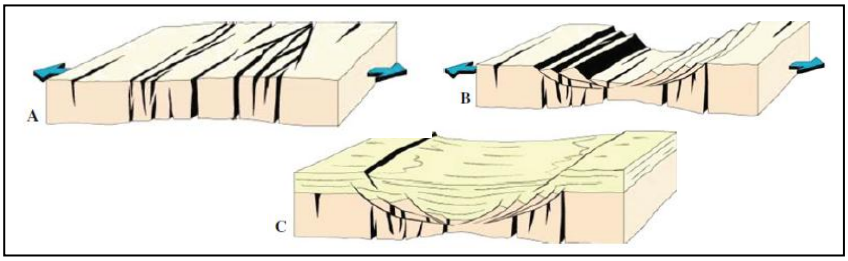

Figure 4.4: Three stages in development of extensional basin. (A) pre-rift, (B) active stretching, (C) post-rift stages (modified from Gabrielsen, 2010).

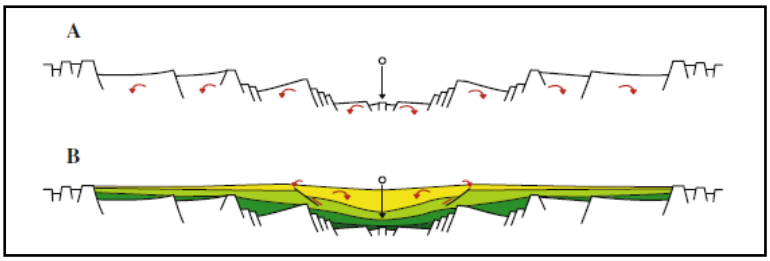

Figure 4.5: Rotation of fault block in (A) syn-rift and (B) post-rift (Gabrielsen, 2010).

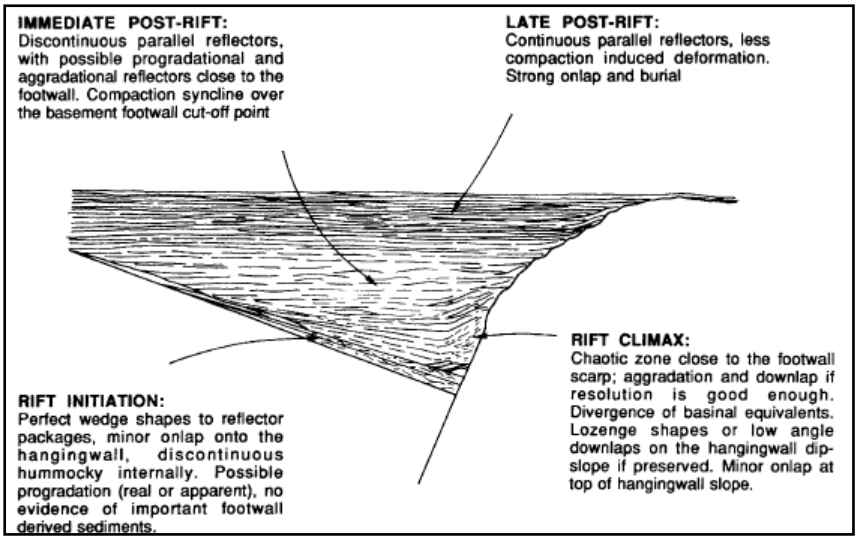

Figure 4.6: Illustration of idealized section through rift basin (Prosser, 1993).

4.1.2.2 Late Permian-Early Triassic and Early-Middle Triassic Intervals

Both late Permian-early Triassic and early-middle Triassic intervals are characterized by relatively similar fault geometries which mainly consist of planar to slightly curved normal faults. Thickening of sediment package across the master fault is observed within lower-middle Triassic succession which is followed by the minor folded layers at upper part of middle-Triassic succession. This sediment thickening with normal drag in the downthrown side of fault is interpreted as the result of growth faulting (*fig. 4.2*). Growth faults are developed by contemporaneous faulting and sedimentation, and theoretically characterized by the abrupt increase in thickness of strata across the fault on the downthrown block (Edwards, 1976).

The occurrence of growth faults in Triassic succession also can be found in Svalbard (Edwards, 1976), as seen in *fig. 4.7*, which are originated from the mass movement in the area close to the paleoslope.

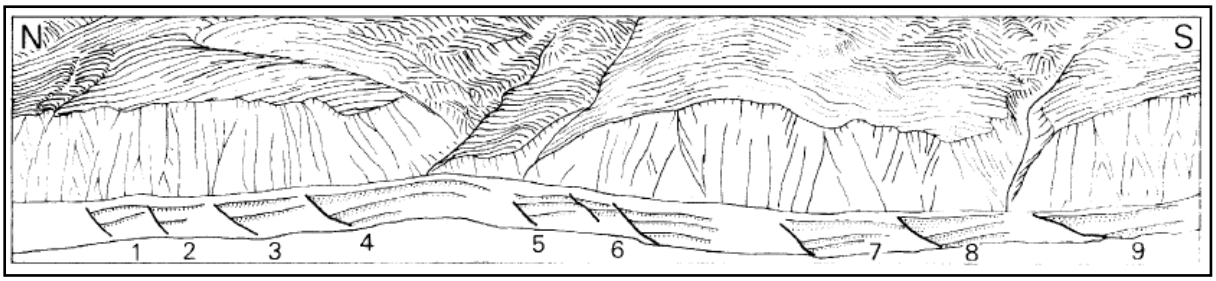

Figure 4.7: Oblique aerial sketch showing the growth faults in the upper Triassic sediment in Kvalpynten, Svalbard. Numbers refer to the growth fault (Edwards, 1976).

Minor fold, which is observed in the upper part of early-middle Triassic interval, reflects mild inversion process after the growth faulting has stopped. The detailed discussion about indication of this mild inversion is explained in subchapter 4.4.

4.1.2.3 Middle Triassic-Base Cretaceous Interval

A set of planar to slightly curved normal faults and its antithetic normal faults within middle Triassic-early Cretaceous interval reflect the extension which actives during late Jurassic-early Cretaceous and forms NE-SW to N-S trending graben system. It is shown by presence of wedge sediment package characterizing syn-rift deposit, just above the base Cretaceous reflection (*fig. 4.2*). The unconformity representing the pre-rift to syn-rift transition, which is characterized by erosional truncation and onlapping of younger reflection, can also be observed along the base Cretaceous reflection. These indications of extensional basin match to the idealized cross section of rift basin (*fig. 4.6*). However, the unconformity reflecting the syn-rift to post-rift deposits is not clearly observed which may indicate gradual transition between those two stages.

4.2 Detachment

Detachment, as mentioned in many published literatures, is basically characterized by disparity in deformation between intervals below and above detachment. The presence of listric faults, which is flatten into a sequence of mechanically weak rocks, is one of the common characteristic of detachment. However, other characteristics reflecting disparity in deformation can also be formed, such as difference in dip of bedding, dip of the fault plane, dip-slip magnitude of fault segments, number of faults above and below detachment.

Based on the differences in fault geometry, as discussed in subchapter 4.1, several detachments are recognized separating different depth-dependent segments. These detachments are major detachment in the upper Carboniferous-lower Permian and minor detachments in upper Permian and middle Triassic successions (*fig. 4.8*).

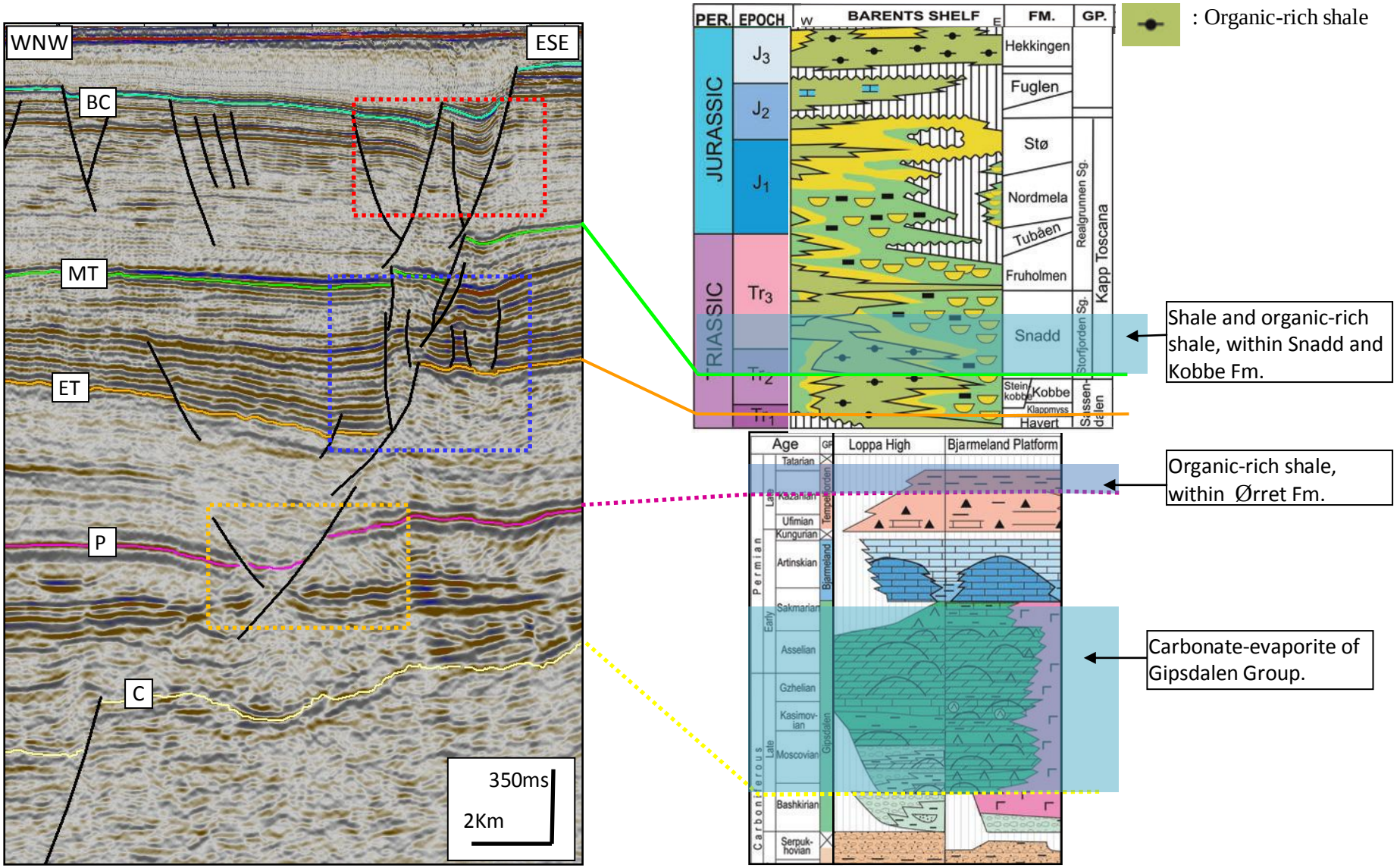

Figure 4.8: 3D Crossline B, with interpreted detachments. See *fig. 3.6* for location of the line. Orange square: late Permian-early Triassic, blue square: early-middle Triassic, red square: middle Triassic-base Cretaceous intervals. All lithostratigraphic columns are modified from Worsley (2008).

4.2.1 Late Carboniferous-Early Permian Detachment

From the difference in the structural arrangement in late Carboniferous and late Permian (*fig. 4.9*), it can be interpreted that faults within post-early Permian interval are decoupled from the deeper late Carboniferous interval, by detachment within the upper Carboniferous-lower Permian succession. The faulting in late Carboniferous affects much wider area compared to that in late Permian where the faulting is concentrated in fewer master faults.

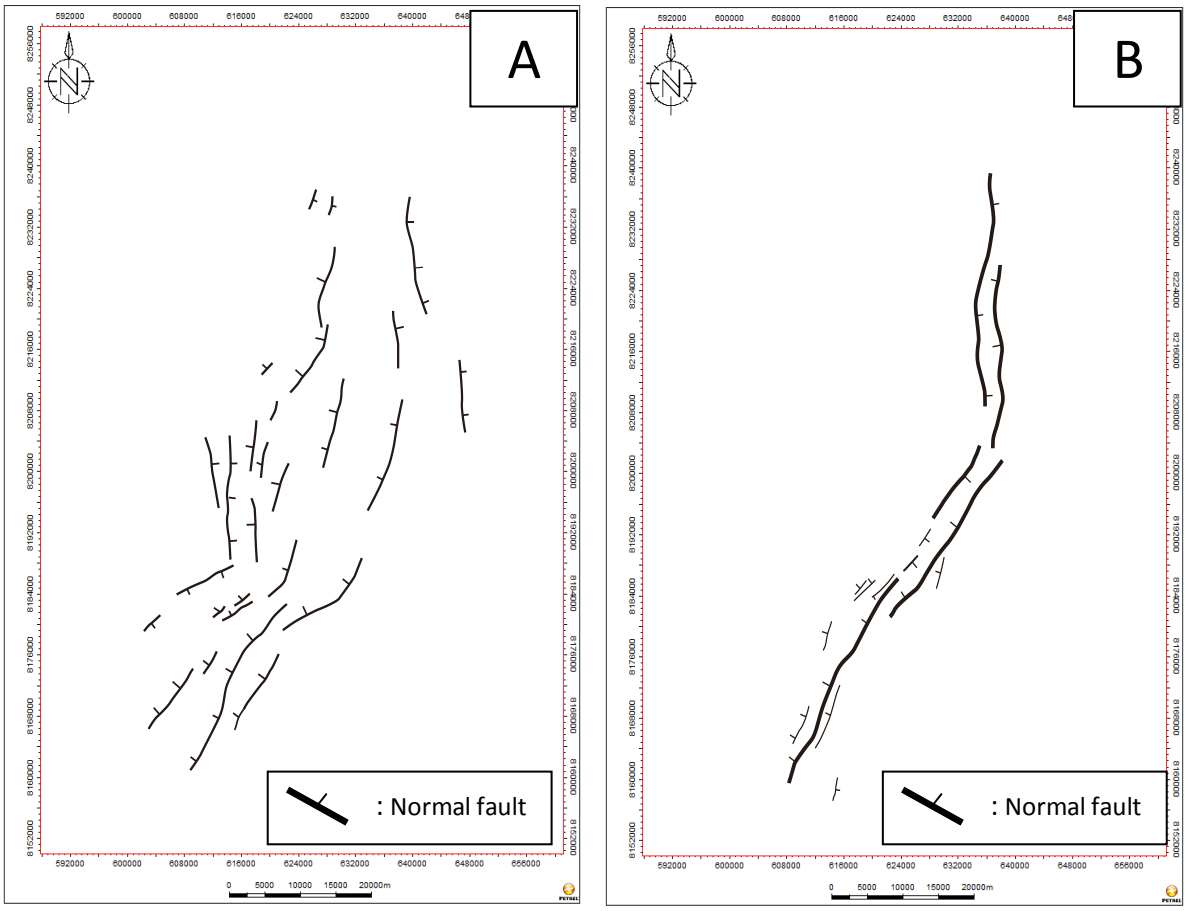

Figure 4.9: (A) Structures of Late Carboniferous. (B) Structures of late Permian, which represents post-early Permian interval.

The presence of this detachment is more clearly observed in seismic section (*fig. 4.10*), where the full graben is confined to the post-early Permian interval only and is separated from deeper horst and minor half graben. The greater dip-slip magnitude and number of faults in post-early Permian interval compared to the late Carboniferous interval have also reflected the presence of this detachment. However, the presence of flatten listric fault is not clearly defined, perhaps it is related to the ductile carbonate-evaporite sequence with low shear strength.

The similar late Carboniferous-early Permian detachment also can be found in Swaen Graben, SW Barents Sea (*fig. 4.11*) as mentioned by Gudlaugsson et al. (1998).

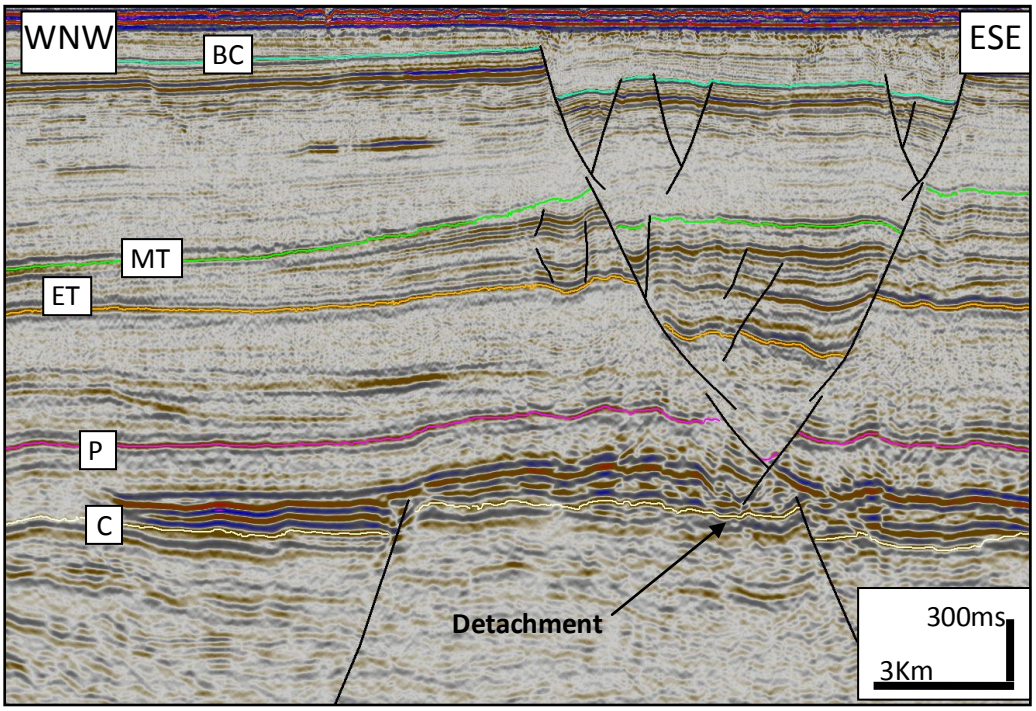

Figure 4.10: 3D crossline D shows separation of structural pattern at above and below upper Carboniferous-lower Permian carbonate-evaporite succession. See *fig. 3.6* for location of the line.

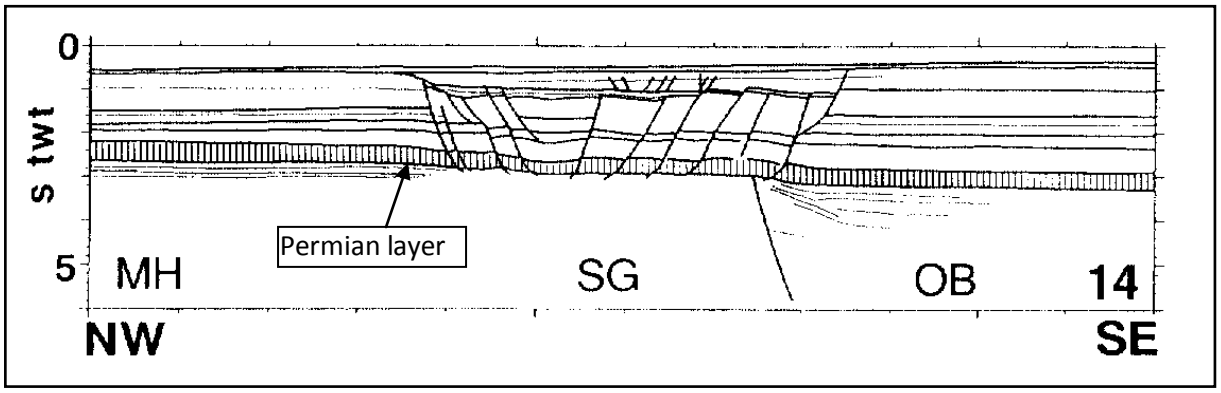

Figure 4.11: Decoupled levels below and above detachment of Permian layer in Swaen Graben, SW Barents Sea (modified from Gudlaugsson, et al., 1998).

4.2.2 Late Permian and Middle Triassic Detachments

From the structural arrangement in late Permian, middle Triassic and base Carboniferous fault maps (*fig. 4.12*), it can be interpreted that the faulting relatively affects wider area toward younger time interval. This difference in structural arrangements indicates the presence of detachments between those mentioned time intervals.

Difference in fault geometry, dip-slip magnitude and number of faults within separated depth-dependent intervals, as discussed in subchapter 4.1.2, have also reflected the presence of these detachments which coincide to the organic-rich shales of late Permian Ørret Formation and middle Triassic Snadd-Kobbe Formations (*fig. 4.8*).

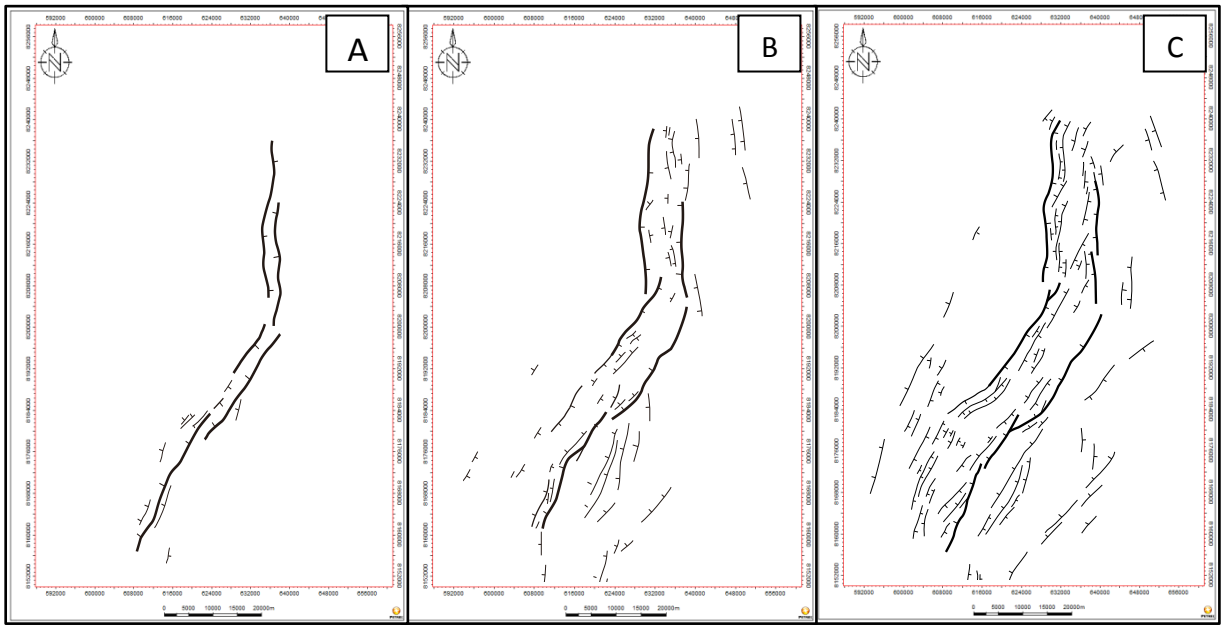

Figure 4.12: Structural pattern of late Permian (A), middle Triassic (B), and base Cretaceous (C).

4.3 Positive Inversion

Minor fold, which is observed at upper part of the hanging wall of slightly curved growth normal fault, as seen in *fig 4.2*, reflects the contraction which is active at least from middle to earliest late Triassic time, after the growth faulting ceased down. It is mainly based on the thinning of folded reflections toward the fault within that time interval. This presence of contraction after extensional growth faulting indicates a positive structural inversion.

The most common characteristics of an positive inverted system are reverse reactivation of extensional faults, generation of new, low angle fault traces, development of secondary contractional structures (folds, reverse faults, thrusts) and uplift of basin margin and central parts of basins (Gabrielsen, 2010). Even though, not all of the mentioned characteristics can be found in the study area, but the presence of fold following the growth faulting can be a strong indication of inversion. Idealized evolution of inverted growth normal fault can be seen in *fig. 4.13*. The absences of other characteristics of inversion, such as reverse fault, in study area may relate to the mild magnitude of the contraction (Grunnaleite, 2004).

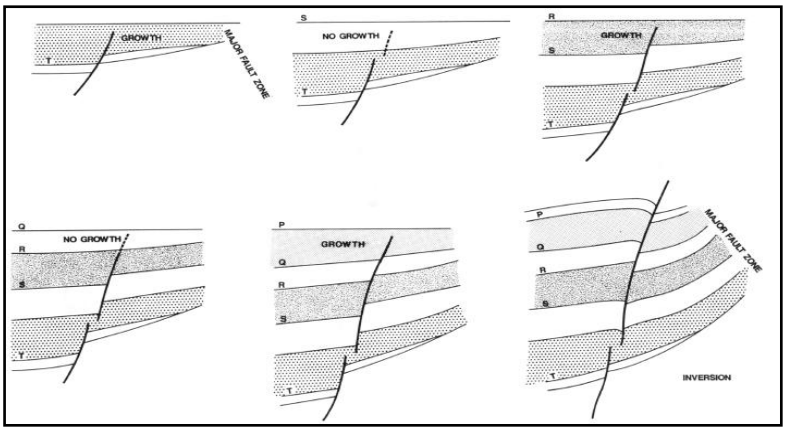

Figure 4.13: Variation of displacement pattern with time of inverted normal growth fault (Chapman and Meneilly, 1991).

This contraction in study area can be originated from head-on contraction or from transpression of secondary strike-slip movement related to the regional NW-SE extension. Inversion due to head-on contraction is characterized by parallel fold axis to the master fault, as seen in the Bjørnøyrenna Fault Complex, SW Barents Sea (*fig. 4.14*). On the other side, fold axis related to the transpression of strike-slip movement is relatively oblique to the master strike-slip fault, as seen in the strain ellipsoid of strike-slip fault in *fig. 4.15*. Due to the limitation on time of this thesis work, it is not possible to map the direction of this minor fold axis. However, contraction related to the transpression is less likely compared to head-on contraction. It is mainly based on the observation that NE-SW trending structures in segment 1 and 2 (*fig. 3.14-3.15*) experience higher degree of contraction, expressed by greater degree of folding, compared to the N-S trending structures in segment 3 (*fig. 3.16*). Whereas if this contraction is due to transpression of the left-stepping strike-slip faults related to regional NW-SE extension, the N-S trending structure should experience greater degree of contraction compared to the NE-SW trending structures.

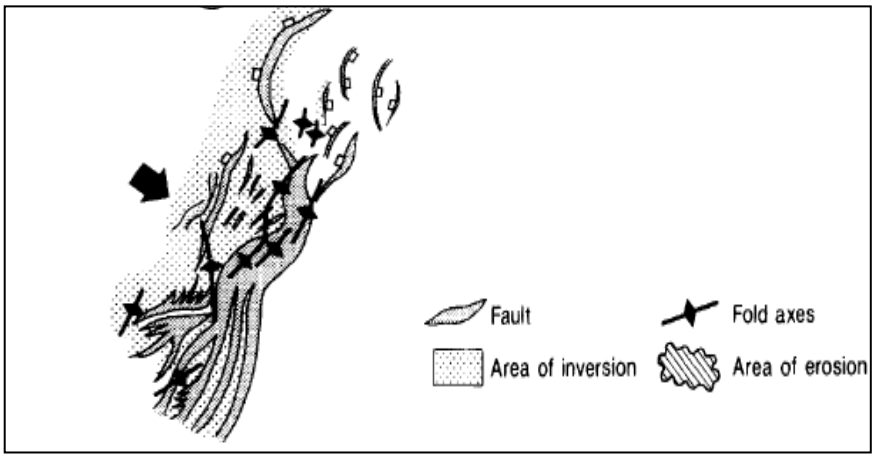

Figure 4.14: Structural pattern of the Bjørnøyrenna Fault Complex during late Cretaceous-early Tertiary inversion (modified from Gabrielsen et al., 1997).

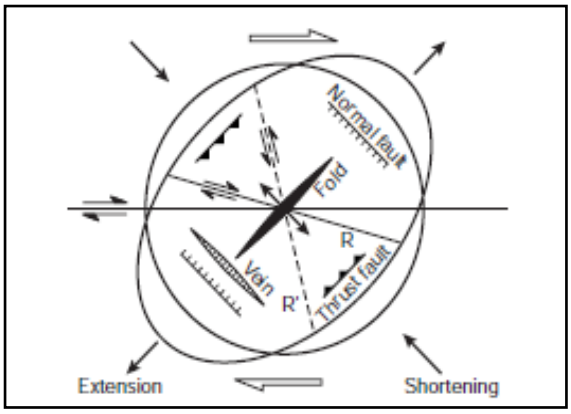

Figure 4.15: Strain ellipsoid of strike slip fault (modified from Pluijm and Marshak, 2003).

4.4 Geological History of The Hoop Fault Complex

This subchapter discusses the evolution of structural configuration of the Hoop Fault Complex, including its possible principal stress configuration and comparison to the regional events.

4.4.1 Late Carboniferous-Late Permian

Evolution of the Hoop Fault Complex is started by the late Carboniferous extensional rifting event which forms NE-SW to NNE-SSW trending wide graben system in the south and faulted platform with minor half graben in the north (*fig. 3.20* and *4.16*). This extension seems to have affected wide area with large number of steeply dipping planar normal faults. Lateral configuration of the Hoop Fault Complex at this time interval is relatively similar to the regional structural configuration which is dominated by NE-SW trends, as seen in *fig. 4.16*.

The local principal stress direction for this late Carboniferous extension is ESE-WNW or perpendicular to the general trend of the structures. This stress configuration is relatively similar to the E-W regional extensional stress configuration during that time interval (Ziegler, 1988 in Smelror et al., 2009).

In the study area, the late Carboniferous active rifting period is followed by thermal subsidence without faulting activity until late Permian time. During transition from late Permian to early Triassic, another regional extensional rifting event occurred (Gudlaugsson et al., 1998) which probably affected northerly trending zone along the entire present western margin of SW Barents Sea. Rift-related renewed faulting, uplift and erosion were also observed at the western margin of the Loppa High during this transition late Permian-early

Triassic time (Faleide et al., 2010). However, no indication of faulting activity during late Permian-early Triassic, such as sediment thickening across the fault, can be found in study area as seen in late Permian-early Triassic time-thickness map (*fig. 3.28*). It may indicate that late Permian-early Triassic rifting only focuses and affects N-S trending structure at western side of SW Barents Sea and have less influence toward the east.

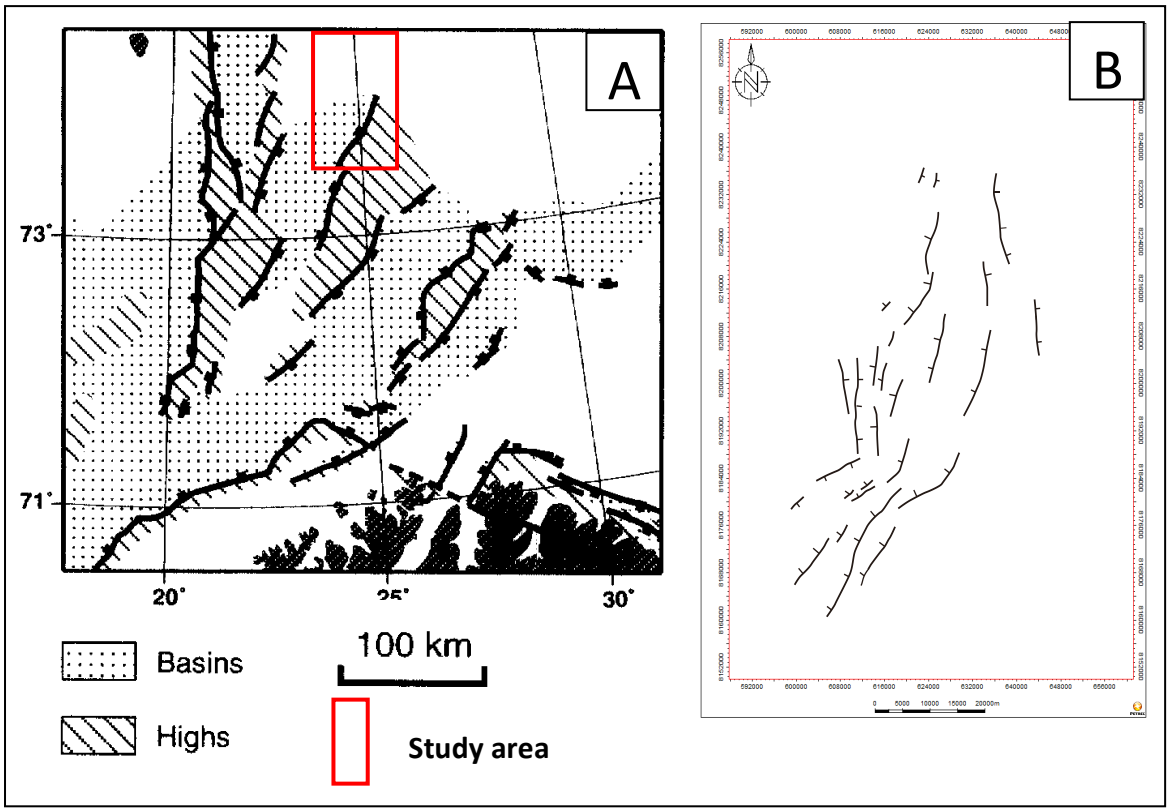

Figure 4.16: Comparison between (A) regional structures of Carboniferous rift system (modified from Gudlaugsson et al., 1998) to (B) structures of late Carboniferous in study area.

4.4.2 Early-Middle Triassic

The early-middle Triassic structural element in study area is characterized by presence of NE-SW and N-S trending growth normal faults forming a sag sediment package in the downthrown side of master faults as seen in seismic section (*fig. 3.14*). However, the origin of this growth fault is still unclearly defined whether it is related to the mass movement at the paleoslope in deltaic environment, as seen in Svalbard (Edwards, 1976), or it is related to the local salt tectonic. Breivik et al. (1995) mentioned the initiation of salt movement in some basins in SW Barents Sea, including Maud Basin, at early-middle Triassic time.

Most of the Barents Sea region experienced calm tectonic period and regional subsidence during Triassic time following late Permian-early Triassic rifting (Glørstad-Clark et al., 2010) and resulted deposition of thick Triassic succession. The Presence of this thick succession may trigger the growth faulting in study area through mass movement related to the failure at the paleoslope in deltaic environment or salt movement which is triggered by differential loading related to mentioned thick succession.

4.4.3 Middle-Late Triassic

The structural development during middle-earliest late Triassic in the study area is marked by the presence of mild contraction which reversely reactivates the early-middle Triassic growth faults. This contraction or positive inversion is characterized by the presence of minor fold at the upper part of hanging wall of master fault (*fig.3.14*). Even though the direction of fold axis is not defined yet, it is interpreted that mentioned mild inversion is resulted by NW-SE trending head-on contraction or relatively perpendicular to the NE-SW trending structures in the south. This interpretation is mainly based on the observation that higher degree of folding is observed in the NE-SW trending structures in the south compared to the one in N-S trending structures in the north of study area.

The linkage of this contraction to the regional tectonic event is also not clearly defined. It is mainly due to most of area in Barents Sea experienced calm tectonic and regional subsidence during Triassic-middle Jurassic time (Glørstad-Clark et al., 2010).

4.4.4 Early-Middle Jurassic

Early-middle Jurassic in study area was characterized by subsidence without any observed faulting activity. It is similar to regional tectonic condition which was characterized by calm tectonic environment (Dengo and Røssland, 1992).

4.4.5 Late Jurassic-Early Cretaceous

Structural development of study area in late Jurassic-early Cretaceous is characterized by presence of major extensional rifting event resulting NE-SW trending half graben in the south, NE-SW trending full graben in the central part and N-S trending full graben in the north (*fig. 3.6*). This extension seems to have concentrated on fewer master faults within narrower area compared to the rifting event in the late Carboniferous.

The local principal extensional stress direction for this late Jurassic-early Cretaceous is NW-SE or relatively perpendicular to the NE-SW trending structures in the south which have greater dip-slip magnitude compared to the one in N-S trending structure in the north (*fig. 3.6*). This stress configuration is relatively similar to the NW-SE regional extensional stress configuration (Ziegler, 1988 in Smelror et al., 2009) creating a wide spread rifting in SW Barents Sea.

4.4.6 Late Cretaceous-Recent

Following rifting event in late Jurassic-early Cretaceous, relatively thick sediment of post-rift stage was deposited inside the full and half grabens during early Cretaceous-earliest late Cretaceous in study area.

In general, late Cretaceous in study area is characterized by uplift and erosion creating widespread unconformity. Approximately 1500 m of strata have been removed during this uplift and erosion (Faleide et al., 1993a).

Following late Cretaceous uplift, most of area in SW Barents Sea experienced Paleogene subsidence related to the breakup in Norwegian-Greenland Sea, and Neogene uplift and erosion related to the combined effects of glacial erosion and isostatic uplift (Faleide et al. 1993a). Thin Tertiary strata in study area reflect these complex tectonic events.

The generalized geological history of study area with the comparoson to the regional events can be seen in *fig. 4.17*.

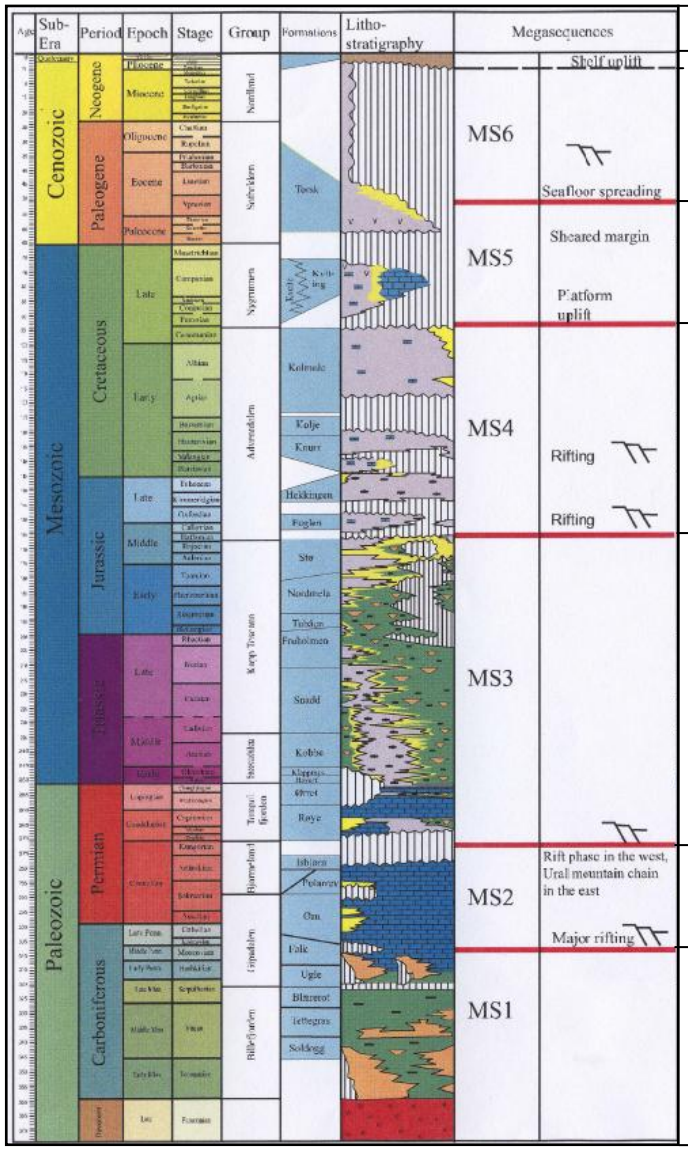

Stress direction (regional)	Tectonic events (local)	Stress direction (local)	Remarks
	Uplift		
NW - SE	subsidence		
	Uplift		
NW - SE	Rifting	NW - SE	
	Subsidence		
	Positive Inversion	NW - SE	Related to head-on contraction
	Growth Faulting		Due to salt tectonic or mass-movement(?)
NW - SE			No indication of active faulting, related to late Permian-early Triassic regional rifting, can be observed in study area.
E - W	Rifting	ESE - WNW	

Figure 4.17: Comparison of regional tectonic evolution in SW Barents Sea (modified from Glørstad-Clark et al., 2011) to the local tectonic events in study area. Regional principal stress configurations are modified from Ziegler (1988) in Smelror et al. (2009).

5. Summary

This thesis describes the structural characteristics of the Hoop Fault Complex with emphasis on structural geometry, its genesis and evolution. Seismic structural interpretation has been done in both 2D and 3D seismic sections to identify and map the detail of structures within the Hoop Fault Complex. A set of time-structure, time-thickness and fault maps corresponding to the selected key seismic reflections has been also constructed in order to analyze the lateral geometry and possible depositional pattern related to the active structures. Eight key seismic lines representing all variations and details of different segments of the Hoop Fault Complex were selected and used to analyze the detail fault geometry, the structural style and its genesis, timing of the faulting, and geological history.

The Hoop Fault Complex is an obviously extensional fault complex which has been repeatedly active since late Carboniferous, being reactivated in Triassic and late Jurassic-early Cretaceous. This fault complex consists of a set of NE-SW and N-S trending normal faults defining three separated lateral segments, namely segment 1, 2 and 3. Segment 1 in the south is characterized by one NE-SW trending master normal faults with a set of minor normal faults, defining a SE tilted half graben. Segment 2 in the central part is characterized by a set of NE-SW trending master normal faults and minor normal faults, which are developed mainly in the hanging wall of master fault, defining full graben morphology. Segment 3 in the north is characterized by a set of N-S trending master normal faults defining full graben in their hanging walls.

Vertically, the Hoop Fault Complex consists of several depth-dependent segments which are characterized by different fault geometry and separated by detachments. The main detachment coincides with upper Carboniferous-lower Permian carbonate-evaporite succession separating late Carboniferous interval from the post-early Permian interval. Late Carboniferous interval is characterized by a set of steeply dipping, extensional planar normal faults defining a wide graben with tilted fault block at the flank of the graben and at the northern platform. These faults were developed during late Carboniferous ESE-WNW major rifting. Post-early Permian interval is characterized by complex geometry of moderate-steeply dipping, extensional normal faults which are ascribed by fault reactivation in early-middle Triassic, middle-late Triassic and late Jurassic-early Cretaceous. However, vertical

variation of the mechanical strength in the rock column has also contributed to the complex geometry of these faults.

Based on the fault geometry, post-early Permian interval can be divided farther into three depth-dependent segments, namely late Permian-early Triassic, early-middle Triassic and middle Triassic-base Cretaceous intervals. Organic rich-shale layers within late Permian Ørret Formation and middle Triassic Snadd-Kobbe Formations have acted as minor detachments separating mentioned depth-dependent segments.

The late Permian-early Triassic interval is characterized by moderate-steeply dipping, slightly curved to planar normal faults, whereas early-middle Triassic interval is characterized by moderately dipping, slightly curved growth normal faults which are possibly related to the mass movement in deltaic environment or to the early-middle Triassic salt movement. Minor fold observed at the upper part of the hanging wall of growth normal fault which reflects mild inversion resulted from NW-SE head-on contraction during middle-earliest late Triassic after growth faulting ceased down. The middle Triassic-base Cretaceous interval is characterized by a set of moderate-steeply dipping planar to slightly curved extensional normal faults and its antithetic faults which are developed during late Jurassic-early Cretaceous NW-SE major rifting.

The evolution of Hoop Fault Complex can be summarized as below:

- Late Carboniferous ESE-WNW rifting event resulting in wide NE-SW to NNE-SSW trending wide graben in the south, as part of Maud Basin, and faulted platform in the north.
- Early-late Permian thermal subsidence. No indication of active faulting related to the regional rifting event can be observed in study area during late Permian to early Triassic transition.
- Early-middle Triassic growth faulting which is possibly related to the mass movement within deltaic environment or to the salt movement during this period.
- Middle-earliest late Triassic mild inversion related to NW-SE head-on contraction.
- Early-middle Jurassic subsidence without faulting activity.
- Late Jurassic-early Cretaceous NW-SE rifting event resulting in NE-SW and N-S trending graben system.
- Late Cretaceous regional uplift and erosion.

- Paleogene subsidence and deposition, associated with break up in Norwegian-Greenland Sea
- Neogene glaciation uplift and erosion.

References

Breivik, A.J., Faleide, J.I. and Gudlaugsson, S.T., 1995, Ottar Basin, SW Barents Sea: a major upper Paleozoic rift basin containing large volume of deeply buried salt, Basin Research 7, 299-312.

Breivik, A.J., Faleide, J.I. and Gudlaugsson, S.T., 1998, Southwestern Barents Sea margin: late Mesozoic, Tectonophysics 293, 21-44.

Chapman, T.J. and Meneilly, A.W., 1991, The displacement patterns associated with reverse-reactivated normal growth fault, In: Roberts, A.M., Yielding, G. and Freeman, B. (ed.), The geometry of normal faults, Geological society special publication 56, 183-191.

Childs, C., Nicol, A., Walsh, J.J., and Watterson, J., 1996, Growth of vertically segmented normal faults, Journal of Structural Geology, v.18(12), 1389-1397.

Dengo, C.A. and Røssland, K.G., 1992, Extensional tectonic history of the western Barents Sea, In: Larsen, R., Brekke, H., Larsen, B. and Talleraas, E. (ed.), Structural and tectonic modelling and its application to petroleum geology, Elsevier, Amsterdam, 91-107.

Dimakis, P., Braathen, B.I., Faleide, J.I., Elverhøi, A. and Gudlaugsson, S.T, 1998, Cenozoic erosion and the preglacial uplift of the Svalbard-Barents Sea region, Tectonophysics 300, 311-327.

Doré, A.G., 1995, Barents Sea geology, petroleum resources and commercial potential, Arctic 8, 207-221.

Edwards, M.B., 1976, Growth faults in upper Triassic deltaic sediments, Svalbard, The American Association of Petroleum Geologist Bulletin, v.60(3), 341-355.

Faleide, J.I., Bjørlykke, K. and Gabrielsen, R.H., 2010, Geology of the Norwegian continental shelf, In: Bjørlykke, K. (ed.), Petroleum geoscience from sedimentary environments to rock physics, Springer, Berlin, 489-499.

Faleide, J.I., Gudlaugsson, S.T. and Jacquart, G., 1984, Evolution of the western Barents Sea, Marine and Petroleum Geology 1, 123-150.

Faleide, J.I., Solheim, A., Fiedler, A., Hjelstuen, B.O., Andersen, E.S. and Vanneste, K., 1996, Late Cenozoic evolution of the western Barents Sea-Svalbard continental margin, Global and Planetary Change 12, 53-74.

Faleide, J.I., Tsikalas, F., Breivik, A.J., Mjelde, R., Ritzmann, O., Engen, O., Wilson, J. and Eldholm, O., 2008, Structure and evolution of the continental margin of Norway and Barents Sea, Episodes 31, 82-91.

Faleide, J.I., Vågnes, E. and Gudlaugsson, S.T., 1993a, Late Mesozoic-Cenozoic evolution of the southwestern Barents Sea, In: Parker, J.R. (ed.), Petroleum Geology of Northwest

Europe, Proceedings of the 4th conference, The Geological Society of London, London, 933-950.

Faleide, J.I., Vågnes, E. and Gudlaugsson, S.T., 1993b, Late Mesozoic-Cenozoic evolution of the south-western Barents Sea in a regional rift-shear tectonic setting, Marine and Petroleum Geology 10, 186-214.

Gabrielsen, R.H., 1984, Long-lived fault zones and their influence on the tectonic development of the south-western Barents Sea, Journal of Geological Society of London 141, 651-662.

Gabrielsen, R.H., 2010, The structure and hydrocarbon traps of sedimentary basins, In: Bjørlykke, K. (ed.), Petroleum geoscience from sedimentary environments to rock physics, Springer, Berlin, 299-327.

Gabrielsen, R.H., Færseth, R.B., Jensen, L.N., Kalheim, J.E. and Riis, F., 1990, Structural elements of the Norwegian continental shelf, Part I: The Barents Sea Region, Norwegian Petroleum Directorate Bulletin 6, 47 pp.

Gabrielsen, R.H., Grunnaleite, I. and Rasmussen, E., 1997, Cretaceous and Tertiary inversion in the Bjørnøyrenna Fault Complex, south-western Barents Sea, Marine and Petroleum Geology, v.14(2), 165-178.

Gérard, J. and Buhrig, C., 1990. Seismic facies of Permian section of the Barents Shelf: analysis and its interpretation, Marine and Petroleum Geology 7, 234-252.

Glørstad-Clark, E., Faleide, J.I., Lundschien, B.A. and Nystuen, J.P., 2010, Triassic seismic sequence stratigraphy and paleogeography of the western Barents Sea Area, Marine and Petroleum Geology 27, 1448-1475.

Glørstad-Clark, E., Clark, S.A., Faleide, J.I., Bjørkesett, S.S., Gabrielsen, R.H. and Nystuen, J.P., 2011, Basin dynamics of the Loppa High area, SW Barents Sea: A history of complex vertical movements in an epicontinental basin, In: Glørstad-Clark, E., Basin analysis in western Barents Sea area: The interplay between accomodation space and depositional system, PhD thesis, University of Oslo, Oslo, 111-178.

Grunnaleite, I., 2004, The development of inverted faults: result from analogue plaster models, In: Bertotti, Buiter, S., Ruffo, P., and Schreurs, G. (ed.), From mountains to sedimentary basins: modelling and testing geological processes, International Journal of Earth Sciences, Switzerland, 217-221.

Gudlaugsson, S.T., Faleide, J.I., Johansen, S.E. and Breivik, A.J., 1998, Late Paleozoic structural development of the South-western Barents Sea, Marine and Petroleum Geology 15,73-102.

Kjemperud, A., Fjeldskaar, W., 1992, Pleistocene glacial isostasy- implication for petroleum geology, In: Larsen, R., Brekke, H., Larsen, B. and Talleraas, E. (ed.), Structural and tectonic modelling and its application to petroleum geology, Elsevier, Amsterdam, Norwegian Petroleum Society, 187-195.

Kusznir, N.J., Roberts, A.M. and Morley, C.K., 1995, Forward and reverse modelling of rift basin formation, in: Lambiase, J.J. (ed.), Hydrocarbon habitat in rift basin, Geological Society Special Publication 80, 33-56.

Larssen, G.B., Elvebakk, G., Henriksen, L.B., Kristensen, S.-E., Nilsson, I., Samuelsberg, T.A., Stemmerik, L. and Worsely, D., 2002, Upper Paleozoic lithostratigraphy of the southern Norwegian Barents Sea, Geological Survey of Norway Bulletin 44, 43 pp.

Nyland, B., Jensen, L., N., Skagen, J., Skarpnes, O., and Vorren, T., 1992, Teriary uplift and erosion in the Barents Sea: magnitude, timing and consequences. In: Larsen, R., Brekke, H., Larsen, B. and Talleraas, E. (ed.), Structural and tectonic modelling and its application to petroleum geology, Elsevier, Amsterdam, Norwegian Petroleum Society, 153-162.

Pluijm, B.A.V.D. and Marshak, S., 2003, Earth structure: An introduction to structural geology and tectonics, WBC/McGraw-Hill.

Prosser, Sarah, 1993, Rift-related linked depositional systems and their seismic expression, Tectonics and Seismic Sequence Stratigraphy, Geological Society Special Publication 71, 35-66.

Ritzmann, O. and Faleide, J.I., 2007, Caledonian basement of the western Barents Sea, Tectonics 26, 417-435.

Smelror, M., Petrov, O.V., Larssen, G.B. and Werner, A.C., 2009, Geological history of the Barents Sea, Trondheim, Geological Survey of Norway.

Talwani, M. and Eldholm, O., 1977, Evolution of the Norwegian-Greenland Sea, Geological Society of America Bulletin 88, 969-999.

Worsley, D., 2008, The post-Caledonian geological development of Svalbard and the Barents Sea, Polar Reasearch 27, 298-317.